Effective Field Theories for Top Quarks at the LHC and Physics Beyond the Higgs Boson

Darren James Scott

A Thesis presented for the degree of
Doctor of Philosophy

Institute for Particle Physics Phenomenology
Department of Physics
Durham University
United Kingdom

August 2017

Effective Field Theories for Top Quarks at the LHC and Physics Beyond the Higgs Boson

Darren James Scott

Submitted for the degree of Doctor of Philosophy

August 2017

Abstract: In this thesis we have considered applications of two different types of effective field theory. The first of these, Soft Collinear Effective Theory (SCET) has been applied to the calculation of top quark pair production at hadron colliders. Building on factorisation theorems developed using SCET we present results for resummed differential cross sections of the top pair invariant mass. The highest accuracy of resummation achieved and matched to fixed order is at NNLO+NNLL$'$. Resummed predictions are compared to fixed order ones and we find that while the (N)NLO results can be sensitive to the choice of factorisation scale, the resummed results exhibit more stable behaviour. We perform a number of additional analyses to further investigate the choice of scale on the invariant mass distribution. In addition, we also present results for the p_T distribution of the top quark.

The second piece of work presented in this thesis concerns the use of the Standard Model Effective Field Theory (SMEFT). The SMEFT augments the Standard Model with higher dimensional operators which can be viewed as the low energy realisation of some as yet undiscovered physics at high scale. We use the dimension-6 SMEFT to calculate the QCD corrections to Higgs decay to bottom quarks at NLO. The main result of this section is the NLO partial decay rate for the Higgs including the

dimension-6 Wilson coefficients. Finally we attempt to remove the presence of large mass logarithms through the conversion of the b-quark mass to the $\overline{\text{MS}}$ scheme. We assess the reliability of this prediction in the limit of massless bottom quarks and find excellent agreement with the result with full mass dependence.

Declaration

The work in this thesis is based on research carried out in The Institute for Particle Physics Phenomenology, Department of Physics at Durham University. No part of this thesis has been submitted elsewhere for any degree or qualification.

The Mellin space resummation formulas in Chapter 3 and their subsequent implementation and results which flow from them presented in Chapter 4 are based on work undertaken by the authour in collaboration with Ben Pecjak, Li Lin Yang, Andrea Ferroglia, Xing Wang, Alex Mitov, Michal Czakon, and David Heymes. Original results obtained at NLO+NNLL′ can be found in the publication

Resummed differential cross sections for top-quark pairs at the LHC
Benjamin D. Pecjak, Darren J. Scott, Xing Wang, Li Lin Yang
Phys.Rev.Lett. 116 (2016) no.20, 202001

The NNLO+NNLL′ predictions presented here have not been published on the date of submission of this thesis.

The content of Chapter 5 which involves computing the NLO QCD corrections to the decay $h \to b\bar{b}$ in the dimension-6 SMEFT constitutes work undertaken by the author in collaboration with Rhorry Gauld and Ben Pecjak. The original work can be found in:

QCD radiative corrections for $h \to b\bar{b}$ in the Standard Model Dimension-6 EFT

Rhorry Gauld, Benjamin D. Pecjak, Darren J. Scott

Phys.Rev. D94 (2016) 074045

This builds upon earlier work also carried out by the same authors in

One-loop corrections to $h \to b\bar{b}$ and $h \to \tau\bar{\tau}$ decays in the Standard Model Dimension-6 EFT: four-fermion operators and the large-m_t limit

Rhorry Gauld, Benjamin D. Pecjak, Darren J. Scott

JHEP 1605 (2016) 080

Acknowledgements

This thesis is based on work carried out during a four year PhD. As such I've had the pleasure of meeting, interacting, learning, and working with a great number of interesting and welcoming people from all walks of life. It is perhaps unsurprising that I am therefore indebted to a great number of people, and these acknowedgments will always fall short of the thanks I owe to so many people.

I wish first and foremost to thank my supervisor Ben Pecjak. His guidance, support and willingness to help has been invaluable over the past four years. His enthusiasm for physics when getting to the heart of a problem has been inspirational. I'd also like to thank the great number of friends I've made through both the IPPP and Grey College. Thank you all, for all the laughs and good times. There are simply too many memories to share here, though it would be wrong not to mention the OC118 powerhouse! In addition I'm also grateful to Rhorry Gauld and Richard Ruiz, both of whom I worked with and learned a great deal from on different projects. Also, thanks to Michael Spannowsky and Frank Krauss for their help and guidance on postdocs and other matters. Special thanks also go to Tom Jubb and Matthew Kirk for proof reading parts of this thesis. I also wish to give thanks in a more encompassing way to all at the IPPP. The privilege to come and study such an amazing subject here has been one of the greatest opportunities ever afforded to me. Thank you to all who have made it possible. Finally, it goes without saying that none of this would have been possible without the love and support of my parents. Thank you for your constant willingness to help and for supporting me throughout, it means so much.

Contents

List of Figures

List of Tables

Chapter 1

Features of the Standard Model

1.1 Introduction

In order to put the rest of this thesis in context we begin with a short review of the Standard Model (SM). We focus on key areas which are of most relevance to the work in this thesis. The SM is a gauge theory built on the gauge group

$$\mathrm{SU}(3)_c \times \mathrm{SU}(2)_L \times \mathrm{U}(1)_Y \,. \tag{1.1.1}$$

The subscripts c, L and Y stand for colour, "left", and hypercharge respectively. As such $\mathrm{SU}(3)_c$ is used to describe the form of the strong interactions, while $\mathrm{SU}(2)_L \times \mathrm{U}(1)_Y$ describes the electroweak sector. We will postpone discussion of the strong interactions until Section 1.4. The groups $\mathrm{SU}(N)$ for $N \geq 2$ are known as non-abelian. This is because the generators of the groups do not commute and obey the Lie algebra

$$\left[t^i, t^j\right] = i f^{ijk} t^k \,, \tag{1.1.2}$$

where t^i is a generator of the group indexed by i and f^{ijk} are known as the structure constants. In the case of SU(2) the structure constants are simply the three dimensional Levi-Civita symbol ϵ^{abc}. For an $\mathrm{SU}(N)$ theory the indices run from $i = 1, \ldots, N^2 - 1$. Gauge fields arising from these non-abelian Lie groups are known

as Yang-Mills theories and were first considered in [1]. Two non-trivial representations of these gauge groups will be important for the SM, the fundamental and adjoint representations. We denote generators in the adjoint representation with capital letters T^A. Fields transforming in the fundamental representation have N components while those in the adjoint have $N^2 - 1$ components. All matter fields in the SM will transform under either the trivial or fundamental representation of these groups, while the gauge fields themselves are in the adjoint representation. Under a gauge transformation, the matter fields in the theory transform as

$$\psi_i(x) \to U_{ij}(x)\psi_j(x)\,, \tag{1.1.3}$$

where

$$U_{ij}(x) = \exp\left(i\alpha^a(x)t^a_{ij}\right)\,, \tag{1.1.4}$$

and $\alpha^a(x)$ is a function parametrising the size of the transformation. Here the indices i, j label the gauge components of the field.

These gauge symmetries together with the spacetime symmetries of the Poincaré group greatly restrict the form of the Lagrangian[1] one can write down for the theory. The various fields in the theory will have different charges under the various gauge groups determining their interactions. Because the theory is based on local symmetries, it is necessary to introduce a covariant derivative in order to write down kinetic terms for the fermions which will appear in the theory. This takes the form

$$D_\mu = \partial_\mu - ig_1 Y B_\mu - ig_2 t^a W^a_\mu - ig_s t^A G^A_\mu\,, \tag{1.1.5}$$

where B_μ, W^a_μ and G^A_μ are the gauge fields associated with the $\mathrm{U}(1)_Y$, $\mathrm{SU}(2)_L$ and $\mathrm{SU}(3)_c$ groups respectively, Y is known as the hypercharge. Not all matter fields are charged under every gauge group and so not all of the gauge fields will necessarily be present in the covariant derivative for each matter field. Because these gauge fields will form dynamical components of the theory it is necessary to provide terms in the Lagrangian of the SM describing their dynamics. The kinetic terms for these

[1]Strictly the Lagrangian density. But we refer to this simply as the Lagrangian from now on.

gauge fields are written

$$\mathcal{L}_{\text{Gauge}} = -\frac{1}{4}B_{\mu\nu}B^{\mu\nu} - \frac{1}{4}W^{a}_{\mu\nu}W^{a\,\mu\nu} - \frac{1}{4}G^{A}_{\mu\nu}G^{A\,\mu\nu}\,, \tag{1.1.6}$$

where

$$\begin{aligned} B_{\mu\nu} &= \partial_\mu B_\nu - \partial_\nu B_\mu\,, \\ W^{a}_{\mu\nu} &= \partial_\mu W^{a}_{\nu} - \partial_\nu W^{a}_{\mu} + g_2 f^{abc} W^{b}_{\mu} W^{c}_{\nu}\,, \\ G^{A}_{\mu\nu} &= \partial_\mu G^{A}_{\nu} - \partial_\nu G^{A}_{\mu} + g_s f^{ABC} G^{B}_{\mu} G^{C}_{\nu}\,. \end{aligned}$$

The field strength tensors for the non-abelian gauge fields have additional terms in them which are quadratic in the fields. The kinetic term for non-abelian gauge fields therefore contain not just the usual $\partial A \partial A$ terms for the fields, but also terms trilinear and quartic in the fields. Non-abelian gauge fields therefore necessarily have self interactions amongst their component fields. Such a phenomenon plays an important role in the phenomenology of the strong interactions. We will encounter this more in Section 1.4.

The presence of the group $\mathrm{SU}(2)_L$, under which only left handed components of fields are charged means that the theory is chiral. As such when it comes to describe the matter content of the SM it is useful to project out the handedness of the field. We write

$$\psi_{L/R} = P_{L/R}\psi\,, \tag{1.1.7}$$

where ψ is a four component Dirac spinor and

$$P_L = \frac{1}{2}\left(1 - \gamma^5\right)\,, \qquad P_R = \frac{1}{2}\left(1 + \gamma^5\right)\,, \tag{1.1.8}$$

are the left and right handed projection operators respectively. Table 1.1 lists the matter fields which are present in the SM and their representation under the different gauge groups. The choices for the hypercharge of the fields is motivated by the resulting electric charge and will be discussed more in Section 1.2. The fields in

Field	$\mathrm{SU}(3)_c$	$\mathrm{SU}(2)_L$	$\mathrm{U}(1)_Y$
Q_L	**3**	**2**	$\frac{1}{6}$
u_R	**3**	**1**	$\frac{2}{3}$
d_R	**3**	**1**	$-\frac{1}{3}$
L_L	**1**	**2**	$-\frac{1}{2}$
e_R	**1**	**1**	-1

Table 1.1: Matter content of the SM and the charges of each field under the different gauge groups. For SU(3) and SU(2) trivial representations are denoted **1** while **3** and **2** denote the fundamental representation of each respectively.

the fundamental representation of $\mathrm{SU}(2)_L$ have as their components

$$Q_L = \begin{pmatrix} u_L \\ d_L \end{pmatrix}, \qquad L_L = \begin{pmatrix} \nu_L \\ e_L \end{pmatrix}.$$

Notice there is no right handed neutrino field. This means we cannot write a mass term for the neutrino, as we shall shortly see. The SM actually contains three copies or "generations" of each field. Each of these fields therefore carries an additional index i (Q_L^i) where $i = \{1, 2, 3\}$ labelling the generation. These generations are identical in every respect apart from their mass. In order to write a Lagrangian description for the theory, we must introduce kinetic terms for the fields. Using the covariant derivative introduced earlier the kinetic terms for the fields are written

$$\begin{aligned}\mathcal{L}_{\text{Dirac}} = &\sum_i \bar{Q}_L^i i \not{D} Q_L^i + \sum_i \bar{L}_L^i i \not{D} L_L^i + \sum_i \bar{u}_R^i i \not{D} u_R^i \\ &+ \sum_i \bar{d}_R^i i \not{D} d_R^i + \sum_i \bar{e}_R^i i \not{D} e_R^i \,. \end{aligned} \tag{1.1.9}$$

As mentioned, the covariant derivative only contains the gauge fields under which the field it is acting on is non-trivially represented. The presence of the covariant derivative in the kinetic term is the source of the interaction terms between the fermions in the theory and the gauge bosons. An apparent problem now arises. Mass terms for spin-$\frac{1}{2}$ fermions take the form

$$\mathcal{L} \supset -m(\bar{\psi}_L \psi_R + \text{h.c.}) \,, \tag{1.1.10}$$

where h.c. stands for the hermitian conjugate. This couples the left and right handed

Field	$\mathrm{SU}(3)_c$	$\mathrm{SU}(2)_L$	$\mathrm{U}(1)_Y$
H	**1**	**2**	$\frac{1}{2}$

Table 1.2: Representation of the Higgs field in the SM.

components of the field. However, because these two components are in different representations of $\mathrm{SU}(2)_L$ such terms would explicitly break this gauge symmetry. Thus it seems we cannot have mass terms for the fermions in the theory. A similar problem exists for the gauge bosons associated with the weak interactions, which are known experimentally to be mediated by massive exchanges. The solution to both these problems is to spontaneously break the symmetry preventing masses via the *Higgs mechanism*. While we postpone detailed discussion of this mechanism until Section 1.2, we note that it relies on the introduction of a scalar field in the fundamental representation of $\mathrm{SU}(2)_L$ which we denote H. Table 1.2 details the representation of the Higgs field under each of the gauge groups in the SM. We also note that the Higgs mechanism gives rise to masses for the fermions through Yukawa type interactions. The SM Lagrangian also contains the following terms

$$\mathcal{L}_{\text{Yukawa}} = -Y_d^{ij}\bar{d}_R^i H^\dagger Q_L^j - Y_u^{ij}\bar{u}_R^i \widetilde{H}^\dagger Q_L^j - Y_e^{ij}\bar{e}_R^i H^\dagger L_L^j + \text{h.c.}\,, \tag{1.1.11}$$

where Y_l^{ij} are the Yukawa coupling matrices in generation space (ij), for l-type[2] fermions. There is an understood contraction between the left hand fields and the Higgs field so as to make each term invariant under $\mathrm{SU}(2)_L$ transformations. In order to get a mass term for the up-type quarks it has been necessary to define $\widetilde{H} = i\sigma^2 H^*$. Our convention here agrees with the one from [2]. The relevance of this will be discussed in Chapter 2. Note that because there is no right handed neutrino field, we cannot write down an interaction with the neutrinos and consequently they will remain massless. Given that neutrinos are known to have a non-zero mass experimentally, one might be tempted to introduce a right handed neutrino and give them mass via the Higgs mechanism. However, the exceedingly small mass of these particles has sparked a lot of interest on other methods to provide a mass. We will

[2] u = up-type quarks, d = down-type quarks, e = charged leptons.

not discuss these here, but simply note that this is a feature of nature which the SM currently doesn't (but could) account for. Finally, we require some terms in the Lagrangian to describe the kinetics of the Higgs field itself. These are given by

$$\mathcal{L}_{\text{Higgs}} = D_\mu H (D^\mu H)^\dagger - V(H)\,, \tag{1.1.12}$$

where $V(H)$ is the potential for the scalar field which we will touch on shortly. The components mentioned thus far then constitute the current formulation of the SM. The classical Lagrangian for the SM is thus given by

$$\mathcal{L}_{\text{SM}} = \mathcal{L}_{\text{Gauge}} + \mathcal{L}_{\text{Dirac}} + \mathcal{L}_{\text{Yukawa}} + \mathcal{L}_{\text{Higgs}}\,, \tag{1.1.13}$$

where the terms on the right hand side are given by Eqs. (1.1.6), (1.1.9), (1.1.11) and (1.1.12). We now turn to the description of the Higgs sector of the SM, which will allow us to account for the masses of the observed particles without explicitly breaking the gauge symmetries.

1.2 Higgs Sector

The purpose of the Higgs sector of the SM Lagrangian is to spontaneously break the electroweak gauge symmetry in order to generate mass terms for the gauge bosons associated with the weak interactions as well as any fermions with mass [3–5]. The symmetry breaking is known as spontaneous since, even though the Lagrangian of the SM respects electroweak gauge symmetry, the potential for the Higgs field is such that the ground state of the theory does not. In Chapter 5 we will study the decays of the Higgs boson into bottom quarks and so we briefly review the Higgs mechanism with emphasis on the coupling to fermions. In spontaneously breaking a continuous (global) symmetry we expect from Goldstone's Theorem [6,7] for there to be massless bosons (Goldstone bosons) in the spectrum of the resulting theory. However, when the symmetry being broken is local and as such has gauge bosons associated with it, these massless Goldstone bosons do not appear in the final spectrum of particles.

Instead the degrees of freedom associated with them are "eaten" by the gauge bosons which gain a degree of freedom giving them a longitudinal polarisation and consequently a mass. Since the Higgs field is introduced to break the electroweak $\mathrm{SU}(2)_L \times \mathrm{U}(1)_Y$ symmetry of the SM, it is necessarily charged under this symmetry. From Table 1.2 we see that the Higgs field is a doublet under $\mathrm{SU}(2)_L$ and is written

$$H = \begin{pmatrix} \phi^+ \\ \phi^0 \end{pmatrix}, \tag{1.2.1}$$

where ϕ^0 and ϕ^+ are complex scalars. The superscripts refer to the electric charge of the bosons and the assignment will be justified later. The form of the potential in the Higgs sector is given by

$$V(H) = -\mu^2 H^\dagger H + \lambda (H^\dagger H)^2 , \tag{1.2.2}$$

where we have chosen the signs such that $\lambda, \mu > 0$. This potential is not minimized at $|H|^2 = 0$. In fact the lowest energy state is obtained for $|H|^2 = v^2$ where

$$v = \sqrt{\frac{\mu^2}{2\lambda}} . \tag{1.2.3}$$

That the Higgs field has a non-zero value in its lowest energy configuration is exactly what gives rise to the spontaneous symmetry breaking. To see this clearly we can expand the Higgs doublet into its components. We require that

$$H^\dagger H = \phi^+ \phi^- + \phi^{0\,\dagger} \phi^0 = v^2 . \tag{1.2.4}$$

This can be achieved by setting the *vacuum expectation value* (VEV), denoted $\langle \phi \rangle$, to be zero for ϕ^+ and $\mathrm{Im}(\phi^0)$ and to v for $\mathrm{Re}(\phi^0)$. In perturbation theory, particles are described by field excitations around local minima. To regain this picture we write $\mathrm{Re}(\phi^0) = v + h$ so that $\langle h \rangle = 0$. The Higgs doublet then becomes

$$H = \frac{1}{\sqrt{2}} \begin{pmatrix} \sqrt{2}\phi^+ \\ v + h + i\chi \end{pmatrix} ,$$

where $\chi = \mathrm{Im}(\phi^0)$. Excitations in the h field correspond to the physical Higgs boson. Expanding the Higgs doublet out in terms of the VEV everywhere in the SM Lagrangian breaks the $\mathrm{SU}(2)_L \times \mathrm{U}(1)_Y$ symmetry of the SM and is known as electroweak symmetry breaking (EWSB). Not all symmetry is removed from this sector and a residual $\mathrm{U}(1)_{em}$ symmetry remains relating to the electromagnetic interactions. The other degrees of freedom in the Higgs doublet, notably $\phi^\pm$ and χ are the Goldstone bosons associated with the symmetry breaking. These will supply the physical gauge bosons $W^\pm$ and Z with a longitudinal polarization necessary to generate a mass. To obtain masses for the gauge bosons in the theory one must expand the Higgs doublets in Eq. (1.1.12). Their masses can be seen from considering the terms proportional to v^2 in Eq. (1.1.12). In doing so, one finds terms mixing B_μ and W^3_μ, indicating that one must perform a field redefinition to obtain the physical spectrum. The physical fields associated with the weak interactions are not W^a_μ and B_μ but linear combinations of them. Specifically

$$W^\pm_\mu = \frac{1}{\sqrt{2}}(W^1_\mu \mp i W^2_\mu)$$

$$\begin{pmatrix} W^3_\mu \\ B_\mu \end{pmatrix} = \begin{pmatrix} \cos\theta_w & \sin\theta_w \\ -\sin\theta_w & \cos\theta_w \end{pmatrix} \begin{pmatrix} Z_\mu \\ A_\mu \end{pmatrix}, \tag{1.2.5}$$

where $W^\pm_\mu$ and Z_μ are the physical bosons associated with the weak interactions while A_μ is the photon. The angle describing this rotation to the mass basis is known as the *weak mixing angle* or *Weinberg angle* and is given as

$$\cos\theta_w = \frac{g_2}{\sqrt{g_1^2 + g_2^2}}\,. \tag{1.2.6}$$

On rotating to the mass basis one finds the masses of these bosons to be

$$M_W = \frac{g_2 v}{2}\,, \quad M_Z = \frac{g_2 v}{2\cos\theta_w}\,, \quad M_A = 0\,, \tag{1.2.7}$$

thus confirming the identification of A_μ as the massless photon. In terms of these physical fields the covariant derivative[3] reads

$$D_\mu = \partial_\mu - ieQ_f A_\mu - i\frac{e}{\sin\theta_w \cos\theta_w}\left(T_{W_3} - Q_f \sin^2\theta_w\right) Z_\mu \,, \tag{1.2.8}$$

where $e = g_2 \sin\theta_w$ is the electric coupling constant and $Q_f = T_{W_3} + Y$ denotes the electric charge of fermion f. T_{W_3} is the third component of weak isospin for the doublets of $\mathrm{SU}(2)_L$. It is this relation for the electric charge which motives the hypercharge assignment for the fields in the beginning of this chapter.

Instead of relating the weak mixing angle to the couplings, we can instead relate it to the mass of the gauge bosons. The angle can thus be expressed as

$$c_w^2 = \frac{M_W^2}{M_Z^2} \,, \qquad s_w^2 = 1 - c_w^2 \,, \tag{1.2.9}$$

where we have introduced the abbreviations $c_w = \cos\theta_w$ and $s_w = \sin\theta_w$. A similar procedure can now also be done for the Higgs VEV

$$v = \frac{2M_W s_w}{e} \,. \tag{1.2.10}$$

The fermions in the SM gain a mass through their Yukawa couplings to the Higgs. Expanding the Higgs doublets in Eq. (1.1.11) and ignoring terms proportional to the Goldstone bosons[4] one finds

$$\mathcal{L}_{\text{Yukawa}} = -\frac{1}{\sqrt{2}}(v+h)\left[Y_d^{ij}\bar{d}_L^i d_R^j - Y_u^{ij}\bar{u}_L^i u_R^j - Y_e^{ij}\bar{e}_L^i e_R^j + \text{h.c.}\right] . \tag{1.2.11}$$

The mass terms are the terms proportional to v. However the Yukawa matrices are not necessarily diagonal (or even hermitian) and so in order to ascertain the physical masses, it is necessary to diagonalise the Yukawa matrices. This can be done using two unitary matrices U and V for each Yukawa matrix

$$Y_d^{ij} = \left[U_d\, y_d\, V_d^\dagger\right]^{ij} \,, \tag{1.2.12}$$

[3] We have dropped the gluon fields here, but they are still present when the derivative acts on the quark fields.

[4] Alternatively we can simply work in unitary gauge where these bosons are absent.

where y_d is diagonal in generation space. In writing the Yukawa matrices in terms of the diagonal matrices y the Lagrangian becomes

$$\mathcal{L}_{\text{Yukawa}} \supset -\frac{(h+v)}{\sqrt{2}} \bar{d}^i_L (U_d)^i{}_j (y_d)^j{}_k (V_d^\dagger)^k{}_l d^l_R + \text{h.c.}\,, \tag{1.2.13}$$

and analogously for the up-type quarks and lepton fields. The final step is to change basis for the fields. Transforming $d^i_R \to (V_d)^i{}_j\, d^j_R$ and $d^i_L \to (U_d)^i{}_j\, d^j_L$ removes the matrices U_d and V_d from the Lagrangian leaving

$$\mathcal{L}_{\text{Yukawa}} \supset -\sum_i \frac{(h+v)}{\sqrt{2}} y^i_d \bar{d}^i_L d^i_R + \text{h.c.}\,, \tag{1.2.14}$$

where we have rewritten y^i_d as a vector. Performing analogous transformations to the up-type quarks and leptons Q_L and e_R brings the Lagrangian to the mass basis where the mass of each of the fermions is manifest. We will not go into details here, but it should be noted that the field rotation $d^i_R \to (V_d)^i{}_j\, d^j_R$ leaves the rest of the Lagrangian unchanged everywhere except in the couplings between the $W^\pm$-bosons and quarks. This introduces mixing between the quark generations mediated by these bosons. The result is parametrised in the Cabibbo-Kobayashi-Maskawa (CKM) matrix V_{CKM} [8, 9] and appears in the Lagrangian as

$$\mathcal{L}_{\text{Dirac}} \supset \frac{e}{\sqrt{2} s_w} \overline{u}^i_L \not{W}^+ (V_{\text{CKM}})^i{}_j\, d^j_L\,. \tag{1.2.15}$$

We see explicitly then that the fermions gain a mass directly proportional to the VEV of the Higgs field,

$$m_f = \frac{v\, y_f}{\sqrt{2}}\,. \tag{1.2.16}$$

The same terms which give rise to the mass of the fermions also generate a Yukawa interaction between the Higgs boson and the fermions. These interaction terms are given by

$$\mathcal{L}_{\text{Yukawa}} \supset -\frac{y_d}{\sqrt{2}} h \bar{d}_L d_R + \text{h.c.}\,, \tag{1.2.17}$$

where we have assumed we have already transformed to the mass basis. From

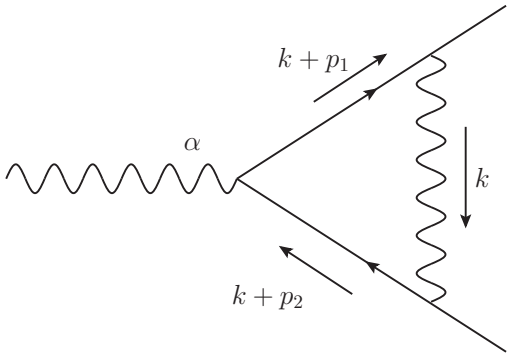

Figure 1.1: The 1-loop correction to the $\gamma\overline{\psi}\psi$ vertex in QED.

Eq. (1.2.16) we can express the Yukawa coupling in terms of the mass

$$y_f = \frac{\sqrt{2}m_f}{v}\,. \tag{1.2.18}$$

This yields an important prediction from the Higgs sector of the SM, namely that the coupling of the Higgs to the fermions (and massive gauge bosons) is directly proportional their mass.

1.3 Renormalisation

In calculating cross sections for processes beyond tree level in Quantum Field Theory (QFT), one often finds the results of calculations produce infinities. These divergences in the theory are of two origins, ultraviolet (UV) and infrared (IR), the exact meaning of which will be clarified shortly. An illustrative example is given by the correction to the vertex coupling a photon to two fermions. Figure 1.1 displays the Feynman diagram representing the 1-loop correction to the photon-fermion-fermion vertex in QED. Applying the Feynman rules, we see that this vertex involves integrating over the unconstrained loop momentum, labelled k in the figure

$$\int \frac{d^4k}{(2\pi)^4} \frac{i(\not{k} + \not{p}_1 + m)}{(k+p_1)^2 - m^2} ie\gamma^\mu \frac{-i\eta_{\mu\nu}}{k^2} ie\gamma^\nu \frac{i(\not{k} + \not{p}_2 + m)}{(k+p_2)^2 - m^2} ie\gamma^\alpha\,. \tag{1.3.1}$$

This integral is divergent in four spacetime dimensions. Firstly, it is divergent as we integrate up to very high energies $k \to \infty$, the origin of the so-called UV divergences.

These infinities can be dealt with by systematically renormalising the theory. This integral is also divergent as $k \to 0$ and these represent IR divergences. In Chapter 5 we will compute the decay of the Higgs boson to b-quarks at NLO in QCD, and as such, we will need to renormalise the theory. In the following sections we introduce the basics of renormalisation as relevant in the SM.

Before dealing with the divergences however we must regularise them. The most common way to do this, though by no means the only, is known as dimensional regularisation. Here instead of calculating in four spacetime dimensions, one calculates in $d = 4 - 2\epsilon$ spacetime dimensions. In this way the divergences become manifest as poles in ϵ and will allow us to quantitatively deal with them. We first illustrate how to remove the UV divergences before moving on to discuss the IR divergences in Section 1.3.2.

1.3.1 UV Divergences

In order to deal with UV divergences, we redefine the so-called *bare* parameters and fields in the Lagrangian. The reason is that unlike at tree level, where we can relate the parameters in the Lagrangian to those quantities as physically measured by experiment (mass or electric charge for example), quantum corrections alter this relation. In fact the relation between the two is altered by UV divergent contributions. As such it is necessary to redefine terms in the Lagrangian beyond tree level absorbing these infinite shifts into *counterterms*. As such, the counterterms are themselves formally divergent quantities. We will illustrate this procedure with a subset of the SM as preparation for Chapter 5 where we will need to perform renormalisation within the Standard Model Effective Field Theory (SMEFT). We write the *bare* terms in the Lagrangian in terms of renormalised quantities. Specifically,

$$\psi_{L,i}^{(0)} = \sqrt{Z_{2,i}^{L}}\,\psi_{L,i}\,, \tag{1.3.2}$$

$$\psi_{R,i}^{(0)} = \sqrt{Z_{2,i}^{R}}\,\psi_{R,i}\,, \tag{1.3.3}$$

$$h^{(0)} = \sqrt{Z_h}\,h\,, \tag{1.3.4}$$

$$M^{(0)} = MZ_M = M(1 + \delta Z_m) = M + \delta M\,, \tag{1.3.5}$$

$$e^{(0)} = eZ_e = e(1 + \delta Z_e) = e + \delta e\,, \tag{1.3.6}$$

where $\psi_{L,i}(\psi_{R,i})$ is a left (right) handed fermion of flavour i, h is the physical Higgs field, M is a generic mass and e the electric coupling constant. Here we have used the superscript (0) to refer to bare parameters and Z to refer to so-called renormalisation constants. In addition to this, one would also have to introduce renormalisation constants for the gauge fields, ghosts and other quantities appearing in the Lagrangian, however this will not be necessary for the calculations performed in Chapter 5 and we avoid introducing unnecessary details. Using these renormalised quantities, one can write the original Lagrangian in terms of renormalised fields and counterterms. Since these divergences first appear at NLO, the counterterms have a perturbative expansion

$$Z = 1 + \delta Z\,, \tag{1.3.7}$$

where δZ starts at the next order in perturbation theory than the leading order process. Expanding the Lagrangian in terms of these renormalised quantities allows one to perform renormalised perturbation theory. One can then set the counterterms to have divergent parts which cancel those from the renormalised part of the Lagrangian rendering the result UV finite. Thus the divergent part of the counterterms are fixed, however one still has complete freedom to set the finite parts in any way. It is important to specify a so-called *renormalisation scheme* then to set these finite parts in a determined way.

Two commonly used schemes for performing renormalisation are the $\overline{\text{MS}}$-scheme and the on-shell scheme. In the Minimal Subtraction (MS) scheme, the finite part of the counterterms are simply set to zero. In the modified Minimal Subtraction ($\overline{\text{MS}}$) scheme, the finite part is extended to include the universal γ_E and $\ln(4\pi)$ factors which appear along with the poles. This scheme has the advantage that it is fairly simple to compute in, one simply determines the divergent parts without needing to worry about additional calculations to fix the finite contributions. However it leaves

physical parameters, such as the mass, dependent on the unphysical renormalisation scale. As such, a quantity like $m_e(\mu)$ may not correspond to the physically measured mass of the electron for example. This isn't necessarily undesirable and in fact we will make use of this fact to resum large logarithmic corrections to the cross section in Chapter 5. The on-shell scheme on the other hand fixes the finite part of the counterterms by requiring that m_e is equal to the position of the pole in the propagator. In practise this means m_e is the same as the physically measured mass. Similarly, the electric coupling e in this scheme is defined as that which would be measured in laboratory experiments in the Thompson limit (no scattering). The advantage of this scheme is that these quantities now correspond to their physically measured values to all orders in perturbation theory. Unlike $\overline{\text{MS}}$ renormalised quantities they do not receive radiative corrections from higher orders in perturbation theory. While it is straightforward to compute in the $\overline{\text{MS}}$-scheme, the on-shell scheme requires a little more detail. A clear presentation deriving the finite part of the counterterms in the on-shell scheme is presented in [10]. We produce the results necessary for the calculations carried out in Chapter 5 here. We first parametrise the two point functions (in Feynman gauge) for the fermions, Higgs, and gauge bosons as

$$\begin{aligned}
\Gamma^f(p) &= i(\not{p} - m_f) + i\left[\not{p}\left(P_L\Sigma_f^L(p^2) + P_R\Sigma_f^R(p^2)\right) + m_f\left(\Sigma_f^S(p^2)P_L + \Sigma_f^{S*}(p^2)P_R\right)\right], \\
\Gamma^H(k) &= i(k^2 - m_H^2) + i\Sigma^H(k^2), \\
\Gamma^W_{\mu\nu}(k) &= -ig_{\mu\nu}(k^2 - M_W^2) - i\left(g_{\mu\nu} - \frac{k_\mu k_\nu}{k^2}\right)\Sigma_T^W(k^2) - i\frac{k_\mu k_\nu}{k^2}\Sigma_L^W(k^2), \\
\Gamma^{ab}_{\mu\nu}(k) &= -ig_{\mu\nu}(k^2 - M_a^2)\delta_{ab} - i\left(g_{\mu\nu} - \frac{k_\mu k_\nu}{k^2}\right)\Sigma_T^{ab}(k^2) - i\frac{k_\mu k_\nu}{k^2}\Sigma_L^{ab}(k^2),
\end{aligned} \tag{1.3.8}$$

respectively, where $a, b = A, Z$, and $M_A^2 = 0$. The counterterms for the masses are then given by

$$\begin{aligned}
\delta M_W^2 = \text{Re}\,\Sigma_T^W\left(M_W^2\right), \qquad \delta M_Z^2 = \text{Re}\,\Sigma_T^{ZZ}\left(M_Z^2\right), \\
\delta M_H^2 = \text{Re}\,\Sigma^H\left(M_H^2\right), \\
\delta m_b = \frac{m_b}{2}\text{Re}\left(\Sigma_b^L\left(m_b^2\right) + \Sigma_b^R\left(m_b^2\right) + \Sigma_b^S\left(m_b^2\right) + \Sigma_b^{S*}\left(m_b^2\right)\right).
\end{aligned} \tag{1.3.9}$$

In practise it will be easier to work with $\delta M_W/M_W$ rather than δM_W^2, and similarly for the Z and Higgs counterterm. The two are related via

$$\frac{\delta M_X}{M_X} = \frac{1}{2}\frac{\delta M_X^2}{M_X^2}\,,$$

where $X = \{W, Z, H\}$. The notation Re simply takes the real part and ensures the resulting renormalised Lagrangian is real[5]. The wavefunction renormalisation counterterms take the form

$$\begin{aligned}\delta Z_b^L = &-\mathrm{Re}\,\Sigma_b^L\left(m_b^2\right) + \Sigma_b^S\left(m_b^2\right) - \Sigma_b^{S*}\left(m_b^2\right) \\ &- m_b^2\frac{\partial}{\partial k^2}\mathrm{Re}\left[\Sigma_b^L\left(k^2\right) + \Sigma_b^R\left(k^2\right) + \Sigma_b^S\left(k^2\right) + \Sigma_b^{S*}\left(k^2\right)\right]\Big|_{k^2=m_b^2}\end{aligned} \tag{1.3.10}$$

$$\begin{aligned}\delta Z_b^R = &-\mathrm{Re}\,\Sigma_b^L\left(m_b^2\right) \\ &- m_b^2\frac{\partial}{\partial k^2}\mathrm{Re}\left[\Sigma_b^L\left(k^2\right) + \Sigma_b^R\left(k^2\right) + \Sigma_b^S\left(k^2\right) + \Sigma_b^{S*}\left(k^2\right)\right]\Big|_{k^2=m_b^2}\end{aligned} \tag{1.3.11}$$

$$\begin{aligned}\delta Z_W = -\mathrm{Re}\frac{\partial\Sigma_T^W(k^2)}{\partial k^2}\bigg|_{k_2=M_W^2}\,, \qquad \delta Z_{ZZ} = -\mathrm{Re}\frac{\partial\Sigma_T^{ZZ}(k^2)}{\partial k^2}\bigg|_{k^2=M_Z^2}\,, \\ \delta Z_{AA} = -\frac{\partial\Sigma_T^{AA}(k^2)}{\partial k^2}\bigg|_{k^2=0}\,, \qquad \delta Z_H = -\mathrm{Re}\frac{\partial\Sigma^H(k^2)}{\partial k^2}\bigg|_{k^2=M_H^2}\,, \\ \delta Z_{ZA} = 2\frac{\Sigma_T^{AZ}(0)}{M_Z^2}\,.\end{aligned} \tag{1.3.12}$$

Finally, we also need the counterterm for the electric charge in the on-shell scheme. This is defined as the on-shell coupling between the photon and the electron. As such it is for zero momentum transfer through the photon. The result can be written entirely in terms of two point functions and reads

$$\delta Z_e = -\frac{1}{2}\delta Z_{AA} - \frac{\sin\theta_w}{2\cos\theta_w}\delta Z_{ZA}\,. \tag{1.3.13}$$

1.3.2 IR Divergences

In order to deal with the IR divergences which arise in loop integrals, it is necessary to consider not just the virtual corrections to the process being dealt with but also

[5]Actually, one should only take the real part of loop integrals and not of terms from the quark mixing matrix. These details will not matter in our calculation.

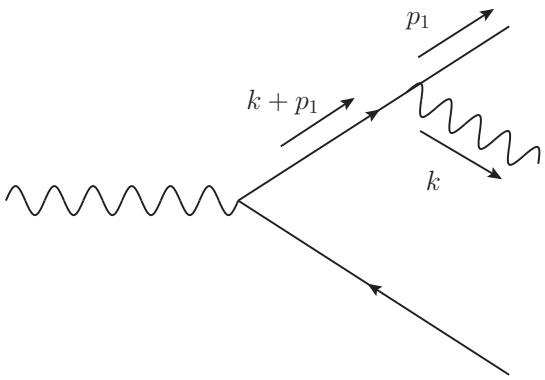

Figure 1.2: Emission of a photon into the final state. Such diagrams give rise to IR poles in phase space integrals.

the emission of massless particles into the final state. Consider the diagram in Figure 1.2. The propagator for the fermion on the top line produces the following contribution to the amplitude

$$\frac{i(\not{p} + \not{k}_1 + m)}{(p + k_1)^2 - m^2} \,. \tag{1.3.14}$$

Expanding out the denominator and using that the final state particles are on shell gives $2p\cdot k_1 = 2E_\gamma(E_p - |\vec{p}|\cos\theta)$. Thus the contribution becomes divergent as the photon energy tends to zero[6]. Hence we can also get IR divergences from real emission, once we integrate over the phase space of the final state particles. These IR divergences from real emissions cancel those from the loop integrals and is known as the KLN theorem [11, 12]. Thus in order to cancel IR divergences from loop integrals, one is forced to consider the same LO process with an additional emission in the final state.

1.4 QCD

As mentioned in Section 1.1 the theory of the strong interactions, Quantum Chromo-Dynamics (QCD), is described by an SU(3) gauge theory. Quarks are represented in the fundamental representation of the group, as in Table 1.1. Collecting the parts

[6]If we consider the fermion massless, the contribution can also be divergent as $\cos\theta \to 1$ leading to collinear divergences.

of the SM Lagrangian after EWSB relevant to QCD gives

$$\mathcal{L}_{\rm QCD} = -\frac{1}{4} G^A_{\mu\nu} G^{A\,\mu\nu} + \sum_i \overline{\psi}_i \left(i \not{D} - m_i \right) \psi_i \,, \tag{1.4.1}$$

where ψ_i is a quark of flavour i and the mass is determined by Eq. (1.2.16). In order to calculate scattering processes in QCD it will be useful to further investigate the algebra (Eq. (1.1.2)) associated with SU(3). For an SU(N) gauge theory the following relations hold between the generators in the fundamental representation

$$\sum_A t^A_{ij} t^A_{jk} = C_F \delta_{ik} \,,$$
$$\mathrm{Tr}\left[t^A t^B \right] = \frac{1}{2} \delta^{AB} \,,$$

where

$$C_F = \frac{N^2 - 1}{2N} \,, \quad C_A = N \,, \tag{1.4.2}$$

and where C_A appears on the right hand side of the first line when considering generators in the adjoint representation. Such relations will appear when one considers processes which involve the exchange of gluons between fermions as will be the case in Chapter 5.

As mentioned at the end of Section 1.1, the Lagrangian in Eq. (1.1.13) describes the classical version of the theory. In quantising the theory there are some subtleties in dealing with gauge fields which we shall now address. A problem in quantising QCD (and gauge theories in general) arises when one considers the partition function

$$Z[J] = \int \mathcal{D}[\{\phi_i\}] \mathcal{D}G \, \exp\left\{ i S[\{\phi\}, G] \right\} \,, \tag{1.4.3}$$

where we have separated out the gauge field G^a_μ from the other fields $\{\phi_i\}$ in the path integral. Because of gauge symmetry however, this integral includes an infinite number of physically equivalent configurations. Gauge transformations of the gluon fields take the form

$$G^A_\mu t^A \to U(x) \left(G^A_\mu t^A + \frac{i}{g_3} \partial_\mu \right) U^\dagger(x) \,, \tag{1.4.4}$$

and so any field configurations related through this will describe the same physical situation. It is possible to isolate the physically inequivalent configurations by adding to the path integral a term of the form

$$\int \mathcal{D}\,\alpha\delta(F(\mathrm{G}_\mu^\alpha))\det\left(\frac{\delta F}{\delta\alpha}\right)=1\,, \tag{1.4.5}$$

which is equivalent to unity under the integral and so does not alter the result. Here $F(\mathrm{G}_\mu^\alpha)$ is a gauge fixing functional where $\mathbf{G}_\mu^\alpha$ corresponds to a gauge transformed field as in Eq. (1.4.4). For example covariant gauges are given by $F(\mathrm{G}_\mu^\alpha)=\frac{1}{2\xi}\partial^\mu\mathrm{G}_\mu^\alpha=0$ for some gauge parameter ξ. The delta function in Eq. (1.4.5) means this integral is then non-zero only for gauge fixed fields. In abelian gauge theories (which suffer from the same problem) this has the effect of adding to the classical Lagrangian, a term of the form

$$\mathcal{L}_{GF}=-\frac{1}{2\xi}(\partial^\mu G_\mu^A)^2\,. \tag{1.4.6}$$

This term is of course different for different choices of $F(G_\mu^A)$. While this introduces an additional arbitrary gauge parameter ξ which can appear in the amplitudes generated from Feynman diagrams, physical observables will always be independent of ξ. This acts as an important check on the results of calculations. In non-abelian gauge theories however, the insertion of Eq. (1.4.5) leads to another feature. Unlike in abelian theories where the determinant falls out in the calculation of Green's functions, it leads to the presence of so-called *Fadeev-Popov ghosts* [13] in non-abelian ones. We label these fields c and they appear in the Lagrangian as

$$\mathcal{L}_{\mathrm{Ghost}}=\partial_\mu c^{A\,\dagger}D_{AB}^\mu c^B\,, \tag{1.4.7}$$

where the covariant derivative acts in the adjoint representation

$$D_{AB}^\mu=\delta_{AB}\partial^\mu-ig_s(T^C G_\mu^C)_{AB}\,. \tag{1.4.8}$$

These ghosts, although scalars, are anti-commuting and are a necessary component to cancel unphysical degrees of freedom which can arise in Feynman diagrams in

non-abelian theories. These ghosts cannot be produced in the final state of a process, but can appear as intermediates within Feynman diagrams. The ghosts can be removed through particular gauge choices. In covariant gauges this corresponds to the unitary gauge $\xi \to \infty$.

An important feature of QCD (and other non-Abelian gauge theories) is that of asymptotic freedom [14, 15]. In Section 1.3 we introduced the idea of dimensional regularisation. A feature of dimensional regularisation is that fields and parameters in the Lagrangian lose their usual mass dimension. In particular the gauge couplings, which are dimensionless in four dimensions, become dimensionful $[g] = \epsilon$. One normally separates out this dimensionful part to leave the coupling dimensionless. Thus writing the bare coupling in terms of the renormalised coupling

$$g_s^{(0)} = Z_g g_s \mu^\epsilon \,, \tag{1.4.9}$$

for some dimensionful parameter μ. Z_g is the renormalisation constant for the strong coupling and has the perturbative expansion

$$Z_g = 1 + \frac{g^2}{(4\pi)^2}\left(\frac{A_1}{\epsilon} + B_1\right) + \mathcal{O}(g^4) \,, \tag{1.4.10}$$

where A_1 and B_1 are constants with $B_1 = 0$ in the MS scheme. It is possible to solve for the running of $g_s(\mu)$. Using the fact that the bare coupling does not depend on μ, we must have that

$$0 = \mu \frac{dZ_g}{d\mu} g_s \mu^\epsilon + Z_g \mu \frac{dg_s}{d\mu} \mu^\epsilon + \epsilon Z_g g_s \mu^\epsilon \,. \tag{1.4.11}$$

Rearranging this for $\partial_\mu g$ and using the expansion of Z_g, one arrives at

$$\frac{dg_s(\mu)}{d\ln\mu} = -\epsilon g_s(\mu) - \frac{g^3(\mu)}{(4\pi)^2} A_1 \,. \tag{1.4.12}$$

The first term here of course vanishes when one takes the limit $\epsilon \to 0$ on returning to four dimensions. This is normally expressed in terms of $\alpha_s = g_s^2/(4\pi)$ and is known

as the β function for QCD

$$\beta(\alpha_s) = \frac{d\alpha_s(\mu)}{d\ln\mu} = -2\alpha_s(\mu)\left[\left(\frac{\alpha_s(\mu)}{4\pi}\right)\beta_0 + \left(\frac{\alpha_s(\mu)}{4\pi}\right)^2\beta_1 + \ldots\right]. \tag{1.4.13}$$

Thus in order to calculate the running of the strong coupling constant one must calculate the renormalisation constant Z_g. This can be done by considering the counterterms required to renormalise the $q\bar{q}g$ vertex as well as the gluon and quark two point functions. In QCD, the leading term is given by

$$\beta_0 = \frac{11N_c - 2n_f}{12}, \tag{1.4.14}$$

where $N_c = 3$ is the number of colours and n_f is the number of active flavours. We can solve the β-function in order to determine how $\alpha_s(\mu)$ runs from one scale to another. Keeping only the β_0 term one arrives at

$$\alpha_s(\mu) = \frac{\alpha_s(\mu_0)}{1 - \alpha_s(\mu_0)\frac{\beta_0}{2\pi}\ln\left(\frac{\mu_0}{\mu}\right)}. \tag{1.4.15}$$

Thus we can obtain the coupling at one scale in terms of the coupling at some other measured scale. Of course, one can include higher order corrections in the β-function to increase the accuracy of the running.

The β-function is negative for $N_c = 3$ and $n_f = 5$. Thus for larger scales μ, the coupling becomes weaker and the theory becomes more susceptible to the application of perturbation theory. Since the renormalisation scale μ is normally chosen around a scale characterising the process of interest high energy scattering in QCD can be computed this way, despite the coupling being strong at low energies. Because the coupling of QCD becomes strong at low energies, quarks are never observed on their own. Instead they are bound together into colourless objects. These are most commonly the baryons, a bound state of three quarks, and the mesons, a bound state of a quark and an antiquark. Thus the running coupling allows us to account for the presence of low energy bound states, while also being able to use perturbative methods in scattering processes.

1.5 Remainder of the Thesis

The rest of this thesis is divided as follows. In Chapter 2 we briefly introduce the two EFTs which will feature in the rest of this thesis; Soft Collinear Effective Theory (SCET) and the Standard Model Effective Theory (SMEFT). In Chapter 3 we will present an application of SCET to the problem of top quark pair production in hadron colliders. In particular we will utilise factorisation theorems which can be derived from the EFT in order to resum potentially large logarithmic corrections to the cross section. Chapter 4 will present results of this work, presenting results at NNLO+NNLL′ accuracy. We will study the results and perform additional analysis comparing with fixed order (N)NLO results along the way. In Chapter 5 we will instead utilise the SMEFT to the problem of Higgs decay to bottom quarks. The SMEFT allows us to parametrise the potential contributions arising from new physics in a largely model independent way. As such we present the NLO QCD corrections to the process $h \to b\bar{b}$ in the SMEFT. Finally, we end the thesis with a conclusion summarising the main findings.

Chapter 2

Effective Field Theories

In this chapter we introduce the two Effective Field Theories (EFTs) which form a central component of this thesis; namely Soft Collinear Effective Theory (SCET) and Standard Model Effective Field Theory (SMEFT). The first part of this chapter deals with SCET while the second introduces the SMEFT.

2.1 Soft Collinear Effective Theory

2.1.1 Method of Regions

Before delving straight into the construction of SCET we will first review an important technique used to obtain results from loop integrals in some limit known as the *Method of Regions* [16, 17]. Occasionally, one is only interested in the result of some loop integral in a particular limit, the idea behind the Method of Regions is to be able to obtain this result by expanding the integrand before carrying out the integral itself. However, this cannot be done naïvely. This can be shown using an example from [17] and also succinctly illustrated in [18]. Consider a bubble diagram in two dimensions with zero external momentum involving two masses. Such an integral can be computed simply using the usual techniques for solving Feynman integrals

$$I = \int d^2k \, \frac{1}{(k^2 - m^2)(k^2 - M^2)} = C \frac{\ln\left(\frac{M}{m}\right)}{M^2 - m^2} \,, \tag{2.1.1}$$

for some constant C. Now suppose we are only interested in the result in the limit $m^2 \ll M^2$. Using the full result above, we easily obtain

$$I_{m^2 \ll M^2} = \frac{C \ln\left(\frac{M}{m}\right)}{M^2}\left(1 + \frac{m^2}{M^2} - \frac{m^4}{M^4} + \dots\right) . \tag{2.1.2}$$

The method of regions can be used to obtain this result by expanding the integrand first. The integral in Eq. (2.1.1) is relatively simple and a method of regions analysis is not necessary, however for more complex integrals perhaps even where exact analytic results are unknown the method of regions can be a useful tool. Conceptually the most straightforward way to proceed would be to introduce a cutoff in the integrand, separating out a low energy region[1] ($k \sim m \ll M$) and a high energy region ($m \ll M \sim k$). Exanding the integrand in $k^2/M^2 \ll 1$ in the low energy region and $m^2/k^2 \ll 1$ in the high energy region and adding the results together reproduces the result in Eq. (2.1.2) and is independent of the cutoff as it should be. However, the use of a hard cutoff is impractical for most calculations and instead we use dimensional regularisation. Using dimensional regularisation ($d = 2 - \epsilon$) one obtains an integral (in Euclidean signature) of the form

$$I \sim \int dk \frac{k^{1-\epsilon}}{(k^2 + M^2)(k + m^2)} , \tag{2.1.3}$$

where we have dropped the angular part. This can now be expanded as described above, once for $k \ll M$ and once for $k \gg m$, though this time the integrals run over the entire range of k i.e. we do not restrict k using a cutoff or something similar. So long as one keeps enough terms in the expansion, the sum of the results from the two regions will reproduce the result in Eq. (2.1.2). Each of the regions produce the following results,

$$I_{\text{Low Energy}} = \frac{m^{-\epsilon}}{2M^2}\Gamma\left(1 - \frac{\epsilon}{2}\right)\Gamma\left(\frac{\epsilon}{2}\right) \tag{2.1.4}$$

$$I_{\text{High Energy}} = -\frac{M^{-\epsilon}}{2M^2}\Gamma\left(1 - \frac{\epsilon}{2}\right)\Gamma\left(\frac{\epsilon}{2}\right) . \tag{2.1.5}$$

[1] We use the notation $a \sim b$ to denote that quantity *a scales like b* in the sense that they have a similar magnitude.

The proceedure is straightforward and we do not detail it here, instead we will use a more illustrative example, namely the integral from the triangle diagram in Figure 1.1. Before doing so however, we first comment on what appears to be a slightly worrying feature of the calculation, namely that despite the fact we have a low energy and a high energy region of the integrand we have expanded in, we still integrate k over the full range of values. Thus one may be lead to believe we have double counted contributions from the two regions identified in the integral. In fact this is not so. This can be seen in a straightforward manner by looking at the scaling of each result with respect to changes in ϵ. The low energy region scales as $m^{-\epsilon}$ while the high energy region never produces a result of this kind, as one can easily see by considering the expansion required in the integrand in order to compute the high energy region. A similar argument holds for the $M^{-\epsilon}$ structure in the high energy region. In this manner, adding results which have been expanded in different regions do not include overlapping contributions.

We now discuss this technique as applied to the diagram in Figure 1.1, which will provide a more concrete connection with the construction of Soft Collinear Effective Theory in the proceeding section. We will treat all the particles as massless in what follows and also ignore the spin structure in the numerator of the propagators since it will play no role in the regions analysis performed here. Before diving straight in however, it will be useful for what follows to introduce an alternative parametrisation of the spacetime coordinates. We choose a parametrisation based on the specifics of the situation. In this case, we have two energetic massless fermions, which emerge from a hard scattering characterised by the scale Q^2. We can specify two reference vectors in the direction of these fermions n^μ and $\bar{n}^\mu$

$$n_\mu = (1, 0, 0, 1)\,, \qquad \bar{n}_\mu = (1, 0, 0, -1)\,. \tag{2.1.6}$$

Any momentum vector can be decomposed into components parallel to and perpen-

dicular to these two light-like directions,

$$p^\mu = (n\cdot p)\frac{\bar{n}^\mu}{2} + (\bar{n}\cdot p)\frac{n^\mu}{2} + p_\perp^\mu = p_+^\mu + p_-^\mu + p_\perp^\mu \,, \tag{2.1.7}$$

and we write $p^\mu = (p_+, p_-, p_\perp)$. Note that the scalar product of two four-vectors is now given as $p\cdot q = p^+\cdot q^- + p^-\cdot\, q^+ + p_\perp\cdot\, q_\perp$. The process is really characterised by 3 different quantities; the hard scale Q, the external particle momenta p_1^μ and p_2^μ in the collinear (anticollinear) directions n^μ ($\bar{n}^\mu$) respectively, and a soft scale p_s^μ about which we will say more shortly. We consider the external particles slightly off their mass shell such that we have the hierarchy $p_1^2 \sim p_2^2 \ll Q^2$. In fact, it will be useful to define the parameter

$$\lambda^2 = \frac{p_1^2}{Q^2} \sim \frac{p_2^2}{Q^2} \ll 1 \,. \tag{2.1.8}$$

The soft scale is then given by $p_s^\mu \sim (\lambda^2, \lambda^2, \lambda^2)Q$ in terms of the light cone coordinates immediatley following Eq. (2.1.7). The parameter λ will also serve the role of our expansion parameter in the Soft Collinear Effective Theory which we construct in the following sections. We can write

$$p_1^\mu \sim \frac{n^\mu}{2}Q \,, \qquad p_2^\mu \sim \frac{\bar{n}^\mu}{2}Q \,. \tag{2.1.9}$$

Then, using that $n\cdot\bar{n} = 2$, $n\cdot n = \bar{n}\cdot\bar{n} = 0$ and $p_1\cdot p_1 \sim p_2\cdot p_2 \sim \lambda^2 Q^2$ we can write

$$p_1^\mu \sim (\lambda^2, 1, \lambda)Q \,, \qquad p_2^\mu \sim (1, \lambda^2, \lambda)Q \,, \tag{2.1.10}$$

allowing us to parametrise the different scales involved via their relation to the expansion parameter. We will use the limit described above ($p_1^2 \sim p_2^2 \ll Q^2$) as the limit of interest for our example at hand, namely the integral from the process in Figure 1.1. The loop integral for this process is written

$$I = \int d^dk \frac{1}{k^2(k+p_1)^2(k+p_2)^2} \,, \tag{2.1.11}$$

where p_1 and p_2 are the momenta of the outgoing fermion and anti-fermion respectively. The limit under consideration allows us to immediatly identify a number of regions for the integral, much like the bubble integral we considered in Eq. (2.1.1). In this instance we find four distinct regions with associated scalings for the loop momenta given by

- Hard region: $k^\mu \sim (1,1,1)Q$
- Collinear to p_1: $k^\mu \sim (\lambda^2,1,\lambda)Q \sim p_1^\mu$
- Collinear to p_2: $k^\mu \sim (1,\lambda^2,\lambda)Q \sim p_2^\mu$
- Soft region: $k^\mu \sim (\lambda^2,\lambda^2,\lambda^2)Q$.

We will find that expanding the integrand in each of these limits just as for the bubble integral and combining the results will produce the result of the integral in the limit under consideration. We will thus see the necessity of considering the soft region, which may appear to have been included in an almost ad-hoc manner. In fact, it is possible to show that scalings $k^\mu \sim (\lambda^a,\lambda^b,\lambda^c)Q$ other than those given above either produce scaleless integrals which we can set to zero immediatley, or give rise to an integral which gives zero in some other way.

The key step is the expansion of the integrand itself. We work here only to leading power in the expansion in λ. Let us consider the region collinear to p_1 as an example ($k^\mu \sim (\lambda^2,1,\lambda)Q$). We expand each factor in the denominator and keep only the pieces leading in λ. We find

$$k^2 = 2k^+\cdot k^- + k_\perp \cdot k_\perp \sim \lambda^2 Q^2\,, \tag{2.1.12}$$

where we simply keep k^2 since each term scales as λ^2. We also find

$$(k+p_1)^2 = k^2 + k^+\cdot p_1^- + k^-\cdot p_1^+ + k_\perp \cdot p_{1,\perp} \sim \lambda^2 Q^2 \tag{2.1.13}$$

and so we again keep each term in this propagator. Finally,

$$(k+p_2)^2 = k^2 + k^+\cdot p_2^- + k^-\cdot p_2^+ + k_\perp \cdot p_{2,\perp} = k^-\cdot p_2^+ + \mathcal{O}(\lambda^2)\,, \tag{2.1.14}$$

where the term we have kept, $k^- \cdot p_2^+$ scales as $\mathcal{O}(\lambda^0)$. Our integral in this region thus becomes

$$I_{\text{col-}p_1} = \int d^d k \frac{1}{k^2 (k+p_1)^2 (k^- \cdot p_2^+)} \,. \tag{2.1.15}$$

We can repeat the analysis for other regions. For example, the hard and soft regions give rise to

$$I_{\text{hard}} = \int d^d k \frac{1}{k^2 (k^2 + k^+ \cdot p_1^-)(k^2 + k^- \cdot p_2^+)} \tag{2.1.16}$$

$$I_{\text{soft}} = \int d^d k \frac{1}{k^2 (k^+ \cdot p_1^-)(k^- \cdot p_2^+)} \,, \tag{2.1.17}$$

respectively. Because of the presence of denominators which are linear in momenta rather than the usual quadratic ones found in basic QCD calculations, some additional parametrisation tricks are useful to aid in solving the integrals. Details of methods and solutions to integrals like these can be found in the Appendix of [18], we only quote the results here in order to highlight some features of this approach. One finds

$$I_{\text{hard}} = \frac{\Gamma(1+\epsilon)}{2 p_1^- \cdot p_2^+} \left(\frac{1}{\epsilon^2} + \frac{1}{\epsilon} \ln \frac{\mu^2}{2 p_1^- \cdot p_2^+} + \frac{1}{2} \ln^2 \frac{\mu^2}{2 p_1^- \cdot p_2^+} - \frac{\pi^2}{6} \right) \tag{2.1.18}$$

$$I_{\text{col-}p_1} = \frac{\Gamma(1+\epsilon)}{2 p_1^- \cdot p_2^+} \left(-\frac{1}{\epsilon^2} - \frac{1}{\epsilon} \ln \frac{\mu^2}{-p_1^2} - \frac{1}{2} \ln^2 \frac{\mu^2}{-p_1^2} + \frac{\pi^2}{6} \right) \tag{2.1.19}$$

$$I_{\text{col-}p_2} = \frac{\Gamma(1+\epsilon)}{2 p_1^- \cdot p_2^+} \left(-\frac{1}{\epsilon^2} - \frac{1}{\epsilon} \ln \frac{\mu^2}{-p_2^2} - \frac{1}{2} \ln^2 \frac{\mu^2}{-p_2^2} + \frac{\pi^2}{6} \right) \tag{2.1.20}$$

$$I_{\text{soft}} = \frac{\Gamma(1+\epsilon)}{2 p_1^- \cdot p_2^+} \left(\frac{1}{\epsilon^2} + \frac{1}{\epsilon} \ln \frac{2\mu^2 p_1^- \cdot p_2^+}{p_1^2 p_2^2} + \frac{1}{2} \ln^2 \frac{2\mu^2 p_1^- \cdot p_2^+}{p_1^2 p_2^2} + \frac{\pi^2}{6} \right) . \tag{2.1.21}$$

There are a number of noteworthy features of these results. Firstly, the sum of the interals from each of the regions reproduces the result of computing the original integral and then expanding in the limit $p_1^2 \sim p_2^2 \ll Q^2$. Secondly, the poles in ϵ in the hard integral arise from the IR region of the integral and these cancel against poles arising from the UV region of the collinear and soft integrals. Though this arises due to our expansion of the integrands, the result is rather important and implies constraints on the pole structure (and as such the anomalous dimensions) of the results of integrals from different regions.

In Soft Collinear Effective theory, we will split the fields in our Lagrangian into fields with momentum scaling in the same manner as each of the regions identified above, with the exception of the hard region which will be accounted for through Wilson coefficients. In general one will need other regions (and hence other fields in the Lagrangian) for more complex situations. Because these fields have a specific momentum scaling, they give rise to propagators of the types we found in each of the regions. Hence the diagrams in Soft Collinear Effective Theory will reproduce exactly the two collinear integrals as well as the soft integral found above.

2.1.2 Degrees of Freedom and SCET Lagrangian

We wish now to introduce Soft Collinear Effective Theory (SCET) [19–25]. We will only scratch the surface of this large topic here, a more encompassing introduction can be found in [18]. However, we introduce the basic concepts here in order to provide some appreciation for the origin of the resummed calculations we perform in Chapter 3. In this section we will introduce the basic degrees of freedom in the theory, construct the effective Lagrangian and show how one can use Wilson lines to decouple soft interactions within the theory.

The situation can be problematic if the incoming momenta, although having large energies, have a small invariant mass such that the ratio $p^2/Q^2 \ll 1$. Large logarithmic corrections of the ratios of these two scales could arise in the perturbative expansion of the cross section and render the expansion invalid. We can use SCET to try and separate these scales in a way we can then deal with. SCET is an EFT which expands in the ratios of momenta. As such the expansion parameter for the EFT in this case would be $\lambda^2 \sim p^2/Q^2$. In order to perform the expansion properly, it is necessary to parametrise the momenta in terms of this expansion parameter. This is exactly the region we conisdered in Section 2.1.1. To describe this situation in SCET then, one splits the fields into several components, each with a specific

momentum scaling. A quark field is thus written

$$\psi(x) \to \psi_c(x) + \psi_{\bar{c}}(x) + \psi_s(x)\,, \tag{2.1.22}$$

where the momentum of field ψ_c ($\psi_{\bar{c}}$) scales as p_1^μ, (p_2^μ) as given in Eq. (2.1.10). As we have also seen, a field with soft momentum scaling has also been introduced, which will be necessary to describe the soft interactions amongst the fields. The momentum scaling of the soft field is given as $p_s^\mu \sim (\lambda^2, \lambda^2, \lambda^2)Q$. While we have fields with momenta restricted to particular scalings it is important to determine the scaling of the fields themselves. The decomposition in Eq. (2.1.22) is not quite sufficient, different components of the quark spinor scale differently from each other. It is necessary to project out pieces with a common scaling. Examining the collinear limits of spinors leads to the identification of the projection operators

$$P_+ = \frac{\not{n}\bar{\not{n}}}{4}\,, \qquad P_- = \frac{\bar{\not{n}}\not{n}}{4}\,, \tag{2.1.23}$$

from which, one defines $\xi_c(x) = P_+\psi_c(x)$ and $\eta_c(x) = P_-\psi_c(x)$. These fields are now the ones we can use to define the effective theory. Note that using $n^2 = \bar{n}^2 = 0$ it follows that

$$\not{n}\xi_c(x) = \bar{\xi}_c(x)\not{n} = 0\,, \qquad \bar{\not{n}}\eta_c(x) = \bar{\eta}_c(x)\bar{\not{n}} = 0\,. \tag{2.1.24}$$

There is no need to decompose the momenta of the soft field, since all the components scale in an identical fashion the field takes the same functional form as in QCD. By considering the form of propagators for these fields, we can see how each of these components scale with respect to the expansion parameter. It can be shown that

$$\xi_c(x) \sim \lambda\,, \qquad \eta_c(x) \sim \lambda^2\,, \tag{2.1.25}$$

from which we see the η_c component of the field is subleading compared to ξ_c. Performing the same analysis with the anticollinear fields $\psi_{\bar{c}}$ yields the opposite result. From now on, we will ignore the anticollinear field since it is treated in a completely analogous manner to the collinear field. The soft field is found to scale

as $\psi_s(x) \sim \lambda^3$. The gluon fields are also decomposed into collinear and soft fields

$$G^\mu(x) \to G_c^\mu(x) + G_{\bar{c}}^\mu(x) + G_s^\mu(x)\,, \tag{2.1.26}$$

where $G_c^\mu = G_c^{A\,\mu} t^A$ for the $\mathrm{SU}(3)_c$ generators t^A. Examination of two point functions again tell us the scaling of the fields. In this case the gluon fields scale the same way as their momentum components

$$\bar{n}\cdot G_c \sim \lambda^0\,, \quad n\cdot G_c \sim \lambda^2\,, \quad G_\perp^\mu \sim \lambda\,, \quad G_s^\mu \sim \lambda^2\,. \tag{2.1.27}$$

An important thing to note here is that although all components of the soft gluon field scale as λ^2 one of the components of the collinear field is of the same order, namely $n \cdot G_c$. Thus we could have terms from the collinear field contributing at the same order in power counting as the soft fields. We will see this explicitly when we construct the Lagrangian describing this EFT.

Having identified the necessary degrees of freedom for the problem, we would now like to construct the Lagrangian of the EFT describing the interactions between these soft and collinear components. In order to obtain this we start with the Lagrangian describing massless quarks

$$\mathcal{L} = \bar{\psi} i \not{D} \psi \tag{2.1.28}$$

where $D_\mu = \partial_\mu - i g_s G_\mu^A$ and we shall deal with the kinetic terms for the gauge fields later. Expanding the fields as in Eqs. (2.1.22) and (2.1.26) and using the relations in Eq. (2.1.24) one recovers

$$\mathcal{L} = \bar{\xi}\frac{\not{\bar{n}}}{2} i n\cdot D\,\xi + \bar{\xi}\, i\not{D}_\perp \eta + \bar{\eta}\, i\not{D}_\perp \xi + \bar{\eta}\frac{\not{n}}{2} i\bar{n}\cdot D\,\eta\,, \tag{2.1.29}$$

where

$$D^\mu = \partial^\mu - i g_s (G_c^\mu + G_s^\mu)\,, \tag{2.1.30}$$

$$D_\perp^\mu = \partial^\mu - i g_s (G_{c\perp}^\mu + G_{s\perp}^\mu)\,, \tag{2.1.31}$$

and we have ignored completely analogous terms for the anticollinear fields and dropped the index c on the quark fields. The reason for keeping both the soft and

collinear gluon fields is related to our earlier observation that the component $n \cdot G_c$ has the same order in the power counting as the corresponding component in the soft field. Recall also that the field η was subleading in λ compared to ξ and as such will not appear to LO in the field theory. Because the Lagrangian is quadratic in η one can simply integrate out this field at the level of the path integral. For the tree level result this is simply a matter of replacing the field using its equation of motion

$$\eta = -\frac{\bar{n}\!\!\!/}{2\bar{n} \cdot D} \not{D}_\perp \xi \,. \tag{2.1.32}$$

Substituting this into Eq. (2.1.29) one recovers

$$\mathcal{L} = \bar{\xi} \frac{\bar{n}\!\!\!/}{2} in \cdot D \xi + \bar{\xi} i \not{D}_\perp \frac{1}{i\bar{n} \cdot D} i \not{D}_\perp \frac{\bar{n}\!\!\!/}{2} \xi \,. \tag{2.1.33}$$

The inverse derivative can be dealt with by considering its action in momentum space. Through a technique known as the multipole expansion [20] (which is required if one wants to calculate subleading corrections from the Lagrangian correctly) one can remove the dependence of certain fields in interaction terms on particular spacetime coordinates. The details shall not be of great importance for what follows, however the procedure is to expand the interaction terms in small momentum components and remove terms subleading in the power counting. The result here is that for soft fields interacting with n^μ collinear fields, we can write the space time dependence of the soft field only on x_-^μ where

$$x_-^\mu = (\bar{n} \cdot x) \frac{n^\mu}{2} \,. \tag{2.1.34}$$

Similarly, soft field interactions with the anticollinear fields can be written with dependence only on x_+^μ.

The form of the gluon field strength tensors in the EFT is identical to that in QCD, but with the gluon fields replaced by their appropriate EFT counterparts. Thus

$$\mathcal{L}_{\text{Gauge}} = -\frac{1}{4} F^s_{\mu\nu} F^{s\,\mu\nu} - \frac{1}{4} F^c_{\mu\nu} F^{c\,\mu\nu} \tag{2.1.35}$$

where the field strengths are defined through

$$F^s_{\mu\nu} = \frac{i}{g_s}\left[D^s_\mu, D^s_\nu\right] , \tag{2.1.36}$$

$$F^c_{\mu\nu} = \frac{i}{g_s}\left[D_\mu, D_\nu\right] , \tag{2.1.37}$$

where $D^\mu = n\cdot D_c \frac{\bar{n}^\mu}{2} + \bar{n}\cdot D_c \frac{n^\mu}{2} + D^\mu_{c\perp}$. The SCET Lagrangian for QCD valid to leading power in the expansion parameter is thus

$$\begin{aligned}\mathcal{L}_{\rm SCET} =& \bar{\psi}_s i\not{D}_s \psi_s + \bar{\xi}\frac{\not{\bar{n}}}{2}\left[in\cdot D + i\not{D}_{c\perp}\frac{1}{i\bar{n}\cdot D_c} i\not{D}_{c\perp}\right]\xi \\ & - \frac{1}{4}F^s_{\mu\nu}F^{s\,\mu\nu} - \frac{1}{4}F^c_{\mu\nu}F^{c\,\mu\nu} ,\end{aligned} \tag{2.1.38}$$

where

$$\begin{aligned} iD^s_\mu &= i\partial_\mu + g_s G^s_\mu , \\ iD^c_\mu &= i\partial_\mu + g_s G^c_\mu , \\ in\cdot D &= in\cdot\partial + g_s n\cdot G_c(x) + g_s n\cdot G_s(x_-) . \end{aligned}$$

This Lagrangian only includes the $\psi_c(x)$ fields and one must remember to add analogous terms for the $\psi_{\bar{c}}$ field. The reason for the appearance of the soft field only in the $n\cdot D$ covariant derivative relates to what we observed in Eq. (2.1.27), that this component of the soft gauge field is not power suppressed compared to its counterpart in the collinear gluon field.

We will not fully address the issue of how the gauge transformations of QCD are represented in the EFT but merely note some important points. Gauge transformations in QCD are realised through transformation matrices

$$\psi_i \to U_{ij}\psi_j , \qquad U_{ij}(x) = \exp\left\{i\alpha^A(x)t^A_{ij}\right\} . \tag{2.1.39}$$

In SCET, the scaling of the gauge parameter $\alpha(x)$ in λ becomes important. Two classes are identified; soft, where $\alpha(x)$ has soft scaling, and collinear for $\alpha(x)$ with collinear scaling. Collinear fields transform under both types of gauge transform, while soft fields only transform under the soft gauge transform. Finally, we note

that the gauge transformations are constructed so as not to introduce any power corrections when they are performed and the power counting of the EFT properly respected.

2.1.3 Wilson Lines and The Decoupling Transformation

Wilson lines play a particularly important role in SCET and as we shall see, can be used to decouple the interactions between soft gluons and the collinear fields (quarks or gluons) in the EFT Lagrangian. Typically a Wilson line is path ordered exponential of a line integral of the gauge field along some path. Because in SCET we have split the gauge field into components with different scaling momenta, we can describe two separate Wilson lines. Introducing two Wilson lines which run from infinity

$$W_c(x) = \mathcal{P}\exp\left\{ig_s\int_{-\infty}^{0} ds\,\bar{n}\cdot G_c(x+s\bar{n})\right\}, \tag{2.1.40}$$

$$S_n(x) = \mathcal{P}\exp\left\{ig_s\int_{-\infty}^{0} ds\,n\cdot G_s(x+sn)\right\}, \tag{2.1.41}$$

where in the collinear Wilson line we have kept the non-power suppressed component and there is an analogous soft Wilson line for the anticollinear component of the soft field.

We use the soft Wilson line to decouple the soft and collinear interactions in the leading power SCET Lagrangian Eq. (2.1.38). Interactions between soft gluons and collinear quarks are described through the covariant derivative

$$\mathcal{L}_{sc} = \bar{\xi}\frac{\bar{\not{n}}}{2} in\cdot D\xi \tag{2.1.42}$$

$$= \bar{\xi}\frac{\bar{\not{n}}}{2}\left[in\cdot\partial + g_s n\cdot G_c(x) + g_s n\cdot G_s(x_-)\right]\xi\,. \tag{2.1.43}$$

It is possible to remove the $n\cdot G_s$ term through a field redefinition involving the soft

Wilson lines. Specifically

$$\begin{aligned} \xi(x) &\to S_n(x_-)\xi^{(0)}(x) \\ G_c^\mu(x) &\to S_n(x_-)G_c^{(0)\,\mu}(x)S_n^\dagger(x_-)\,, \end{aligned} \tag{2.1.44}$$

where the superscript (0) indicates these fields no longer interact via soft gluons. In fact, the same transformation also decouples the soft gluons from interacting with the collinear gluons. The Lagrangian remaining after this transformation is given by

$$\mathcal{L}_{sc} = \bar{\xi}^{(0)}\frac{\bar{n}\!\!\!/}{2} in\cdot D^{(0)}\xi^{(0)}\,, \tag{2.1.45}$$

where the $n\cdot G_s$ term is no longer present in $n\cdot D^{(0)}$. In this manner we have eliminated the interactions between the soft gluons and collinear fields to leading power.

The decoupling relation used the soft Wilson line $S_n(x)$. The collinear Wilson line $W_c(x)$ on the other hand can be used to construct manifestly gauge invariant operators which can be used in order to describe other processes taking place within the EFT. It is possible to construct operators which are invariant under the collinear gauge transformations mentioned earlier

$$\chi(x) = W_c^\dagger(x)\xi(x)\,. \tag{2.1.46}$$

A similar procedure can be used to obtain a gluon field also invariant under collinear gauge transformations.

$$\mathcal{G}^\mu = W^\dagger(x)\left(iD_c^\mu W(x)\right)\,. \tag{2.1.47}$$

Since these operators are explicitly collinear gauge invariant it is most convenient to construct other composite operators with them. For example, the factorisation theorem used in Chapter 3 makes use of an additional operator to describe the LO top pair production production processes $q\bar{q}\to t\bar{t}$. The operator considered has the form

$$O^{q\bar{q}} = c_a\bar{\chi}_{\bar{n}}(x+t_2n)\Gamma_r'\chi_n(x+t_1\bar{n})\,\bar{h}_{v_3}(x)\,\Gamma_r''\,h_{v_4}(x)\,. \tag{2.1.48}$$

We see the explicit appearance of the gauge invariant operator χ, while Γ_r represents

possible Dirac structures, c_a is the Wilson coefficient for the operator and $h_{v_i}(x)$ are fields from Heavy Quark Effective Theory (HQET). There is an analogous operator for initial state gluons producing tops. The operator has an important feature which is worth pointing out. The two χ fields are not necessarily evaluated at the same spacetime point. The reason for this follows from the power counting in the effective theory.

Although we can build operators in the EFT using just the fields in the theory, we can also include operators with derivatives acting on fields, provided we respect the power counting. Using the Fourier space representation of the fields we can see that derivatives on the fields scale like the momentum component the derivative is with respect to. Thus

$$n\cdot\partial\chi_n \sim \lambda^2\chi_n\,, \quad \bar{n}\cdot\partial\chi_n \sim \lambda^0\chi_n\,, \quad \partial_\perp^\mu\chi_n \sim \lambda^1\chi_n\,, \tag{2.1.49}$$

and we see that derivatives along the direction of largest energy flow are not suppressed. Thus to leading power in the effective theory, we could include any number of such derivatives. Such contributions can be included by writing the field as a Taylor expansion along the $\bar{n}^\mu$ direction

$$\chi_c(x+t_1\bar{n}) = \sum_{k=0}^{\infty}\frac{t_1^k}{k!}\left(\bar{n}\cdot\partial\right)\chi_c(x)\,, \tag{2.1.50}$$

and typically one integrates overt_1. So we see that we can get the appearance of non-local operators in SCET which arise from considering operators with derivatives of fields.

Typically, one decouples the soft gluons from these operators by using the decoupling relations in Eq. (2.1.44). These Wilson lines will still be present in the operator however. Instead of being viewed as separate Wilson lines, they can be viewed as one continuous Wilson line. For the quark fields in Eq. (2.1.48), this would constitute a Wilson line coming in from $-\infty$ in the $\bar{n}^\mu$ direction to the point x, turning around and leaving towards $+\infty$ in the n^μ direction. As such, this Wilson line has a cusp in it at the point x where it changes direction. It turns out, that Wilson lines with

cusps require renormalisation [26, 27]. Thus we will see in Chapter 3 the presence of so called *cusp anomalous dimensions*, related to the renormalisation of these Wilson lines.

2.2 Standard Model Effective Field Theory

2.2.1 Introduction

We now turn our attention to The SMEFT. The SMEFT is an example of a *bottom up* EFT and is built upon the SM Lagrangian by augmenting it with operators that have a mass dimension greater than four. No new degrees of freedom are added, and these higher dimensional operators are built out of the SM fields. Clearly these composite operators must obey the Poincaré symmetries as well as the gauge symmetries of the SM Eq. (1.1.1). Each composite operator is accompanied by a *Wilson Coefficient*, essentially the coupling constant for the operator. However, because the operators now have a mass dimension higher than four, the corresponding Wilson Coefficient must have a negative mass dimension in order for the Lagrangian density to have mass dimension four. Specifically for an operator of dimension d the associated Wilson Coefficient has mass dimension $4-d$. Thus a typical term in the SMEFT Lagrangian will have the form $C_i^{(d)}Q_i^{(d)}$ with $C_i^{(d)}$ the Wilson Coefficient of mass dimension $4-d$ for operator $Q_i^{(d)}$ with mass dimension d. It is also convenient to separate out the mass dependence of the Wilson coefficient explicitly and so we also define $\widetilde{C}_i^{(d)} = \Lambda_{\rm NP}^{d-4}C_i^{(d)}$ such that $\widetilde{C}_i^{(d)}$ is dimensionless. The subscript "NP" refers to the fact that $\Lambda_{\rm NP}$ specifies the scale of the New Physics which gives rise to these operators. In this way, one can view the operators arising from integrating out heavier degrees of freedom related to new phenomena beyond the SM. The Wilson Coefficients encode the high energy information of this phenomena while the remaining composite operators describe the low energy appearance of the new physics. This is an important example of the Appelquist-Carazzone decoupling

theorem [28] which states that at low energies, the effects of heavy (and as yet unobserved) degrees of freedom in a theory manifest themselves at low energies as changes in the couplings or masses of the light degrees of freedom.

A familiar example is the Fermi theory of weak interactions, where, before knowledge of the W-boson, fermions decaying weakly did so through 4-fermion operators. Fermi originally used this to explain β-decay, but another classic example is that of the decay of the muon. An operator contributing to this decay would be written as

$$G_F(\overline{\psi}\psi)(\overline{\psi}\psi)\,, \tag{2.2.1}$$

where the ψs denote the relevant particles and G_F denotes the coupling constant of this operator. Simple dimensional analysis tells us this coefficient has mass dimension -2. Later, after the development of the Electroweak theory [29] it was possible to derive the form of G_F by integrating the W-boson out of the theory to reveal that $G_F \propto 1/M_W^2$.

In this instance we do not know the form of heavy new physics beyond the SM and so we will not be able to solve for the Wilson coefficients that appear in our EFT in terms of the parameters of the underlying theory. The most general SMEFT Lagrangian simply consists in adding to the SM all possible higher dimensional terms that respect the spacetime and gauge symmetries as mentioned earlier. We can thus write the SMEFT Lagrangian as

$$\mathcal{L} = \mathcal{L}_{\text{SM}} + \sum_{n=1} \mathcal{L}^{(n+4)}\,, \tag{2.2.2}$$

where

$$\mathcal{L}^{(k)} = \sum_i C_i^{(k)} Q_i^{(k)} = \sum_i \frac{\widetilde{C}_i^{(k)}}{\Lambda_{\text{NP}}^{k-4}} Q_i^{(k)}\,, \tag{2.2.3}$$

and the $C_i^{(k)}$ and $Q_i^{(k)}$ are the Wilson Coefficients and operators mentioned earlier. The presence of higher dimensional operators makes the theory non-renormalisable in the traditional sense; namely that we cannot remove all divergences which could arise at higher orders using a finite number of counterterms. Instead the theory is

renormalisable order by order in the expansion in $\Lambda_{\rm NP}$. What this means in practise is that the theory will be renormalisable if we only consider diagrams up to order $\Lambda_{\rm NP}^{-n}$ and we include all operators up to $d = n + 4$. In what follows we work with dimension-6 operators and so the Wilson Coefficients will have mass dimension -2. Including two such operators in a diagram would give a term proportional to $\Lambda_{\rm NP}^{-4}$ and so may require a tree-level dimension-8 term to renormalise it. However our theory will be renormalisable if we truncate all calculations to contain terms suppressed by no more than $\Lambda_{\rm NP}^{-2}$.

One of the first attempts to characterise the operators which can appear at dimension-6 appears in [30], where only explicitly hermitian operators which conserve baryon and lepton number were considered. Naïvely writing down everything which could appear at dimension-6 would lead to many hundereds of operators. However, it is not necessary to consider all such operators which appear, instead one can consider a basis. Specifically, one can use the SM equations of motion to write a given operator at dimension-6 as a linear sum of other dimension-6 operators. For example, the e_R field has the equation of motion [2]

$$i\not{D} e_R = Y_e L H^\dagger \,, \tag{2.2.4}$$

which can be used to perform the following conversion

$$\left(H^\dagger H\right) \bar{e}_R i\not{D} e_R \to \left(H^\dagger H\right) \bar{e}_R Y_e L H^\dagger \,. \tag{2.2.5}$$

Eliminiating operators in this fashion, one can arrive at a minimal basis. The basis is not unique however and there are many sets one can choose to work with. We will also exclude baryon number violating operators from our work[2]. For this work, we choose to work with the "Warsaw Basis". Originally derived in [31] with a basis of 80 such operators, though this was further refined down to 59 in [32]. This basis (excluding baryon number violating operators) is presented in Table A.1 in

[2]Normally, one might expect such operators to be heavily suppressed due to the fact the proton appears stable on timescale comparable to the age of the universe.

Appendix A.3.

One might worry that reducing the number of operators through use of the equations of motion is only valid at tree level and that such a route is not valid when quantum corrections are included. This is not the case however, and infact the basis obtained by reducing the number of operators through relations built out of SM equations of motion (EOM) can be used to perform loop calculations safely [33, 34]. The reasons for this rely on the fact that use of the EOM is equivalent to performing field redefinitions. Provided the field redefinitions preserve one particle states[3] and obey the symmetries of the theory, the redefinitions have no effect on the observables in the low energy theory.

2.2.2 Effect on SM Parameters

Extending the SM in this way has a number of immediate consequences. Many of these are highlighted in [35] and we review some of them here. The first point to address is that the addition of the only class 2 operator $C_H(H^\dagger H)^3$ alters the Higgs potential

$$V(H) = -\mu^2 H^\dagger H + \lambda (H^\dagger H)^2 - C_H (H^\dagger H)^3 \,, \tag{2.2.6}$$

which leads to the new VEV, denoted v_T

$$v_T = \left(1 + \frac{3 C_H v_T^2}{8\lambda}\right) \hat{v}_T \,, \tag{2.2.7}$$

where $\hat{v}_T$ is the SM VEV as in Eq. (1.2.10). Hatted quantities take the same form as their equivalents in the SM, while those without hats may have additional dependence on dimension-6 Wilson coefficients. As such any quantity explicitly multiplying a dimension-6 Wilson coefficient can be replaced by its hatted version without consequence to the order we are working.

Another effect of adding dimension-6 operators is that kinetic terms for the Higgs

[3] That they are of the form $\phi_i \to \phi_i + T[\{\phi\}]/\Lambda^2_{\rm NP}$ in this case, where $T[\{\phi\}]$ is any local dimension-6 combination of the fields in the theory.

and gauge bosons lose their canonical normalisation. For example, addition of the class 4 operators leads to terms of the form $\sim v_T^2 C_{HG}\, G^A_{\mu\nu} G^{A\,\mu\nu}$ in addition to the $G^A_{\mu\nu} G^{A\,\mu\nu}$ term already present in the SM Lagrangian. In order to obtain kinetic terms which are canonically normalised, a field redefinition is performed. For the gluon field this takes the form

$$G^A_{\mu\nu} = \mathcal{G}^A_{\mu\nu} \left(1 + C_{HG} v_T^2\right) , \tag{2.2.8}$$

and there are analogous transformations for the W and B fields. Simultaneously, one can transform the gauge field coupling by

$$g_3 = \overline{g}_3 \left(1 - C_{HG} v_T^2\right) , \tag{2.2.9}$$

such that the product $g_3 G^A_{\mu\nu} = \overline{g}_3 \mathcal{G}^A_{\mu\nu}$ remains unchanged to this order and we have canonically normalised kinetic terms. For the terms in the Higgs doublet to be canonically normalised we use

$$H(x) = \frac{1}{\sqrt{2}} \begin{pmatrix} -\sqrt{2} i \phi^+(x) \\ \left[1 + C_{H,\mathrm{kin}}\right] h(x) + i \left[1 - \frac{v^2}{4} C_{HD}\right] \chi(x) + v_T \end{pmatrix} , \tag{2.2.10}$$

where

$$C_{H,\mathrm{kin}} \equiv \left(C_{H\Box} - \frac{1}{4} C_{HD}\right) v^2 , \qquad v_T \equiv \left(1 + \frac{3 C_H v^2}{8\lambda}\right) v , \tag{2.2.11}$$

and ϕ^+ and χ are the Goldstone bosons. These contributions in the Higgs sector also show up in the coupling of the Higgs to fermions. In the SM the Higgs couples to fermions directly via Yukawa couplings. The dimension-6 terms introduce additional couplings between the Higgs and fermions

$$\mathcal{L} \supset -Y_b\, \overline{d}_R H^\dagger Q_L + C_{dH} (H^\dagger H)(\overline{Q}_L H d_R) + \mathrm{h.c.} . \tag{2.2.12}$$

The interaction between a single Higgs and two fermions is given by $\mathcal{Y}\, h \bar{b}_R b_L + \mathrm{h.c.}$ where

$$[\mathcal{Y}_f]^{ij} = \frac{1}{\sqrt{2}} \left([Y_f]^{ij} (1 + C_{K,\mathrm{kin}}) - \frac{3}{2} v_T^2 C_{fH}^{ij*} \right) . \tag{2.2.13}$$

Similarly the mass matrix is given by

$$[M_f]^{ij} = \frac{v_T}{\sqrt{2}}\left([Y_f]^{ij} - \frac{1}{2}v_T^2 C_{fH}^{ij*}\right), \tag{2.2.14}$$

where the indices (ij) run over generation space. Because the mass and Yukawa matrices are no longer directly proportional to each other, it does not necessarily hold that they are simultaneously diagonalisable without some further constraints on C_{fH}. This can in principle lead to additional flavour changing interactions with the Higgs. These can of course be interesting in their own right, however, for the rest of this thesis we will work under the assumption that both matrices are simultaneously diagonalisable. An example of this would be Minimal Flavour Violating (MFV) scenarios in which no additional flavour violating effects take place beyond those from the CKM matrix.

We can rewrite the SM Yukawa coupling in terms of the physical mass and C_{bH}

$$y_b = \sqrt{2}\frac{m_b}{v_T} + \frac{v_T^2}{2}C_{bH}^* \,. \tag{2.2.15}$$

Another important consequence of the SMEFT operators is the presence of

$$C_{HWB}\left(H^\dagger \frac{1}{2}t^a H\right) W^a_{\mu\nu} B^{\mu\nu} \,. \tag{2.2.16}$$

Because this introduces additional mixing between the W and B fields, the simple field rotation in Eq. (1.2.5) no longer takes us to the mass basis. Instead the rotation required to get to the mass basis is

$$\begin{pmatrix} \mathcal{W}^3_\mu \\ \mathcal{B}_\mu \end{pmatrix} = \begin{pmatrix} 1 & -\frac{1}{2}v_T^2 C_{HWB} \\ -\frac{1}{2}v_T^2 C_{HWB} & 1 \end{pmatrix} \begin{pmatrix} \cos\bar{\theta}_w & \sin\bar{\theta}_w \\ -\sin\bar{\theta}_w & \cos\bar{\theta}_w \end{pmatrix} \begin{pmatrix} \mathcal{Z}_\mu \\ \mathcal{A}_\mu \end{pmatrix}, \tag{2.2.17}$$

where $\sin\bar{\theta}_w$ and $\cos\bar{\theta}_w$ also have dependence on C_{HWB} now and can be found in [35].

As for the fields, the relations between various parameters in the broken phase of the theory also become modified by dimension-6 Wilson coefficients.

The covariant derivative can be expressed as

$$D_\mu = \partial_\mu + i\frac{\overline{g}_2}{\sqrt{2}}\left[\mathcal{W}_\mu^+ t^+ + \mathcal{W}_\mu^- t^-\right] + i\bar{g}_Z\left[T_{W_3} - \bar{s}_w^2 Q_f\right]\mathcal{Z}_\mu + i\bar{e}Q_f\mathcal{A}_\mu + i\bar{g}_s\mathcal{G}_\mu^A T^A\,, \tag{2.2.18}$$

so that the barred quantities are those that appear in the covariant derivatives like in the SM. These now have dependence on the dimension-6 Wison coefficients. In particular, the VEV can be written[4]

$$\frac{1}{v_t} = \frac{1}{\hat{v}_T} + \frac{\hat{c}_w}{\hat{s}_w}\left(C_{HWB} + \frac{\hat{c}_w}{4\hat{s}_w}C_{HD}\right)\hat{v}_T^2\,. \tag{2.2.19}$$

This will be important in Chapter 5 when we consider the decays of the Higgs boson.

[4]We have written $1/v_T$ since often the VEV appears on the denominator of expressions when calculating cross sections.

Chapter 3

Top Quark Pair Production in SCET

3.1 Features of Fixed Order Calculations

We now turn to the problem of top quark pair production at the LHC. In particular we will review the underlying factorisation theorems which allow the calculation of resummed cross sections for top quark pair production and show how these resummed results are subsequentley matched to to fixed order NNLO calculations. The factorisation theorems are formulated within the SCET framework. As such we build heavily on results derived in [36] and [37] and recast them in Mellin space where the resummation is actually performed. The factorisation theorems will allow us to perform threshold resummation as well as a joint, threshold boosted resummation; the exact meaning of which will be clarified later in this chapter. We begin however, with a short review of top quark pair production at hadron colliders and examine some features of the fixed order calculations.

The total cross section for top quark pair production was first calculated to NLO in [38, 39] and to NNLO in [40]. Differential distributions were also obtained at

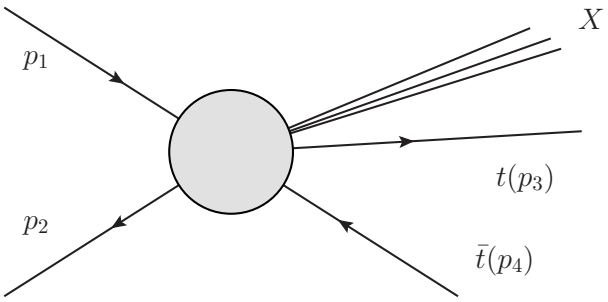

Figure 3.1: Diagrammatic representation of top quark pair production from two initial partons with momentum p_1 and p_2. X represents any additional radiation which may enter the final state.

NNLO, first with a fixed factorisation scale $\mu_f = m_t$ in [41] and later with dynamical choices of factorisation scale in [42], where the authors also performed an analysis of different choices of scale for various distributions. At the LHC, inclusive top quark pair production proceeds through the process

$$p(P_1) + p(P_2) \to t(p_3) + \bar{t}(p_4) + X\,, \tag{3.1.1}$$

for protons p, top quarks t and X refers to any additional particles which may enter into the final state. The variables P_1 and P_2 denote the 4-momenta of the incoming protons, while p_3 and p_4 denote the 4-momenta of the outgoing top and anti-top quarks respectively. At leading order two partonic channels contribute

$$\begin{aligned} q(p_1) + \bar{q}(p_2) &\to t(p_3) + \bar{t}(p_4)\,, \\ g(p_1) + g(p_2) &\to t(p_3) + \bar{t}(p_4)\,, \end{aligned} \tag{3.1.2}$$

where we have used the variables $p_1(p_2)$ to denote the 4-momentum of parton 1(2) in the initial state of the process. Each is related to the momentum of its parent hadron P_i via the relation $p_i = x_i P_i$ where x_i denotes the momentum fraction carried by that parton with respect to the momentum of its parent. We denote the top pair invariant mass squared as $M^2_{t\bar{t}} = M^2 = (p_3 + p_4)^2$ and the incoming partonic centre of mass energy squared as $\hat{s} = (p_1 + p_2)^2$. We also make use of the Mandelstam invariant $t_1 = (p_1 - p_3)^2 - m_t^2$. For what follows, it is convenient to introduce two

further variables

$$\tau = \frac{M^2}{s}\,, \qquad z = \frac{M^2}{\hat{s}}\,,$$

τ and z describe the fraction of the incident hadronic and partonic energy which is consumed by the final state top quarks respectively. In particular $(1-z)$ gives the fraction of the incident parton energy which is available for final state radiation.

In order to calculate the cross section for the process in Eq. (3.1.1), one typically employs the well known QCD factorisaton theorem [43]. From this we can write the cross section for the hadronic process as a convolution between the *parton distribution functions* (PDFs) and the corresponding partonic cross section, summing over the different possible initial state partons. Explicitly we can write the double differential cross section as

$$\frac{d^2\sigma(\tau)}{dM\, d\cos\theta} = \frac{8\pi\beta_t}{3sM}\sum_{ij}\int_\tau^1 \frac{dz}{z}\,\mathcal{L}_{ij}(\tau/z,\mu_f)\,C_{ij}(z,M,m_t,\cos\theta,\mu_f)\,, \tag{3.1.3}$$

where the sum (ij) is over initial state partons, C_{ij} are the so-called *hard-scattering kernels* which are proportional to the partonic cross section and $\mathcal{L}_{ij}$ is the *parton luminosity* defined as

$$\mathcal{L}_{ij}(y,\mu_f) = \int_y^1 \frac{dx}{x}\,\phi_{i/N_1}(x,\mu_f)\,\phi_{j/N_2}(y/x,\mu_f)\,. \tag{3.1.4}$$

The functions $\phi_{i/N_k}(x,\mu_f)$ are the PDFs and describe the probability of finding parton species i in hadron N_k carrying a fraction x of the hadron's total momentum. It is convenient to introduce the variable β_t which gives the 3-velocity of the (anti)top quark in the $\bar{t}t$ rest frame

$$\beta_t = \sqrt{1-\frac{4m_t^2}{M^2}}\,.$$

The perturbative expansion of C_{ij} is given by calculating higher order corrections to the partonic process. In calculating these corrections, one typically encounters logarithms of the ratios of different scales which appear in the process. One kind,

which feature heavily in this work, are so called *threshold logarithms*. These logarithms remain after the cancellation of IR divergences and are related to the emission of real gluons. These logarithms generally appear in differential cross sections in the form

$$C_{ij}(z,\mu_f) = \sum_{m,n} \alpha_s^n(\mu_f) \left(c_{n,m}^{(0)} \left[\frac{\ln^m(1-z)}{1-z} \right]_+ + c_{n,m}^{(1)} \ln^m(1-z) + \dots \right), \qquad (3.1.5)$$

where the coefficients $c_{n,m}^{(k)}$ are functions of the other variables in the process $(m_t, \cos\theta, ..)$ and can be functions of z which remain finite as $z \to 1$. We notice that these logarithms become large as $(1-z) \to 0$ and therefore, based on the preceding discussion, correspond to precisely the region of phase space where additional radiation in the final state is constrained to necessarily be soft. We see that Eq. (3.1.5) has the form of an expansion in $(1-z)$ with the leading divergent term beginning at $(1-z)^{-1}$. Later, when we develop the EFT to resum threshold logarithms, our power counting will be in $(1-z)$ and we will work only to leading power.

One may not necessarily feel the need to worry about such logarithms destroying the applicability of the perturbative expansion. After all one might expect the limit $z \to 1$ to be very rarely realised. Indeed, from Eq. (3.1.3) we see $z \in [\tau, 1]$ and even for $M \sim 500$ GeV, $\tau \sim 0.0015$ at the 13 TeV LHC. One obvious region where $z \to 1$ is relevant is when $\tau \sim 1$. However, from the form of Eqs. (3.1.3) and (3.1.4) we see that this requires PDFs at large x where they become numerically small. Hence the parton luminosity becomes extremely small in this region and the result becomes less phenomenologically interesting. There is another possibility however. Considering Eq. (3.1.3), if the parton luminosity is such that it falls steeply for $\tau/z \to 1$ then the largest contributions to the cross section will come from values away from this limit and hence the largest values of z. Such an effect, where these larger values of z become relevant is known as *Dynamical Threshold Enhancement* and was discussed in the context of Drell-Yan production in [44]. Evidence for such an effect in $t\bar{t}$ production at hadron colliders was observed in [45]. Indeed, in [36] it is shown that the leading threshold terms at NLO are a very good approximation to the full NLO

in the invariant mass distribution.

Another type of logarithm which can appear is one of the ratio of the top pair invariant mass M, to the top mass itself m_t, namely $\ln(m_t/M)$. Provided one considers the region of phase space where $M \sim m_t$, these logarithms are not necessarily harmful. However, if one considers *boosted* top quark pairs for which $M \gg m_t$, the resummation of such logarithms can become a necessity in order to maintain convergence in the perturbative expansion.

We will explore the resummation of the threshold logarithms as well a joint resummation of small-mass and threshold logarithms in the coming sections. In order to perform the resummation it is necessary to separate the various scales leading to these large logarithms into separate functions.

3.2 Factorisation for Threshold Resummation

The origin of the potentially dangerous logarithms in Eq. (3.1.5) comes from the presence of the dynamically generated soft scale $\sqrt{\hat{s}}(1-z)$ compared to the other larger scales present in the calculation. We thus identify the following separation of scales

$$\text{Soft limit:} \quad \hat{s}, t_1, m_t^2, M^2 \gg \hat{s}(1-z)^2 \,. \tag{3.2.1}$$

As mentioned in Chapter 2, one must be careful to properly take account of the power counting in the EFT. In this instance, the expansion parameter is $\lambda \sim (1-z) \ll 1$, and we work to leading power in this expansion. This means we will only pick up the contributions proportional to $c^{(0)}_{n,m}$ from Eq. (3.1.5) to all orders in n through our resummation. We will also only account for terms to a given logarithmic order m specified by the accuracy of our calculation which we will discuss in Section 3.4.7. A factorised form of the hard-scattering kernels was derived in this limit using techniques from SCET in [36]. The resummation performed in that work was carried out in momentum (z) space. We will convert the main results of that work into Mellin

space for the current project in Section 3.4.1.

Our starting point is the factorised form of the hard-scattering kernels in the soft limit which from [36] can be written as the product of so called *hard* and *soft* functions

$$C_{ij}^{\text{Soft}}(z, M, m_t, \cos\theta, \mu_f) = \text{Tr}\left[\mathbf{H}_{ij}^m(M, m_t, \cos\theta, \mu_f)\mathbf{S}_{ij}^m(\sqrt{\hat{s}}(1-z), M, m_t, \cos\theta, \mu_f)\right] + \mathcal{O}(1-z)\,. \tag{3.2.2}$$

We have include the superscript "soft" on C_{ij}^{soft} to denote that this hard-scattering kernel has been obtained in soft limit and we have included the indices (ij) denoting the partonic channel $(ij) \in \{q\bar{q}, \bar{q}q, gg\}$. The superscript m indicates the dependence of these matching functions on m_t in order to distinguish them from the hard and soft functions with $m_t = 0$ which will appear in Section 3.3. Convolving this with the parton luminosity as shown in Eq. (3.1.3) gives our factorised form of the cross section in the soft limit. The key use of this result is that we now have two separate functions; the hard function $\mathbf{H}^m$ which no longer depends on z (and so is regular as $z \to 1$), and the soft function $\mathbf{S}^m$ which contains the threshold logarithms. Specifically, $\mathbf{H}^m$ contains logarithms of the form $\ln^m(M/\mu_f)$, while the soft function contains $\ln^m\left(\hat{s}(1-z)^2/\mu_f^2\right)$. Having separated the different scales, we can clearly see that there is no appropriate choice of μ_f which can simultaneously remove the large logarithms from both the hard and soft functions. Ideally, we would like to evaluate the hard function at a scale $\mu_f \sim M$ and the soft function at a scale $\mu_f \sim \sqrt{\hat{s}}(1-z)$. However, the fact that there are now two functions which each depend on logarithms of the ratio of only one scale and the factorisation scale is what will ultimately allow the resummation of these threshold logarithms. This will be discussed in more detail in Section 3.4.

Before moving on there is a feature of the soft limit we can exploit in order to also be able to produce p_T distributions. In the limit $z \to 1$, the top quarks are back-to-back

in their rest frame. It is possible then to express the top quark p_T and rapidity $\hat{y}$ as

$$p_T = \frac{M\beta_t}{2}\sin\theta\,, \quad \hat{y} = \frac{1}{2}\ln\frac{1+\beta_t\cos\theta}{1-\beta_t\cos\theta}\,. \tag{3.2.3}$$

We can then perform a change of variables in order to obtain the double differential cross section with respect to p_T and $\hat{y}$. This change of variables takes the form

$$\frac{d^2\sigma(\tau)}{dp_T\,d\hat{y}} = 2\sin\theta\,\frac{d^2\sigma(\tau)}{dM\,d\cos\theta} \tag{3.2.4}$$

where in the expression involving the original double differential cross section it is understood that M and $\cos\theta$ should be expressed in terms of the integration variables according to

$$M = 2m_T\cosh(\hat{y}) \equiv 2\sqrt{p_T^2+m_t^2}\cosh(\hat{y})\,, \quad \cos\theta = \frac{1}{\beta_t}\tanh(\hat{y})\,, \tag{3.2.5}$$

where we have defined the transverse mass m_T. The transverse momentum distribution can be obtained by integrating over $\hat{y}$ in the range

$$|\hat{y}| \leq \operatorname{arccosh}\left(\frac{\sqrt{s}}{2m_T}\right), \tag{3.2.6}$$

while the range of p_T is

$$0 \leq p_T \leq \sqrt{\frac{s}{4}-m_t^2}\,. \tag{3.2.7}$$

3.3 Factorisation for Boosted Top Quarks

We now extend the results of Section 3.2 to the case where the top quarks are highly boosted. Specifically, the region of phase space where the pair invariant mass is much larger than the top mass itself. We will see the emergence of the following scale separation

$$\text{Boosted Soft limit:} \quad \hat{s}, t_1, M^2 \gg m_t^2 \gg \hat{s}(1-z)^2 \gg m_t^2(1-z)^2\,. \tag{3.3.1}$$

In what follows, we will see the further factorisation of the hard-scattering kernels into four distinct functions, one for each of these scales. The results here were first de-

rived in z space in [37]. We will reproduce their result, but now recast in Mellin space.

Rather than building directly on Eq. (3.2.2), it is simpler to take a step back and take the small mass limit first by expanding the partonic cross section in m_t/M. The same result can be achieved by taking the small mass limit of Eq. (3.2.2) and this will be discussed at the end of the section. It was shown in [46] that by introducing perturbative *heavy quark fragmentation functions* one can write the partonic cross section for the production of a heavy quark (which we suggestively denote t) as

$$\frac{d\sigma_t}{dz}(z, m_t, \mu) = \sum_a \int_z^1 \frac{dx}{x} \frac{d\hat{\sigma}_a}{dx}(x, m_t, \mu) D_{a/t}^{(n_l+n_h)} \left(\frac{z}{x}, m_t, \mu\right) . \tag{3.3.2}$$

Here, $D_{a/t}^{(n_f)}(x, m_h, \mu)$ is the heavy quark fragmentation function, defined with α_s using n_f flavours and gives the probability of producing a heavy quark t of mass m_t with momentum fraction x of the initial state from a massless parent parton a. The cross section $d\hat{\sigma}_a/dx$ describes the production of a massless parton a and is computed using standard techniques from perturbative QCD. Finally, we sum over massless partons a including the heavy quark we wish to produce, treating it as massless in $d\hat{\sigma}_a/dx$. As will be highlighted later, the heavy quark framgnetation functions satisfy a DGLAP type evolution in a similar manner to PDFs. However, because the scale associated with heavy quark fragmentation is the mass of the heavy quark itself, $\alpha_s(m_{\text{heavy}})$ is still in the perturbative regime. Essentially this means only an initial condition for $D_{i/h}^{(n_f)}$ need be calculated. The heavy quark fragmentation functions were first calculated in [46] by essentially de-convolving Eq. (3.3.2); that is computing both the massless and massive ampitudes to leading order in α_s. The $\mathcal{O}(\alpha_s^2)$ corrections were obtained in [47]. To apply these results to the case of $t\bar{t}$ production two modifications must be made. First, since we are producing two heavy quarks, we need to apply Eq. (3.3.2) twice. It is also necessary, as discussed in [37], to introduce additional matching functions (*heavy-flavour coefficients*) to match six-flavour PDFs, fragmentation functions, and α_s onto five-flavour PDFs. We will cluster the matching coefficients for these contributions together and generically

denote them as c_t^{ij}. The hard scattering kernel thus becomes, in the small mass limit

$$\begin{aligned} C_{ij}(z, M, m_t, t_1, \mu_f) = \sum_{a,b} C_{ij}^{ab}(z, M, t_1, \mu_f) \otimes D_{a/t}^{(n_f)}(z, m_t, \mu_f) \\ \otimes D_{b/\bar{t}}^{(n_f)}(z, m_t, \mu_f) \otimes c_t^{ij}(z, m_t, \mu_f) + \mathcal{O}\left(\frac{m_t}{M}\right) , \end{aligned} \tag{3.3.3}$$

where C_{ij}^{ab} is related to the massless partonic inclusive cross section for the production of partons a, b from i, j and the symbol $\otimes$ denotes a convolution. Note that a and b can include the top quark itself which is treated as massless in the scattering kernel C_{ij}^{ab}. Next, we take the soft limit ($z \to 1$) of Eq. (3.3.3). First of all, at leading power only the choices $a = t$ and $b = \bar{t}$ contribute in the fragmentation functions and partonic cross section. The soft limit of $C_{ij}^{t\bar{t}}$ follows exactly from the results of Section 3.2, but for massless top quarks. We therefore obtain

$$\begin{aligned} C_{ij}^{t\bar{t}}(z, M, m_t, \cos\theta, \mu_f) = \mathrm{Tr}\left[\mathbf{H}_{ij}(M, \cos\theta, \mu_f)\mathbf{S}_{ij}(\sqrt{\hat{s}}(1-z), M, \cos\theta, \mu_f)\right] \\ + \mathcal{O}(1-z) , \end{aligned} \tag{3.3.4}$$

where compared to Eq. (3.2.2) we have dropped the superscript ^{m} on $\mathbf{H}$ and $\mathbf{S}$ indicating that these functions no longer depend on m_t. It was shown in [48] that after matching on to n_l flavours, the heavy quark fragmentation function factorises at leading power in the soft limit. Specifically, one finds that

$$D_{t/t}^{n_l}(z, m_t, \mu_f) = C_D(m_t, \mu_f) S_D(m_t(1-z), \mu_f) + \mathcal{O}(1-z) . \tag{3.3.5}$$

The fragmentation function thus decomposes into two one-scale functions; one depending on the collinear scale m_t and one on the dynamically generated soft-collinear scale $m_t(1-z)$. In the same fashion as the hard and soft functions in Eqs. (3.2.2) and (3.3.4), C_D is related to virtual corrections while S_D is related to the emission of soft collinear radiation. The factorisation for $D_{\bar{t}/\bar{t}}$ is completely analogous to that for $D_{t/t}$. Putting these results together, one obtains the factorised form of the hard

scattering kernel in the joint, soft and small mass limits,

$$\begin{aligned} C_{ij}^{\text{Boosted}}(z, M, m_t, \cos\theta, \mu_f) = \text{Tr}\left[\mathbf{H}_{ij}(M, \cos\theta, \mu_f)\, \mathbf{S}_{ij}\left(\sqrt{\hat{s}}(1-z), M, \cos\theta, \mu_f\right)\right] \\ \times C_D^2(m_t, \mu_f) \otimes S_D\left(m_t(1-z), \mu_f\right) \\ \otimes S_D\left(m_t(1-z), \mu_f\right) \otimes c_t^{ij}(z, m_t, \mu_f) \\ + \mathcal{O}(1-z) + \mathcal{O}\left(\frac{m_t}{M}\right), \end{aligned} \tag{3.3.6}$$

where we have introduced the "Boosted" superscript to emphasise that this hard-scattering kernel has been obtained in the joint small mass and threshold limits.

As mentioned at the start of this section the same result can also be achieved by taking the small mass limit of Eq. (3.2.2). It is useful for matching with fixed order later to examine the first step of this. Ignoring again for a moment the contributions from closed heavy quark loops, the massive hard $\mathbf{H}^m$ and soft $\mathbf{S}^m$ functions can be further factorised in the $m_t \to 0$ limit

$$\mathbf{H}_{ij}^m(M, m_t, \cos\theta, \mu_f) = \mathbf{H}_{ij}(M, \cos\theta, \mu_f) C_D^2(m_t, \mu_f) + \mathcal{O}\left(\frac{m_t}{M}\right) \tag{3.3.7}$$

$$\begin{aligned} \mathbf{S}_{ij}^m\left(\ln\frac{M^2(1-z)^2}{\mu_f^2}, M, m_t, \cos\theta, \mu_f\right) = \mathbf{S}_{ij}\left(\ln\frac{M^2(1-z)^2}{\mu_f^2}, M, \cos\theta, \mu_f\right) \\ \times S_D^2\left(\ln\frac{m_t(1-z)}{\mu_f}, \mu_f\right) + \mathcal{O}\left(\frac{m_t}{M}\right). \end{aligned} \tag{3.3.8}$$

Here we see explicitly that the combination $\mathbf{H}\, C_D^2$ is just the small mass limit of the massive hard function and similarly $\mathbf{S}$, S_D^2 is the corresponding limit for the massive soft function. Such relations will be useful when we wish to combine the results from pure threshold resummation and the resummation performed in the boosted-soft limit in Section 3.5.

3.4 Resummed Differential Cross Sections

3.4.1 Mellin Space

We now turn to the issue of performing resummation from our factorised results. While it is possible to proceed directly in momentum space as was done for the threshold resummation in [36], we choose to implement the joint resummation in Mellin space. We first introduce the necessary transform to this space and some features of it, before deriving the resummed cross sections.

The Mellin transform[1] and its inverse are defined by

$$\tilde{f}(N) = \mathcal{M}[f](N) = \int_0^1 dx\; x^{N-1} f(x)\,, \tag{3.4.1}$$

$$f(x) = \mathcal{M}^{-1}[\tilde{f}](x) = \frac{1}{2\pi i}\int_{c-i\infty}^{c+i\infty} dN\; x^{-N} f(N)\,, \tag{3.4.2}$$

where N is the Mellin space variable and c is a real number chosen such that the contour in the inverse transform is to the right of all singularities in the integrand. Under a Mellin transform, convolutions of functions instead become simple products. We take the Mellin transform of Eq. (3.1.3) with respect to the variable τ,

$$\begin{aligned}\frac{d^2\tilde{\sigma}(N)}{dM\, d\cos\theta} &= \int_0^1 d\tau\; \tau^{N-1}\frac{d^2\sigma(z)}{dM\, d\cos\theta}\\ &= \frac{8\pi\beta_t}{3sM}\sum_{ij}\int_0^1 \frac{dz}{z}\, z^N\, C_{ij}(z,\mu_f)\int_0^1 \frac{dp}{p}\, p^N \mathcal{L}_{ij}(p,\mu_f)\\ &= \frac{8\pi\beta_t}{3sM}\sum_{ij}\; \tilde{\mathcal{L}}_{ij}(N,\mu_f)\,\tilde{C}_{ij}(N,\mu_f)\,,\end{aligned} \tag{3.4.3}$$

where we have changed the order of integration on the second line and suppressed the dependence on $\cos\theta$, m_t and M in the hard-scattering kernel. The PDFs, and hence the parton luminosity $\mathcal{L}_{ij}$, are usually provided in momentum space. To obtain $\mathcal{L}_{ij}$ in Mellin space, we employ techniques first suggested in [49] and more recently utilised for resummation in Higgs production in [50, 51] where $\mathcal{L}_{ij}(z,\mu_f)$ is fit to a basis of polynomials whos Mellin transform can be taken analytically. The latter

[1] Normally the upper limit on the Mellin transform is ∞, however in our case this is restricted to 1 since $z < 1$ and $\tau < 1$.

reference [51] contains a detailed appendix on how to implement this in practice.

The Mellin transform of C_{ij} is with respect to z. The effect on the leading power threshold logarithms

$$P_n(z) = \left[\frac{\ln^n(1-z)}{1-z}\right]_+ , \tag{3.4.4}$$

can be computed from the Mellin transform of their generating function [52]. We simply quote the result

$$\mathcal{M}[P_k](N) = \frac{1}{1+k}\sum_{j=0}^{k}\binom{k+1}{j}\Gamma^{(j)}(1)\left[\Gamma(N)\Delta^{(k+1-j)}(N) - \Delta^{(k+1-j)}(1)\right] , \tag{3.4.5}$$

where

$$\Delta^{(p)}(N) = \frac{d^p}{dN^p}\left(\frac{1}{\Gamma(N)}\right) ,$$

and the notation (j) on the gamma function also implies a derivative. Evaluating Eq. (3.4.5) usually produces a sequence of polygamma functions $\psi^{(k)}(N)$, where

$$\psi^{(k)}(N) = \frac{d^{k+1}}{dN^{k+1}}\ln\Gamma(N) .$$

The momentum space limit $z \to 1$ corresponds to the Mellin space limit $N \to \infty$. As such the resummation is normally performed in the large-N limit, a procedure which we adopt here. In this limit, the transformed plus distributions become a series of logarithms in N, rather than a collection of polygamma functions. The first few of these are

$$\begin{aligned}
\mathcal{M}[P_0](N) &= -\ln\bar{N} + \mathcal{O}\left(\frac{1}{N}\right) , \\
\mathcal{M}[P_1](N) &= \frac{1}{2}\left(\ln^2\bar{N} + \frac{\pi^2}{6}\right) + \mathcal{O}\left(\frac{1}{N}\right) , \\
\mathcal{M}[P_2](N) &= -\frac{1}{3}\left(\ln^3\bar{N} + \frac{\pi^2}{2}\ln\bar{N} + 2\zeta(3)\right) + \mathcal{O}\left(\frac{1}{N}\right) , \\
\mathcal{M}[P_3](N) &= \frac{1}{4}\left(\ln^4\bar{N} + \pi^2\ln^2\bar{N} + 8\zeta(3)\ln\bar{N} + \frac{3\pi^4}{20}\right) + \mathcal{O}\left(\frac{1}{N}\right) ,
\end{aligned} \tag{3.4.6}$$

where the notation $\bar{N} = Ne^{\gamma_E}$ has been introduced to tidy factors of γ_E. We note that the cross section contains terms of the form $\alpha_s^n P_k(z)$ where $0 \le k \le 2n-1$ at N^{n}LO in its perturbative expansion. In Mellin space this becomes $\alpha_s^n L^k$ where $L = \ln\bar{N}$ and $0 \le k \le 2n$. Since the resummation is performed in Mellin space, the

number of these logarithms which are reproduced by the resummation formula at each order in perturbation theory determines the accuracy of the resummation. This point will be addressed further in Section 3.4.7. The soft and boosted soft limits in Eqs. (3.2.1) and (3.3.1) become

$$\text{Mellin-space soft limit:} \quad \hat{s}, t_1, m_t^2 \gg \frac{\hat{s}}{N^2}\,, \tag{3.4.7}$$

$$\text{Mellin-space boosted soft limit:} \quad \hat{s}, t_1 \gg m_t^2 \gg \frac{\hat{s}}{N^2} \gg \frac{m_t^2}{N^2}\,. \tag{3.4.8}$$

Since the Mellin transform only acts upon functions depending on z, it has no effect on the hard functions $\mathbf{H}^{(m)}$ or C_D and so we obtain

$$\begin{aligned}\widetilde{C}_{ij}^{\text{Soft}}(N,\mu_f) = \text{Tr}\left[\mathbf{H}_{ij}^{m}(M, m_t, \cos\theta, \mu_f)\,\widetilde{\mathbf{S}}_{ij}^{m}\left(\ln\frac{M^2}{\bar{N}^2\mu_f^2}, M, m_t, \cos\theta, \mu_f\right)\right] \\ +\mathcal{O}\left(\frac{1}{N}\right)\,,\end{aligned} \tag{3.4.9}$$

$$\begin{aligned}\widetilde{C}_{ij}^{\text{Boosted}}(N,\mu_f) = \text{Tr}\left[\mathbf{H}_{ij}(M, \cos\theta, \mu_f)\,\widetilde{\mathbf{S}}_{ij}\left(\ln\frac{M^2}{\bar{N}^2\mu_f^2}, M, \cos\theta, \mu_f\right)\right] \\ \times C_D^2(m_t,\mu_f)\,\widetilde{S}_D^2\left(\ln\frac{m_t}{\bar{N}\mu_f}, \mu_f\right)\widetilde{c}_{ij}^{\,t}\left(\ln\frac{1}{\bar{N}^2}, m_t, \mu_f\right) \\ +\mathcal{O}\left(\frac{1}{N}\right)+\mathcal{O}\left(\frac{m_t}{M}\right)\,,\end{aligned} \tag{3.4.10}$$

for the factorised hard-scattering kernel in the soft, and boosted soft limit respectively. In order to free the matching functions from large logarithmic corrections we would like to evaluate the hard function at a scale $\mu_h \sim M$, the soft function at $\mu_s \sim M/\bar{N}$ and the collinear functions C_D and S_D at scales $\mu_{dh} \sim m_t$ and $\mu_{ds} \sim m_t/\bar{N}$ respectively. In order to do so, we now derive Renormalisation Group (RG) equations for each of these matching functions. The solutions to these equations will allow us to relate each of the matching functions evaluated at μ_f in terms of itself evaluated at another scale (chosen to eliminate the large logs) and an evolution function which interpolates between the two. Schematically, we will be able to write $F(\mu_a) = U(\mu_a,\mu_b)F(\mu_b)$.

3.4.2 Hard Function RG Equation

In order to perform resummation it is necessary to derive and solve RG equations for each of the component functions in Eqs. (3.4.9) and (3.4.10). This allows each function to be evaluated at a factorisation scale where it is free from large logarithms. The RG equation for the hard function and its solution can be taken from [36] since it is unaffected by the Mellin transform. We will review the techniques and its solution here as a model for how to solve the other RG equations which we will encounter.

The RG equation for the massive hard function [36] is given by

$$\begin{aligned}\frac{d}{d\ln\mu}\mathbf{H}^m(M,m_t,\cos\theta,\mu) = \boldsymbol{\Gamma}^m_{\mathbf{H}}(M,m_t,\cos\theta,\mu)\,\mathbf{H}^m(M,m_t,\cos\theta,\mu)\\ + \mathbf{H}^m(M,m_t,\cos\theta,\mu)\,\boldsymbol{\Gamma}^{m\,\dagger}_{\mathbf{H}}(M,m_t,\cos\theta,\mu)\,,\end{aligned} \tag{3.4.11}$$

where we have removed the indices labelling the initial state partons. It should be remembered that the form of the anomalous dimensions and hard functions (as well as their dimension) is different between the $q\bar{q}$ and gg channels. In what follows, we remove dependence on M, m_t and $\cos\theta$ from the arguments of the functions. The solution can be written as

$$\mathbf{H}^m(\mu) = \mathbf{U}^m_H(\mu_h,\mu)\mathbf{H}^m(\mu_h)\mathbf{U}^{m\,\dagger}_H(\mu_h,\mu)\,, \tag{3.4.12}$$

which implies

$$\begin{aligned}&\frac{d\mathbf{U}^m_H}{d\ln\mu}\,\mathbf{H}^m(\mu_h)\mathbf{U}^{m\,\dagger}_H + \mathbf{U}^m_H\,\mathbf{H}^m(\mu_h)\,\frac{d\mathbf{U}^{m\,\dagger}_H}{d\ln\mu} = \boldsymbol{\Gamma}^m_{\mathbf{H}}(\mu)\mathbf{H}^m(\mu) + \mathbf{H}^m(\mu)\boldsymbol{\Gamma}^{m\,\dagger}_{\mathbf{H}}(\mu)\\ &\qquad\Longrightarrow\ \frac{d\mathbf{U}^m_{\mathbf{H}}}{d\ln\mu} = \boldsymbol{\Gamma}^m_{\mathbf{H}}(\mu)\mathbf{U}^m_H\,.\end{aligned} \tag{3.4.13}$$

Recalling that $\boldsymbol{\Gamma}^m_{\mathbf{H}}$ is matrix valued, this equation can be solved using iterative methods. The result is the path ordered exponential

$$\mathbf{U}^m_H(\mu_h,\mu) = \mathcal{P}\exp\left\{\int_{\mu_h}^{\mu}\frac{d\mu'}{\mu'}\boldsymbol{\Gamma}^m_{\mathbf{H}}(\mu')\right\}. \tag{3.4.14}$$

The form of the hard anomalous dimension in both the $q\bar{q}$ and gg channel contains terms which have explicit logarithmic μ dependence. These are related to the

Sudakov double logarithms and, since they are proportional to the identity matrix in colour space, can be extracted from the path ordering all together. Writing the anomalous dimension as

$$\mathbf{\Gamma}_{\mathbf{H}}^{m} = \Gamma_{\text{cusp}}\left(\alpha_s\right)\left(\ln\frac{M^2}{\mu^2} - i\pi\right)\mathbf{1} + \gamma^{h,m}(\alpha_s)\,, \tag{3.4.15}$$

we can simplify the evolution factor $\mathbf{U}_H^m$,

$$\mathbf{U}_H^m(\mu_h,\mu) = \exp\left\{\int_{\mu_h}^{\mu}\frac{d\mu'}{\mu'}\Gamma_{\text{cusp}}(\alpha_s)\left(\ln\frac{M^2}{\mu^2} - i\pi\right)\right\}\mathcal{P}\exp\left\{\int_{\mu_h}^{\mu}\frac{d\mu'}{\mu'}\gamma^{h,m}(\alpha_s)\right\}.$$

Here we see the appearance of the cusp anomalous dimension Γ_{cusp} as mentioned in Section 2.1.3 due to the presence of Wilson lines in the collinear fields describing the incoming partons. The cusp anomalous dimension takes on slightly different forms in the $q\bar{q}$ channel compared to the gg channel and can be found in the appendix of [36]. Using the definition of the QCD β-function, it is possible to change variables in the first exponent and solve the integrals perturbatively. Namely, using

$$\beta(\alpha) = \frac{d\alpha}{d\ln\mu}\,, \quad d\ln\mu = \frac{d\mu}{\mu} = \frac{d\alpha}{\beta(\alpha)}\,, \tag{3.4.16}$$

we can write

$$\begin{aligned}\mathbf{U}_H^m(\mu_h,\mu) = \exp&\left\{2S(\mu_h,\mu) - a_\Gamma(\mu_h,\mu)\left(\ln\frac{M^2}{\mu_h^2} - i\pi\right)\right\}\\ &\times\mathcal{P}\exp\left\{\int_{\mu_h}^{\mu}\frac{d\mu'}{\mu'}\gamma^{h,m}\right\},\end{aligned} \tag{3.4.17}$$

where

$$S(\mu_h,\mu) = -\int_{\alpha_s(\mu_h)}^{\alpha_s(\mu)}d\alpha\frac{\Gamma_{\text{cusp}}(\alpha)}{\beta(\alpha)}\int_{\alpha_s(\mu_h)}^{\alpha}\frac{d\alpha'}{\beta(\alpha')}\,, \qquad a_\gamma(\mu_h,\mu) = -\int_{\alpha_s(\mu_h)}^{\alpha_s(\mu)}d\alpha\frac{\gamma(\alpha)}{\beta(\alpha)}\,.$$

The subscript on a_γ can be any of the anomalous dimensions, in particular a_Γ refers specifically to the cusp anomalous dimension $\Gamma_{\text{cusp}}(\alpha_s)$.

The result for the massless hard function $\mathbf{H}$ will be discussed along with the massless soft function $\widetilde{\mathbf{S}}$ in Section 3.4.5.

3.4.3 Soft Function RG Equation

We now derive and solve the soft function RG equation in Mellin space. It is first necessary to determine the anomalous dimension of the soft function. This can be achieved by using the fact that the hadronic cross section itself should be invariant under changes in the factorisation scale. In Mellin space this implies

$$\mu\frac{d}{d\mu}\left(\mathrm{Tr}[\mathbf{H}^m(\mu)\widetilde{\mathbf{S}}^m(\mu)]\widetilde{\mathcal{L}}(\mu)\right)=0\,,$$
$$\mathrm{Tr}[\frac{d\mathbf{H}^m(\mu)}{d\ln\mu}\widetilde{\mathbf{S}}^m(\mu)]\widetilde{\mathcal{L}}(\mu)+\mathrm{Tr}[\mathbf{H}^m(\mu)\frac{d\widetilde{\mathbf{S}}^m(\mu)}{d\ln\mu}]\widetilde{\mathcal{L}}(\mu)+\mathrm{Tr}[\mathbf{H}^m(\mu)\widetilde{\mathbf{S}}^m(\mu)]\frac{d\widetilde{\mathcal{L}}(\mu)}{d\ln\mu}=0\,. \tag{3.4.18}$$

The above equation can be rearranged to express the evolution equation for the soft function in terms of those for the hard function and parton luminosity. We addressed the issue of the RG equation for the hard function in Section 3.4.2. In Mellin space the evolution equation for the parton luminosities takes the form

$$\frac{d\widetilde{\mathcal{L}}}{d\ln\mu}=2\frac{d\widetilde{\phi}(N)}{d\ln\mu}\widetilde{\phi}(N)\,. \tag{3.4.19}$$

The form of the evolution equation for the PDFs is governed by the DGLAP equations [53–55]. We only require these in the soft limit, $z\to 1$ (resp $N\to\infty$) however. This greatly simplifies the form of the resulting equations, which normally involve mixing between different flavours and gluons. In the $z\to 1$ limit we can write the evolution equation for PDFs as,

$$\frac{d\phi(z,\mu)}{d\ln\mu}=\int_z^1\frac{d\xi}{\xi}\,P(\xi)\,\phi(z/\xi,\mu),\quad P(\xi)=\frac{2\Gamma_{\mathrm{cusp}}(\alpha_s)}{(1-\xi)_+}+2\gamma^\phi(\alpha_s)\,\delta(1-\xi)\,, \tag{3.4.20}$$

where $P(\xi)$ is the part of the usual Altarelli-Parisi splitting kernels which become singular as $\xi\to 1$. In Mellin space, this becomes

$$\frac{d\widetilde{\phi}(N,\mu)}{d\ln\mu}=\widetilde{P}(N)\widetilde{\phi}(N,\mu),\quad \widetilde{P}(N)=-2\Gamma_{\mathrm{cusp}}(\alpha_s)\ln\bar{N}+2\gamma^\phi(\alpha_s)\,. \tag{3.4.21}$$

Rearranging Eq. (3.4.3) for the evolution of the soft function, and inserting Eqs. (3.4.11) and (3.4.21) one arrives at

$$\frac{d\widetilde{\mathbf{S}}^m}{d\ln\mu} = -\widetilde{\mathbf{S}}^m\,\mathbf{\Gamma}^m_{\mathbf{H}} - \mathbf{\Gamma}^{m\,\dagger}_{\mathbf{H}}\,\widetilde{\mathbf{S}}^m - (2\Gamma_{\rm cusp}(\alpha_s)\,\ln\frac{1}{\bar{N}^2} + 4\gamma^\phi) \tag{3.4.22}$$

$$= -\widetilde{\mathbf{S}}^m\,\mathbf{\Gamma}^m_{\mathbf{S}} - \mathbf{\Gamma}^{m\,\dagger}_{\mathbf{S}}\widetilde{\mathbf{S}}^m\,, \tag{3.4.23}$$

where we have used Eq. (3.4.15) and, since $\gamma^{\phi\dagger} = \gamma^\phi$, defined

$$\mathbf{\Gamma}^m_{\mathbf{S}} = \Gamma_{\rm cusp}(\alpha_s)\,\left(\ln\frac{M^2}{\bar{N}^2\mu^2} - i\pi\right)\mathbf{1} + \gamma^{s,m}\,, \tag{3.4.24}$$

$$\gamma^{s,m} = \gamma^{h,m} + 2\gamma^\phi\mathbf{1}\,.$$

Solving the RG equation for the soft function proceeds in a completely analogous manner to that of the hard function. We write the solution as

$$\widetilde{\mathbf{S}}^m(\mu) = \mathbf{U}^m_S(\mu_s,\mu)\widetilde{\mathbf{S}}^m(\mu_s)\mathbf{U}^{m\,\dagger}_S(\mu_s,\mu)\,, \tag{3.4.25}$$

where

$$\begin{aligned}\mathbf{U}^m_S(\mu_s,\mu) = \exp\Bigg\{ &-2S(\mu_s,\mu) + 2a_{\gamma^\phi}(\mu_s,\mu) + a_\Gamma(\mu_s,\mu)\left(\ln\frac{M^2}{\bar{N}^2\mu_s^2} + i\pi\right)\Bigg\} \\ &\times\mathcal{P}\exp\left\{-\int_{\mu_s}^{\mu}\frac{d\mu'}{\mu'}\gamma^{h,m\,\dagger}\right\}.\end{aligned} \tag{3.4.26}$$

Since the RG equation for the soft function was derived using the RG equations of the other functions appearing in the hadronic cross section, we postpone the discussion of the RG equation for the massless soft function until Section 3.4.5 due to the presence of additional matching functions in the boosted-soft limit.

3.4.4 Fragmentation Function RG Equation

In the factorised form of the hard-scattering kernels in the joint soft and small mass limits (Eq. (3.3.6)) we also have the factorised form of heavy quark fragmentation functions in addition to the massless hard and soft functions. In order to perform the joint resummation, these functions must also be RG evolved from a scale where

they are perturbatively well behaved, to some common scale μ_f. In [37] we see that the relevant fragmentation function obeys the following RG equation

$$\frac{d}{d\ln\mu} D_{t/t}(z, m_t, \mu) = P_{qq}(z, \mu) \otimes D_{t/t}(z, m_t, \mu)\,, \tag{3.4.27}$$

which in Mellin space, becomes simply

$$\frac{d}{d\ln\mu} \widetilde{D}(N) = \widetilde{P}_{qq}(N)\widetilde{D}(N)\,, \tag{3.4.28}$$

where we have dropped the t/t subscript. In the soft limit, the fragmentation function factorises, $\widetilde{D}(N) = C_D(m_t, \mu)\widetilde{S}_D(N, \mu) + \mathcal{O}(1/N)$ and so the RG equation becomes

$$\frac{dC_D(m_t,\mu)}{d\ln\mu}\widetilde{S}_D(N,\mu) + C_D(m_t,\mu)\frac{d\widetilde{S}_D(N,\mu)}{d\ln\mu} = \widetilde{P}_{qq}(N)C_D(m_t,\mu)\widetilde{S}_D(N,\mu)\,. \tag{3.4.29}$$

Here the evolution equation for S_D is known from B-physics. Specifically, S_D is equivalent to the perturbative shape function use in the decay of B-mesons [48, 56]. Its RG equation in Mellin space is given by

$$\frac{d\widetilde{S}_D}{d\ln\mu} = 2\left[\Gamma_{\rm cusp}(\alpha_s)\ln\frac{m_t}{\bar{N}\mu} - \gamma^S(\alpha_s)\right]\widetilde{S}_D\,. \tag{3.4.30}$$

Note that γ^S appearing in Eq. (3.4.30) is NOT the same as γ^s appearing in the anomalous dimension of the soft function in Eq. (3.4.24). The solution to this equation is obtained in the same way as the hard and soft functions. We write the solution as

$$\widetilde{S}_D(\mu) = U_{ds}(\mu_{ds}, \mu)\widetilde{S}_D(\mu_{ds})\,, \tag{3.4.31}$$

where

$$\begin{aligned} U_{ds}(\mu_{ds},\mu) &= \exp\left\{\int_{\mu_{ds}}^{\mu}\frac{d\mu'}{\mu'}\left(2\Gamma_{\rm cusp}(\alpha_s)\ln\frac{m_t}{\bar{N}\mu} - 2\gamma^S(\alpha_s)\right)\right\} \\ &= \exp\left\{2S(\mu_{ds},\mu) - a_\Gamma(\mu_{ds},\mu)\ln\frac{m_t^2}{\bar{N}^2\mu_{ds}^2} + 2a_{\gamma^S}(\mu_{ds},\mu)\right\}. \end{aligned} \tag{3.4.32}$$

Knowledge of the anomalous dimension for S_D in Eq. (3.4.30) allows us to rearrange Eq. (3.4.29) for the RG equation of C_D to obtain

$$\frac{dC_D(m_t,\mu)}{d\ln\mu} = \left[2\gamma^S(\alpha_s) + 2\gamma^{\phi_q}(\alpha_s) - 2\Gamma_{\rm cusp}(\alpha_s)\ln\frac{m_t}{\mu}\right] C_D(m_t,\mu)\,. \tag{3.4.33}$$

Like the function S_D, we write the solution to this as

$$C_D(m_t,\mu) = U_{dh}(\mu_{dh},\mu) C_D(m_t,\mu_{dh})\,, \tag{3.4.34}$$

where

$$\begin{aligned} U_{dh}(\mu_{dh},\mu) &= \exp\left\{\int_{\mu_{dh}}^{\mu}\frac{d\mu'}{\mu'}\left(2\gamma^S(\alpha_s) + 2\gamma^{\phi_q}(\alpha_s) - 2\Gamma_{\rm cusp}\ln\frac{m_t}{\mu}\right)\right\} \\ &= \exp\left\{ - 2a_{\gamma^S}(\mu_{dh},\mu) - 2a_{\gamma^{\phi_q}}(\mu_{dh},\mu) - 2S(\mu_{dh},\mu) \right. \\ &\qquad \left. + a_\Gamma(\mu_{dh},\mu)\ln\frac{m_t^2}{\mu_{dh}^2}\right\}. \end{aligned} \tag{3.4.35}$$

This completes the derivation and solution of the necessary evolution equations in order to perform the resummation.

3.4.5 Massless Hard and Soft Function RG Equations

The RG equations for the massless hard and soft functions are similar to those in the massive case and are solved in exactly the same manner. The massless hard function satisfies

$$\begin{aligned} \frac{d}{d\ln\mu}\mathbf{H}(M,\cos\theta,\mu) = \mathbf{\Gamma_H}(M,\cos\theta,\mu)\,\mathbf{H}(M,\cos\theta,\mu) \\ + \mathbf{H}(M,\cos\theta,\mu)\,\mathbf{\Gamma_H^\dagger}(M,\cos\theta,\mu)\,, \end{aligned} \tag{3.4.36}$$

where we have removed the superscript ^{m} compared with the massive case in Eq. (3.4.36) to reflect the fact that the hard function no longer depends on the top mass. The anomalous dimension for the massless case is given by

$$\mathbf{\Gamma_H}(M,t_1,\mu) = A(\alpha_s)\left(\ln\frac{M^2}{\mu^2} - i\pi\right) + \gamma^h(\alpha_s)\,, \tag{3.4.37}$$

where $A(\alpha_s) = 2\Gamma^q_{\text{cusp}}$ in the $q\bar{q}$ channel and $A(\alpha_s) = \Gamma^q_{\text{cusp}} + \Gamma^g_{\text{cusp}}$ in the gg channel. Here we have explicitly indicated whether the factors in the cusp anomalous dimension should be evaluated in the fundamental (q) or adjoint representation (g). The solution proceeds in the same way as the massive case resulting in

$$\begin{aligned}\mathbf{U}_H(\mu_h,\mu) = \exp&\left\{2S_A(\mu_h,\mu) - a_A(\mu_h,\mu)\left(\ln\frac{M^2}{\mu_h^2} - i\pi\right)\right\}\\ &\times\mathcal{P}\exp\left\{\int_{\mu_h}^{\mu}\frac{d\mu'}{\mu'}\gamma^h\right\},\end{aligned} \tag{3.4.38}$$

where

$$S_A(\mu_h,\mu) = -\int_{\alpha_s(\mu_h)}^{\alpha_s(\mu)} d\alpha\frac{A(\alpha)}{\beta(\alpha)}\int_{\alpha_s(\mu_h)}^{\alpha}\frac{d\alpha'}{\beta(\alpha')}\,, \qquad a_A(\mu_h,\mu) = -\int_{\alpha_s(\mu_h)}^{\alpha_s(\mu)} d\alpha\frac{A(\alpha)}{\beta(\alpha)}\,.$$

The RG equation for the massless soft function changes slightly. For the massive case, we derived the RG equation for the soft function using the invariance of the hadronic cross section under changes in the factorisation scale. In the boosted-soft limit, we also have the heavy quark fragmentation function (in the soft limit) which contribute to the anomalous dimension of the soft function. Using the same technique as in Eq. (3.4.3) we can write

$$\frac{d\widetilde{\mathbf{S}}}{d\ln\mu} = -\widetilde{\mathbf{S}}\,\mathbf{\Gamma_S} - \mathbf{\Gamma_S}^\dagger\,\widetilde{\mathbf{S}}\,, \tag{3.4.39}$$

where

$$\mathbf{\Gamma_S} = \Gamma_{\text{cusp}}(\alpha_s)\left(\ln\frac{M^2}{\bar{N}^2\mu^2} - i\pi\right) + \gamma^s + 2\gamma^{\phi_q}\mathbf{1}\,, \tag{3.4.40}$$

and similarly $\gamma^s = \gamma^h + 2\gamma^\phi\mathbf{1}$. Thus, compared to the anomalous dimension for the massive soft function in Eq. (3.4.24), we pick up an additional contribution from the quark PDF anomalous dimension as necessary for RG invariance of the hadronic cross section. The solution proceeds in complete analogy to the massive case from this point, and we simply state the result as

$$\begin{aligned}\mathbf{U}_S(\mu_s,\mu) = \exp&\Big\{-2S_A(\mu_s,\mu) + 2a_{\gamma^\phi}(\mu_s,\mu) + 2a_{\gamma^{\phi_q}}(\mu_s,\mu)\\ &+ a_A(\mu_s,\mu)\left(\ln\frac{M^2}{\bar{N}^2\mu_s^2} + i\pi\right)\Big\}\mathcal{P}\exp\left\{-\int_{\mu_s}^{\mu}\frac{d\mu'}{\mu'}\gamma^{h\,\dagger}\right\}.\end{aligned} \tag{3.4.41}$$

3.4.6 Resummed Cross Sections

We now bring together the solutions to the RG equations for each of the matching functions. This will allow us to evaluate each matching function in Eqs. (3.4.9) and (3.4.10) independently at a scale where it is free from large logarithmic corrections. The evolution factors U_i then resum the respective logs to all orders in perturbation theory. The resummed hard-scattering kernel in the soft limit is thus

$$\begin{aligned}\widetilde{C}_{ij}^{\text{Soft}}(N,\mu_f) = \text{Tr}\Bigg[&\mathbf{U}_H^m(\mu_h,\mu_f)\mathbf{H}_{ij}^m(\mu_h)\mathbf{U}_H^{m\,\dagger}(\mu_h,\mu_f)\\ &\times \mathbf{U}_S^m(\mu_s,\mu_f)\widetilde{\mathbf{S}}_{ij}^m\left(\ln\frac{M^2}{\bar{N}^2\mu_f^2},\mu_s\right)\mathbf{U}_S^{m\,\dagger}(\mu_s,\mu_f)\Bigg] + \mathcal{O}\left(\frac{1}{N}\right)\\ = \text{Tr}\Bigg[&\mathbf{U}_1^m(\mu_h,\mu_s\,\mu_f)\mathbf{H}_{ij}^m(\mu_h)\mathbf{U}_1^{m\,\dagger}(\mu_h,\mu_s,\mu_f)\\ &\times \widetilde{\mathbf{S}}_{ij}^m\left(\ln\frac{M^2}{\bar{N}^2\mu_s^2},\mu_s\right)\Bigg] + \mathcal{O}\left(\frac{1}{N}\right), \end{aligned} \tag{3.4.42}$$

where we have defined $\mathbf{U}_1^m(\mu_h,\mu_s.\mu_f) = \mathbf{U}_S^{m\,\dagger}(\mu_s,\mu_f)\,\mathbf{U}_H^m(\mu_s,\mu_f)$, which can be written as

$$\begin{aligned}\mathbf{U}_1^m(\mu_h,\mu_s.\mu_f) = \exp\Bigg\{&2S(\mu_h,\mu_s) + 2a_{\gamma^\phi}(\mu_s,\mu_f) - a_\Gamma(\mu_h,\mu_s)\ln\frac{M^2}{\mu_h^2}\\ &- a_\Gamma(\mu_s,\mu_f)\ln\bar{N}^2 + i\pi\,a_\Gamma(\mu_s,\mu_h)\Bigg\}\\ &\times\mathcal{P}\exp\left\{\int_{\alpha_s(\mu_h)}^{\alpha_s(\mu_s)}\frac{d\alpha}{\beta(\alpha)}\gamma^{h,m}(\alpha)\right\}. \end{aligned} \tag{3.4.43}$$

Evaluating Eq. (3.4.42) with appropriate choices of μ_h and μ_s will resum[2] to all orders in perturbation theory the leading power threshold logarithms appearing in Eq. (3.1.5). We can repeat this exercise for the boosted soft limit, resulting in

$$\begin{aligned}\widetilde{C}_{ij}^{\text{Boosted}}(N,\mu_f) = \text{Tr}\Bigg[&\mathbf{U}_H(\mu_h,\mu_f)\mathbf{H}_{ij}(\mu_h)\mathbf{U}_H^\dagger(\mu_h,\mu_f)\\ &\times\mathbf{U}_S(\mu_s,\mu_f)\widetilde{\mathbf{S}}_{ij}\left(\ln\frac{M^2}{\bar{N}^2\mu_s^2},\mu_s\right)\mathbf{U}_S^\dagger(\mu_s,\mu_f)\Bigg]\\ &\times U_{dh}^2(\mu_{dh},\mu_f)C_D^2(\mu_{dh})\,U_{ds}^2(\mu_{ds},\mu_f)\widetilde{S}_D^2\left(\ln\frac{m_t}{\bar{N}\mu_{ds}},\mu_{ds}\right) \end{aligned}$$

[2]There are some subtleties concerning exactly what is resummed and the number of these logs captured at each order to be discussed in Section 3.4.7.

$$
\begin{aligned}
&+\mathcal{O}\left(\frac{1}{N}\right)+\mathcal{O}\left(\frac{m_t}{M}\right)\\
&=\mathrm{Tr}\left[\mathbf{U}_1(\mu_h,\mu_s,\mu_f)\mathbf{H}_{ij}(\mu_h)\mathbf{U}_1^\dagger(\mu_h,\mu_s\mu_f)\,\widetilde{\mathbf{S}}_{ij}\left(\ln\frac{M^2}{\bar{N}^2\mu_s^2},\mu_s\right)\right]\\
&\times U_D^2(\mu_{dh},\mu_{ds},\mu_f)C_D^2(\mu_{dh})\,\widetilde{S}_D^2\left(\ln\frac{m_t}{\bar{N}\mu_{ds}},\mu_{ds}\right)\\
&+\mathcal{O}\left(\frac{1}{N}\right)+\mathcal{O}\left(\frac{m_t}{M}\right),
\end{aligned}
\tag{3.4.44}
$$

where

$$
\begin{aligned}
\mathbf{U}_1(\mu_h,\mu_s,\mu_f)=&\exp\Bigg\{2S_A(\mu_h,\mu_s)+2a_{\gamma^\phi}(\mu_s,\mu_f)+2a_{\gamma^{\phi_q}}(\mu_s,\mu_f)\\
&-a_A(\mu_h,\mu_s)\ln\frac{M^2}{\mu_h^2}-a_A(\mu_s,\mu_f)\ln\bar{N}^2\\
&+i\pi\,a_A(\mu_s,\mu_h)\Bigg\}\\
&\times\mathcal{P}\exp\left\{\int_{\mu_h}^{\mu_s}\frac{d\alpha}{\beta(\alpha)}\gamma^h(\alpha)\right\},
\end{aligned}
\tag{3.4.45}
$$

and

$$
\begin{aligned}
U_D(\mu_{dh},\mu_{ds},\mu_f)=&\exp\Bigg\{-2S(\mu_{dh},\mu_{ds})+a_\Gamma(\mu_{dh},\mu_{ds})\ln\frac{m_t^2}{\mu_{dh}^2}-2a_\Gamma(\mu_{dh},\mu_{ds})\\
&-2a_{\gamma^{\phi_q}}(\mu_{dh},\mu_f)+a_\Gamma(\mu_{ds},\mu_f)\ln\bar{N}^2\Bigg\}.
\end{aligned}
\tag{3.4.46}
$$

We expand the functions S, S_A and a_{γ_i} in terms of α_s evaluated at the different matching scales. The perturbative expansion of the functions appearing in the exponents leads to [36]

$$
\begin{aligned}
S(\mu_1,\mu_2)=&\frac{\Gamma_0}{4\beta_0^2}\Bigg\{\frac{4\pi}{\alpha_s(\mu_1)}\left(1-\frac{1}{r}+\ln r\right)+\left(\frac{\Gamma_1}{\Gamma_0}-\frac{\beta_1}{\beta_0}\right)(1-r+\ln r)+\frac{\beta_1}{2\beta_0}\ln^2 r\\
&+\frac{\alpha_s(\mu_1)}{4\pi}\left[\left(\frac{\beta_1\Gamma_1}{\beta_0\Gamma_0}-\frac{\beta_2}{\beta_0}\right)(1-r+r\ln r)+\left(\frac{\beta_1^2}{\beta_0^2}-\frac{\beta_2}{\beta_0}\right)(1-r)\ln r\right.\\
&\left.-\left(\frac{\beta_1^2}{\beta_0^2}-\frac{\beta_2}{\beta_0}-\frac{\beta_1\Gamma_1}{\beta_0\Gamma_0}+\frac{\Gamma_2}{\Gamma_0}\right)\frac{(1-r)^2}{2}\right]\Bigg\},
\end{aligned}
\tag{3.4.47}
$$

$$
a_\Gamma(\mu_1,\mu_2)=\frac{\Gamma_0}{2\beta_0}\left\{\ln r+\left(\frac{\Gamma_1}{\Gamma_0}-\frac{\beta_1}{\beta_0}\frac{\alpha_s(\mu_2)-\alpha_s(\mu_1)}{4\pi}\right)\right\},
\tag{3.4.48}
$$

where $r = \alpha_s(\mu_2)/\alpha_s(\mu_1)$. In our resummation formalism however, we have chosen the soft scales μ_s and μ_{ds} to depend on the Mellin space variable N which can be complex valued. We therefore choose to express all α_s dependence in terms of $\alpha_s(\mu_h)$ using the running coupling (see e.g. [57])

$$\alpha_s(\mu) = \frac{\alpha_s(\mu_h)}{X}\left[1 - \frac{\alpha_s(\mu_h)}{4\pi}\frac{\beta_1}{\beta_0}\frac{\ln X}{X} + \left(\frac{\alpha_s(\mu_h)}{4\pi}\right)^2 \frac{1}{X^2}\left[\frac{\beta_1^2}{\beta_0^2}\left(\ln^2 X - \ln X - 1 + X\right) + \frac{\beta_2}{\beta_0}(1-X)\right] + \mathcal{O}(\alpha_s^3(\mu_h))\right], \tag{3.4.49}$$

where

$$X = 1 - \frac{\alpha_s(\mu_h)}{2\pi}\beta_0 \ln\frac{\mu_h}{\mu}\,. \tag{3.4.50}$$

The exponent will then explicitly contain logarithms of the form $\ln^p \mu_h/\mu_s$, for example, which for appropriate choices of μ_h and μ_s is a large logarithm. In fact using Eq. (3.4.16) we can see

$$\ln\frac{\mu_h}{\mu_s} = \int_{\alpha_s(\mu_s)}^{\alpha_s(\mu_s)} \frac{d\alpha}{\beta(\alpha)}\,, \tag{3.4.51}$$

and recalling that $\beta(\alpha_s) = -2\alpha_s^2 + \mathcal{O}(\alpha_s^3)$ indicates that we should treat such logarithms as scaling like $1/\alpha_s$. On expanding in the coupling α_s we therefore treat $\alpha_s L \sim \mathcal{O}(1)$. To this end, we define $\mathcal{O}(1)$ parameters

$$\lambda_i = \frac{\alpha_s(\mu_h)}{2\pi}\beta_0 \ln\frac{\mu_h}{\mu_i}\,, \tag{3.4.52}$$

for $i = \{s, dh, ds, f\}$. Expanding in this fashion, one obtains for the evolution matrix appearing in the soft limit

$$\widetilde{\mathbf{U}}^m(\mu_f, \mu_h, \mu_s) = \exp\left\{\frac{4\pi}{\alpha_s(\mu_h)}\, g_1^m(\lambda_s, \lambda_f) + g_2^m(\lambda_s, \lambda_f) + \frac{\alpha_s(\mu_h)}{4\pi}\, g_3^m(\lambda_s, \lambda_f) + \cdots\right\} \times \mathcal{P}\exp\left\{\int_{\alpha_s(\mu_h)}^{\alpha_s(\mu_s)} \frac{d\alpha}{\beta(\alpha)}\gamma^{h,m}(\alpha)\right\}, \tag{3.4.53}$$

where as indicated the g-functions are functions of the $\mathcal{O}(1)$ parameters λ_f and λ_s leaving the power counting the strong coupling explicit. Repeating this procedure

for the two evolution matrices appearing in the boosted soft limit one obtains

$$\widetilde{\mathbf{U}}(\mu_h,\mu_s,\mu_f) = \exp\left\{\frac{4\pi}{\alpha_s(\mu_h)}\,g_1(\lambda_s,\lambda_f) + g_2(\lambda_s,\lambda_f) + \frac{\alpha_s(\mu_h)}{4\pi}\,g_3(\lambda_s,\lambda_f)\right\} \times \mathcal{P}\exp\left\{\int_{\alpha_s(\mu_h)}^{\alpha_s(\mu_s)}\frac{d\alpha}{\beta(\alpha)}\gamma^h(\alpha)\right\}, \tag{3.4.54}$$

and

$$U_D(\mu_{dh},\mu_{ds},\mu_f) = \exp\left\{\frac{4\pi}{\alpha_s(\mu_h)}\,g_1^D(\lambda_{dh},\lambda_{ds},\lambda_f) + g_2^D(\lambda_{dh},\lambda_{ds},\lambda_f) + \frac{\alpha_s(\mu_h)}{4\pi}\,g_3^D(\lambda_{dh},\lambda_{ds},\lambda_f)\right\}. \tag{3.4.55}$$

The functions $g_i^{(m)}$ can be rather lengthy expressions, explicit results are given in Appendix A.1.

The part of the evolution matrix involving the path ordered exponential is a little more involved to evaluate. In the following section we denote this as $\mathbf{u}(\mu_1,\mu_2)$ such that

$$\mathbf{u}(\mu_h,\mu_s) = \mathcal{P}\exp\left\{\int_{\alpha_s(\mu_h)}^{\alpha_s(\mu_s)}\frac{d\alpha}{\beta(\alpha)}\gamma^h(\alpha)\right\}. \tag{3.4.56}$$

The exponential of a matrix is defined by its power series. Difficulties arise because we need to integrate the non-cusp anomalous dimensions $\gamma^{h,(m)}(\alpha_s)$ over a range of α_s and, because the matrices evaluated at different values of α_s don't necessarily commute, keep the matrices path ordered in the process. Because $\gamma^{h,(m)}(\alpha_s)$ is given by its perturbative expansion

$$\gamma^h(\alpha_s) = \left(\frac{\alpha_s}{4\pi}\right)\gamma^0 + \left(\frac{\alpha_s}{4\pi}\right)^2\gamma^1 + \left(\frac{\alpha_s}{4\pi}\right)^3\gamma^2 + \mathcal{O}(\alpha_s^4)\,, \tag{3.4.57}$$

the exponent actually turns into the integral of a sum of matrices. A method developed in [58] and further used in [36, 59, 60] involves expanding $\gamma^{h,m}(\alpha_s)$ only to leading power. This way the integral in the exponent can be carried out without breaking the path ordering (since clearly γ^0 commutes with itself) and higher order corrections to this are incorporated perturbatively outside the exponent. Explicitly

we compute

$$\mathbf{u}(\mu_h, \mu_s) = \mathbf{V}(\alpha_s(\mu_s)) \exp\left\{\frac{\gamma_0}{2\beta_0} \ln \frac{\alpha_s(\mu_h)}{\alpha_s(\mu_s)}\right\} \mathbf{V}^{-1}(\alpha_s(\mu_h))\,, \tag{3.4.58}$$

for some matrix $\mathbf{V}$ defined by its perturbative expansion

$$\mathbf{V}(\alpha_s) = \mathbf{1} + \frac{\alpha_s}{4\pi}\mathbf{V}_2\,, \tag{3.4.59}$$

the first term being the unit matrix since to leading order we already have the exponentiated γ-matrix. Details can be found in the appendix in [36], but the result is that we can express the non-trivial matrix valued part of the evolution equations as

$$\mathbf{u}(\mu_h, \mu_s) = \left(\mathbf{1} + \frac{\alpha_s(\mu_s)}{4\pi}\mathbf{V}_2\right) \mathbf{U} \exp\left\{\frac{\gamma_{D,0}}{2\beta_0} \ln \frac{\alpha_s(\mu_h)}{\alpha_s(\mu_s)}\right\} \mathbf{U}^{-1} \left(\mathbf{1} - \frac{\alpha_s(\mu_h)}{4\pi}\mathbf{V}_2\right)\,, \tag{3.4.60}$$

where γ_D^0 is a diagonal matrix related to γ^0 by

$$\gamma_D^0 = \mathbf{U}^{-1}\gamma^0\mathbf{U}\,, \tag{3.4.61}$$

for some matrix $\mathbf{U}$. The term in the middle of Eq. (3.4.60) can therefore easily be computed since the exponential of a diagonal matrix is simply given by exponentiating each of the diagonal entries individually. This is often denoted

$$\left(\left[\frac{\alpha_s(\mu_h)}{\alpha_s(\mu_s)}\right]^{\frac{\vec{\gamma}^{h}(0)}{2\beta_0}}\right)_D = \exp\left\{\frac{\gamma_D^0}{2\beta_0} \ln \frac{\alpha_s(\mu_h)}{\alpha_s(\mu_s)}\right\}, \tag{3.4.62}$$

where the vector $\vec{\gamma}^0$ consists of the eigenvalues of γ^h; the diagonal entries in γ_D^0. The matrix $\mathbf{V}_2$ encodes higher order corrections to this, details can be found in [36].

3.4.7 Resummation Accuracy

Having obtained resummed hard scattering kernels in the soft Eq. (3.4.42) and boosted soft Eq. (3.4.44) limits, we now examine what level of resummation can be achieved given the current status of perturbative calculations. In Table 3.1, we list the perturbative orders at which the matching functions and anomalous dimensions

need to be evaluated in order to achieve resummation at a given logarithmic accuracy. We use the so-called *Notation′* (primed notation) as outlined in [50] to denote the accuracy of our resummation.

	Γ^i_{cusp}	γ_i	$\mathbf{H}^{(m)}, \widetilde{\mathbf{S}}^{(m)}, C_D, \widetilde{S}_D$
NLL	NLO	LO	LO
NNLL	NNLO	NLO	NLO
NNLL′	NNLO	NLO	NNLO

Table 3.1: Perturbative orders at which the cusp anomalous dimension, all other anomalous dimensions γ_i, and matching functions need to be evaluated in order to obtain resummation at a given logarithmic order.

The cusp anomalous dimension is fully known to three-loop order [61], results for the other anomalous dimensions to NLO can be found in [62–68], The massive hard $\mathbf{H}^m_{ij}$ and soft functions $\widetilde{\mathbf{S}}^m_{ij}$ have been extracted to NLO only [36], as a result we can perform resummation in the threshold limit only to NNLL accuracy. On the other hand, the matching functions $\mathbf{H}_{ij}, \widetilde{\mathbf{S}}_{ij}, C_D$ and $\widetilde{S}_D$ are all known to NNLO accuracy [37, 69, 70], enabling resummation to NNLL′ accuracy in the boosted soft limit. In terms of the perturbative expansion of the exponents in the evolution factors Eqs. (3.4.53), (3.4.54) and (3.4.55) this corresponds to keeping the first three g-functions (note both NNLL and NNLL′ require anomalous dimensions at the same order). Keeping only the first two g-functions results in NLL resummation as can be seen by the lower perturbative order of the anomalous dimensions in the first line of Table 3.1.

As highlighted in Section 3.4.1 in the discussion following Eq. (3.4.6), in Mellin space the perturbative expansion of the cross section gives corrections of the form $\alpha_s^n L^k$ where $L = \ln \bar{N}$ and $0 \leq k \leq 2n$. The logarithms accounted for by the resummation at each order in perturbation theory for a given resummation accuracy is indicated in Table 3.2. The difference between the NNLL and NNLL′ accuracies to which our different resummed results can be calculated amounts to a single logarithm at each order in perturbation theory.

Accuracy	$\alpha_s^n L^k$
NLL	$2n-1 \leq k \leq 2n$
NNLL	$2n-3 \leq k \leq 2n$
NNLL′	$2n-4 \leq k \leq 2n$

Table 3.2: Powers of $L = \ln \bar{N}$ at N^{n}LO captured by the resummed result for a given resummation accuracy.

3.4.8 Mellin Inversion

We now need to apply the inverse Mellin transform in order to return our Mellin space results to momentum space where predictions can be made. This amounts to applying Eq. (3.4.2) to our hadronic cross sections with the resummed hard scattering kernels. Explicitly we want

$$\frac{d^2\sigma}{dM\, d\cos\theta} = \frac{8\pi\beta_t}{3sM} \sum_{ij} \frac{1}{2\pi i} \int_{c-i\infty}^{c+i\infty} dN\, \tau^{-N}\, \widetilde{C}_{ij}(N, M, m_t, \cos\theta, \mu_f)\, \widetilde{\mathcal{L}}_{ij}(N, \mu_f)\,, \tag{3.4.63}$$

where $\widetilde{C}$ is either $\widetilde{C}^{\text{Soft}}$ or $\widetilde{C}^{\text{Boosted}}$ as given by Eqs. (3.4.42) and (3.4.44) respectively. Unfortunately, because we choose the soft scales $\mu_s \sim M/\bar{N}$ (and $\mu_{ds} \sim m_t/\bar{N}$) in Mellin space the inverse transform develops a Landau singularity as we integrate over N. The prescence of this singularity requires the adoption of a prescription to define the result. We adopt the so-called *Minimal Prescription* (MP) [71]. In this prescription, the integration contour's interception with the real axis (the variable c) is chosen to run to the right of all singularities *except* that from the Landau pole. It is shown in [71] that this is equivalent to performing the inverse transform of the expansion of the resummed hard-scattering kernel order by order in α_s and that it renders a finite result for this asymptotic series. Figure 3.2 gives a pictorial representation of the inverse Mellin transform. On the left is shown the conventional choice for a the inverse transform. The right plot however shows the implementation of the MP contour. In addition to placing the interception with the real axis to the left of the Landau pole at large N, denoted N_L, the contour is also deformed towards the negative real axis in order aid the numerical convergence.

A final point to address on inverting the resummed result back into momentum space

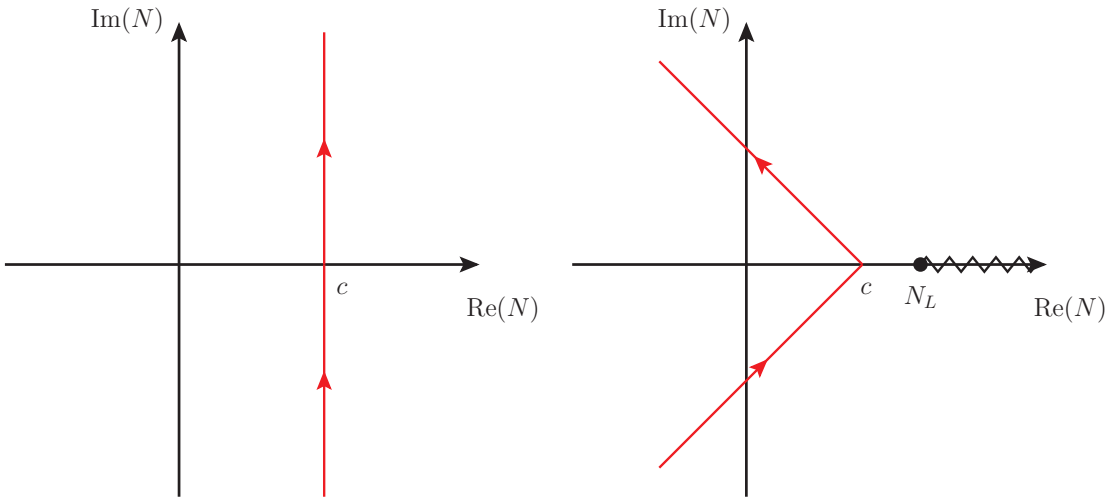

Figure 3.2: Contours chosen to perform the inverse Mellin transform.

is the nature of the threshold logs which are recovered. In Section 3.4.1 we discussed the effects of the Mellin transform on the leading power threshold logarithms. The limit $z \to 1$ corresponds to $N \to \infty$ in Mellin space and we subsequently took this limit on the Mellin transformation of the threshold logs to obtain a series in $\ln N$ as in Eq. (3.4.6). An effect of taking this limit in Mellin space means that on performing the inverse transform, we do not recover exactly the threshold logarithms in Eq. (3.4.4). Instead we recover distributions of the form

$$P'_n(z) = \left[\frac{\ln^n(-\ln z)}{-\ln z}\right]_+ . \tag{3.4.64}$$

These distributions exhibit the same behaviour as $z \to 1$ and therefore reproduce the same dynamics in this region. We should stress however, that the inverse transform is taken numerically and so we never explicitly see such terms appearing. That the inverse transform is also taken with the product of the parton luminosities in Mellin space could further complicate this issue.

3.5 Matching to Fixed Order Calculations

The resummed formulas Eqs. (3.4.42) and (3.4.44) are only valid to leading power in their respective limits. The pure threshold resummed calculation Eq. (3.4.42) misses power corrections away from partonic threshold, while the small-mass resummed result in the threshold limit Eq. (3.4.44) misses the very same power corrections as well as those subleading in m_t/M. Away from regions of phase space where these formulas dominate it is necessary to match these to exact fixed order calculations in order to obtain results applicable to the whole of phase space. As such we end this chapter by discussing how to match the resummed cross sections Eqs. (3.4.42) and (3.4.44) to fixed order (N)NLO calculations. This will result in predictions which are exact to (N)NLO and include the resummation of threshold logs, as well as small mass logs from the threshold limit. While matching to NNLO will form the main results of this work, it is also illustrative for the analysis performed in Chapter 4 to discuss matching on to NLO results.

An important idea in what follows is that of expanding the resummed results to some given order. The resummed results contain logarithmic terms to all orders in α_s, as can be seen via the exponentials in Eqs. (3.4.53)-(3.4.55). Expanding these as a power series in α_s reproduces the resummed logarithms, including those at (N)NLO. As will be detailed explicitly below, we wish to add to these resummed results the exact results at (N)NLO. Simply adding the two together results in a double counting of the resummed terms at (N)NLO. It is therefore important to be able to expand the resummed results to (N)NLO in order to subtract these contributions from the sum of fixed order and resummed results which would otherwise double count such contributions.

We will first match the threshold resummed result Eq. (3.4.42) to fixed order, before addressing how to also include the contributions from the joint boosted-soft resummation. This is achieved by adding to the resummed result the exact (N)NLO and subtracting the expansion of the resummed result to (N)NLO in order to avoid

double counting such contributions. We thus have

$$d\sigma^{(\mathrm{N})\mathrm{NLO}+\mathrm{NNLL}_m} = d\sigma^{\mathrm{NNLL}_m} + \left(d\sigma^{(\mathrm{N})\mathrm{NLO}} - d\sigma^{\mathrm{NNLL}_m}\Big|_{\substack{(\mathrm{N})\mathrm{NLO}\\ \text{expansion}}} \right), \tag{3.5.1}$$

where $d\sigma^{\mathrm{NNLL}_m}$ denotes the (differential) cross section obtained from using Eq. (3.4.42) in Eq. (3.4.3) to obtain a resummed hadronic cross section. The notation $d\sigma^{(\mathrm{N})\mathrm{NLO}}$ simply refers to the exact fixed order (N)NLO result and $d\sigma^{\mathrm{NNLL}_m}\Big|_{(\mathrm{N})\mathrm{NLO}}$ to the (N)NLO expansion the first term. The expansion of the resummed result is somewhat different depending on whether one expands to NLO or NNLO. The expansion to NLO is rather straightforward; we simply set each of the matching scales in the soft resummed result equal to the factorisation scale $\mu_h = \mu_s = \mu_f$

$$d\sigma^{\mathrm{NNLL}_m}\Big|_{\substack{\mathrm{NLO}\\ \text{expansion}}} = d\sigma^{\mathrm{NNLL}_m}\Big|_{\substack{\mu_h=\mu_f\\ \mu_s=\mu_f}}. \tag{3.5.2}$$

This works because the matching functions in the massive hard and soft functions $\mathbf{H}^{(m)}$, $\widetilde{\mathbf{S}}^{(m)}$ are known exactly to NLO. On expanding the exponents, the μ_h and μ_s dependence must cancel to leave only μ_f dependence at this order. Since setting the matching scales equal to the factorisation scale effectively turns of the resummation off ($\mathbf{U}_1^m \to 1$), we simply retrieve the matching functions in fixed order. Expanding to NNLO is a little more involved. At NNLO the μ_h and μ_s dependence which is generated from the expansion of the evolution function is not entirely cancelled by the matching functions, since the NNLO terms are not present in them. However we know that the μ_h and μ_s dependence *would* cancel if the NNLO terms were present. We can use this to quickly ascertain the form of the expanded exponent. Writing the NNLO expansion as

$$d\sigma^{\mathrm{NNLL}_m}\Big|_{\substack{\mathrm{NNLO}\\ \text{expansion}}} = d\sigma^{\mathrm{NNLL}_m}\Big|_{\substack{\mathrm{NLO}\\ \text{expansion}}} + d\sigma^{\mathrm{NNLL}_{m,(2)}}, \tag{3.5.3}$$

where $d\sigma^{\mathrm{NNLL}_{m,(2)}}$ is the cross section obtained from the NNLO terms generated by the expansion of the evolution function. We can write this as the contribution generated by the NNLO correction to the hard-scattering kernel at two different

scales

$$\begin{aligned}\widetilde{C}^{(2)} = &\operatorname{Tr}\left[\mathbf{H}_m^{(2)}(\mu_f)\widetilde{\mathbf{S}}_m^{(0)}(\mu_f) + \mathbf{H}_m^{(1)}(\mu_f)\widetilde{\mathbf{S}}_m^{(1)}(\mu_f) + \mathbf{H}_m^{(0)}(\mu_f)\widetilde{\mathbf{S}}_m^{(2)}(\mu_f)\right] \\ &- \operatorname{Tr}\left[\mathbf{H}_m^{(2)}(\mu_h)\widetilde{\mathbf{S}}_m^{(0)}(\mu_s) + \mathbf{H}_m^{(1)}(\mu_h)\widetilde{\mathbf{S}}_m^{(1)}(\mu_s) + \mathbf{H}_m^{(0)}(\mu_h)\widetilde{\mathbf{S}}_m^{(2)}(\mu_s)\right] , \end{aligned} \tag{3.5.4}$$

where we have used the perturbative expansion of the hard and soft function as

$$\begin{aligned}\mathbf{H}^m &= \alpha_s^2\left[\mathbf{H}_m^{(0)} + \left(\frac{\alpha_s}{4\pi}\right)\mathbf{H}_m^{(1)} + \left(\frac{\alpha_s}{4\pi}\right)^2\mathbf{H}_m^{(2)} + \dots\right] , \\ \widetilde{\mathbf{S}}^m &= \widetilde{\mathbf{S}}_m^{(0)} + \left(\frac{\alpha_s}{4\pi}\right)\widetilde{\mathbf{S}}_m^{(1)} + \left(\frac{\alpha_s}{4\pi}\right)^2\widetilde{\mathbf{S}}_m^{(2)} + \dots . \end{aligned} \tag{3.5.5}$$

While we do not have exact results for $\mathbf{S}_m^{(2)}$ or $\mathbf{H}_m^{(2)}$ the dependence on μ_h and μ_s arises only through logarithms. These logarithms are completely determined to NNLO by the NNLL resummation (as can be seen from Table 3.2) and so we are able to explicitly evaluate Eq. (3.5.4). The reason this procedure works is down to the fact that the second line of Eq. (3.5.4) would vanish if the NNLO contributions were actually present in the matching functions, leaving only μ_f dependence. But since we know these contributions won't cancel in this instance, we can obtain the form of the NNLO term in the expansion by evaluating the logarithmic terms at NNLO at μ_f and subtracting the same result using μ_h in the hard function and μ_s in the soft function which remains un-cancelled. As mentioned, the μ dependence appears only in logarithmic terms, so any non-logarithmic terms (which are unknown) which could appear in the NNLO contributions to the hard and soft function simply cancel between the two lines in Eq. (3.5.4) and have no implications for the matching procedure. This completes the matching with the pure threshold resummation calculation and we now turn to the issue of combining this result with the boosted-soft resummation.

This will proceed in two steps; we will first match the boosted-soft resummation to the pure threshold result to produce a double resummation, before matching this on to fixed order. To produce results matched to NNLO this takes the form

$$d\sigma^{\text{NNLO+NNLL}'} = d\sigma^{\text{NNLL}'_b} + \left(d\sigma^{\text{NNLL}_m} - d\sigma^{\text{NNLL}_b}\Big|_{\substack{\mu_{ds}=\mu_s \\ \mu_{dh}=\mu_h}}\right)$$

$$+\left(d\sigma^{\rm NNLO} - d\sigma^{\rm NNLL'_{b+m}}\Big|_{\substack{\rm NNLO\\ \rm Expansion}}\right). \tag{3.5.6}$$

The notation $d\sigma^{\rm NNLL'_b}$ denotes the NNLL$'$ resummed (differential) hadronic cross section obtained by using Eq. (3.4.44). The first line in Eq. (3.5.6) matches the boosted-soft resummed result to the threshold resummed result. The boosted-soft resummed result, being built upon the pure threshold resummed result, already contains a subset of the threshold logs, namely those leading in the small-mass limit. In order to avoid double counting this subset, we must subtract them out. We can achieve this by considering Eqs. (3.3.7) and (3.3.8) which highlights that the product of C_D^2 and $\mathbf{H}$ is just the small-mass limit of the massive hard function $\mathbf{H}^m$ used in the threshold resummation and similarly for $\widetilde{S}_D^2$ and $\widetilde{\mathbf{S}}$ for $\widetilde{\mathbf{S}}^m$. Thus setting $\mu_{dh} = \mu_h$ and $\mu_{ds} = \mu_s$ removes the scale separation between these matching functions and we simply recover the threshold resummed result in the small mass limit. We can then use this result to remove the double counting after adding the boosted-soft resummed result to the purely threshold resummed one. The second line of this equation matches this joint resummation to the exact fixed order result at NNLO. The notation $d\sigma^{\rm NNLL'_{b+m}}$ refers to the joint resummed result which is achieved on the first line. The NNLO expansion of this is achieved through expanding each of the terms to NNLO. The expansion of the NNLL$'$ result is given simply by setting each of the matching scales equal to the factorisation scale since each of the matching functions is known to NNLO in this instance. The NNLO expansion of the two NNLL resummed terms is performed in complete analogy to the NNLO expansion performed in Eq. (3.5.3). This completes the matching of the two resummed formulas and the NNLO fixed order result.

Matching to NLO proceeds in much the same manner as matching to NNLO. Specifically, it is achieved as follows

$$\begin{aligned} d\sigma^{\rm NLO+NNLL'} = d\sigma^{\rm NNLL'_b} &+ \left(d\sigma^{\rm NNLL_m} - d\sigma^{\rm NNLL_b}\Big|_{\substack{\mu_{ds}=\mu_s\\ \mu_{dh}=\mu_h}}\right) \\ &+ \left(d\sigma^{\rm NLO} - d\sigma^{\rm NNLL_m}\Big|_{\substack{\mu_s=\mu_f\\ \mu_h=\mu_f}}\right). \end{aligned} \tag{3.5.7}$$

The first line of Eq. (3.5.7) is identical to that in the NNLO matching in Eq. (3.5.6). The difference occurs in the matching to fixed order on the second line. In this case, since all the matching functions we use are known to NLO, the result after matching the two resummation formulas reproduces the NLO result in the threshold limit. Therefore, when matching to the exact NLO result, we need only subtract the threshold logarithms at this order. Alternatively, one can see that the NLO contributions in the boosted soft limit will cancel on the first line, leaving only threshold logs double counted when combining with the NLO result.

There are some additional considerations which arise from the contributions from heavy quark loops when matching for the NLO+NNLL′ result. As mentioned in Section 3.3 there are contributions from such heavy quarks (which we include in the coefficient $\widetilde{c}^{t}_{ij}$ in Eq. (3.4.10)) that factorise out of the cross section in the boosted-soft limit. When matching to NLO we could like to include the contributions from these heavy quark loops which are known to NNLO in the $m_t \to 0$ limit. These contributions are proportional to the number of heavy quarks n_h considered. The issue is that such contributions do not factorise out of the threshold resummed piece $d\sigma^{\mathrm{NNLL}_m}$ which partially contains some of these contributions at NNLO (and beyond). When including these effects it is therefore necessary to subtract the contributions in $d\sigma^{\mathrm{NNLL}_m}$ proportional to n_h at NNLO only. This is simply because the NNLO expansion of the threshold resummed result will not correctly reproduce the n_h terms at this order since the matching functions are only known to NLO.

Chapter 4

Phenomenology of Resummed Calculations

We now turn to the phenomenological predictions which can be made using the factorised form of the cross sections we have obtained in the previous section. That is we numerically evaluate Eqs. (3.5.7) and (3.5.6) to obtain differential distributions which can be compared with experimental data. Throughout this Chapter we make use of the NNPDF3.0 PDF sets [72], using (N)NLO PDFs for fixed order (N)NLO predictions and NNLO PDFs for all resummed calculations unless otherwise specificed. To incorporate these into the numerical implementation we have made use of LHAPDF6 [73] with $\alpha_s(M_Z) = 0.118$ and set $m_t = 173.3$ GeV. In addition, the necessary numerical integration for the resummed results is carried out with the use of the `CUBA` integration libraries [74, 75]. Results for the exact (N)NLO results are obtained from the authors of [42]. Some NLO results are generated through the use of `MCFM` [76]. Results presented in this Chapter are for the LHC operating at a centre-of-mass energy $\sqrt{s} = 13$ TeV, thought it is of course possible to produce results for the LHC running at 8 TeV or for $p\bar{p}$ collisions at the Tevatron. Uncertainties are estimated by varying (independently) each of the matching scales μ_h, μ_s, μ_{dh}, μ_{ds} and the factorisation scale μ_f about their default value by a factor of two in each direction whilst keeping the others fixed. In the fixed order calculations,

we keep the renormalisation and factorisation scales equal and vary them in unison. As discussed in Section 3.4.6, in order to free the matching functions $\mathbf{H}^{(m)}$, $\widetilde{\mathbf{S}}^{(m)}$, C_D and $\widetilde{S}_D$ from large logarithmic corrections we set the default values of the matching scales as

$$\mu_h = M \qquad \mu_s = M/\bar{N}$$
$$\mu_{dh} = m_t \qquad \mu_{ds} = m_t/\bar{N}\,.$$

The choice of factorisation scale μ_f depends on the type of distribution under study and will be specified in each case. The final results are obtained by computing each of the terms $d\sigma$ in Eq. (3.5.6) separately and combining the resulting distributions.

We will first study the pair invariant mass distributions (PIM) of the produced $t\bar{t}$ system and assess the impact of resummation improved results compared with respect to those obtained in fixed order calculations. Following this we will also present predictions for the p_T distribution of the (anti-)top quark using Eq. (3.2.4). Finally, this Chapter will conclude with a short analysis regarding the effect of the resummation performed here on the total cross section.

4.1 Invariant Mass Distributions

4.1.1 Predictions for LHC Phenomenology

When considering PIM distributions (and others), it is typical to select a factorisation scale correlated to the observable being predicted. With that in mind, we first present results obtained using $\mu_f = M$ and $\mu_f = M/2$ in the left and right hand plots of Figure 4.1 respectively. Each plot displays the results from a fixed order NNLO (red) and resummed NNLO+NNLL$'$ (blue hatched) calculation. In the lower panel the ratio of these two distributions to the NNLO result at its default scale is displayed such that

$$\text{Ratio} = \frac{d\sigma}{d\sigma^{\text{NNLO}}(\mu_f = \mu_f^{\text{default}})}\,. \tag{4.1.1}$$

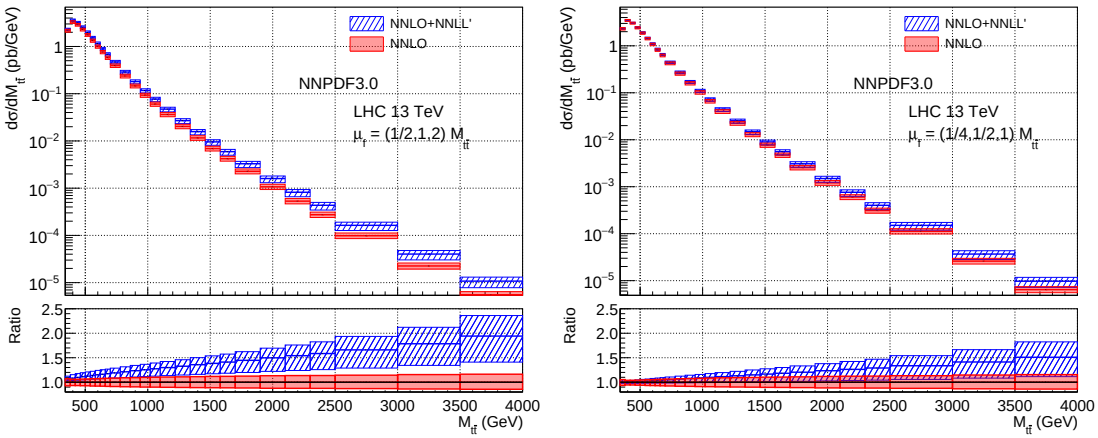

Figure 4.1: Pair invariant mass distributions at NNLO (red) and NNLO+NNLL′ (blue hatched) accuracy. Results are obtained using $\mu_f = M$ (left) and $\mu_f = M/2$ (right)

The same scale is used on the vertical axes for ease of comparison and the bands around the central values correspond to the uncertainties obtained by varying each of the scales as described at the beginning of this Chapter. We see that the effect of the resummed result compared to fixed order for both scale choices is to enhance the tail of the cross section at large values of M. The enhancement is more pronounced for the choice $\mu_f = M$ than $\mu_f = M/2$, which essentially doubles the cross section in the highest energy bins displayed. For $\mu_f = M$ the uncertainty bands do not overlap for $M \gtrsim 1.5$ TeV, while there is very slight overlap for $\mu_f = M/2$ across the entire range.

While we have presented results for the canonical choices $\mu_f \sim M$ the authors of the NNLO fixed order predictions with dynamical scales [42] also performed an analysis of different possible scale choices which one might consider for each type of observable. Based on maximizing the convergence of the perturbative series in fixed order, it was found that for PIM distributions $\mu_f = H_T/4$ was an appropriate choice for the factorisation scale. Here H_T is defined as the sum of the transverse mass of the final state particles of interest. In this case,

$$H_T = \sqrt{m_t^2 + p_{T,t}^2} + \sqrt{m_t^2 + p_{T,\bar{t}}^2}\,, \tag{4.1.2}$$

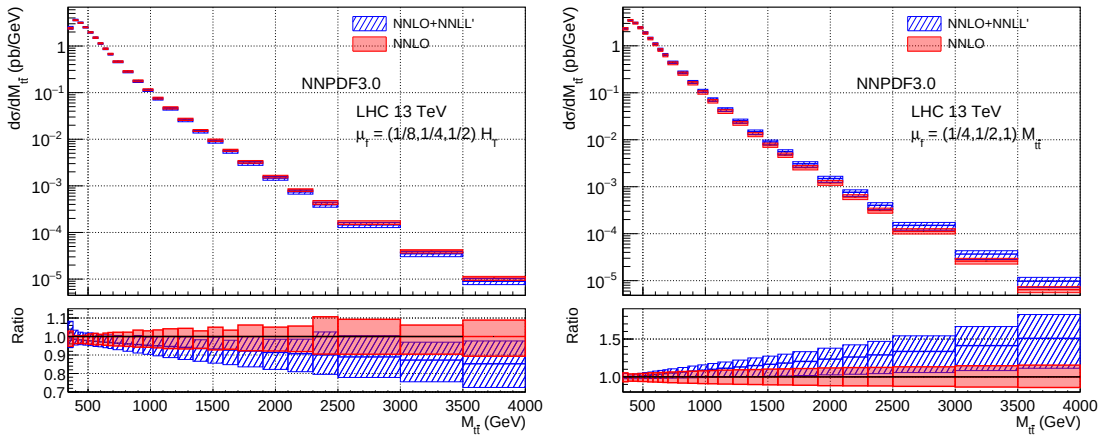

Figure 4.2: Pair invariant mass distributions at NNLO (red) and NNLO+NNLL′ (blue hatched) accuracy. Results are obtained using $\mu_f = H_T/4$ (left) and $\mu_f = M/2$ (right).

where $p_{T,t}$ denotes the transverse momentum of the top quark. In Figure 4.2 we display predictions obtained using $\mu_f = H_T/4$ (left) next to those obtained from $\mu_f = M/2$ (right) for comparison. With the choice $\mu_f = H_T/4$ the effect of the resummed result compared to fixed order is, in contrast to $\mu_f = M/2$, to soften the high energy tail of the distribution. The uncertainty bands for $\mu_f = H_T/4$ have a much more significant overlap with the fixed order result than those from $\mu_f = M/2$. To study this further, it is helpful to take ratios of predictions at the two different scale choices. We show in the top (middle) plot of Figure 4.3 the ratios of the results from NLO (NNLO) calculations evaluated with the two different scale choices normalised to the result with $\mu_f = H_T/4$, while the bottom plot displays the analogous predictions from the NNLO+NNLL′ calculation. We see that the NLO calculation displays strong dependence on the parametric choice of factorisation scale. This discrepancy is not remedied at NNLO and the two scale choices still exhibit serious disagreement, particularly for large values of M. Indeed the uncertainty bands do not overlap for $M \gtrsim 1.1$ TeV. By definition, the difference between the NNLO predictions at two different scale choices must arise from terms N^{3}LO and higher. This is suggests that such terms are not negligible, at least in the high energy tails of the distributions. The resummed predictions at NNLO+NNLL′ at the two

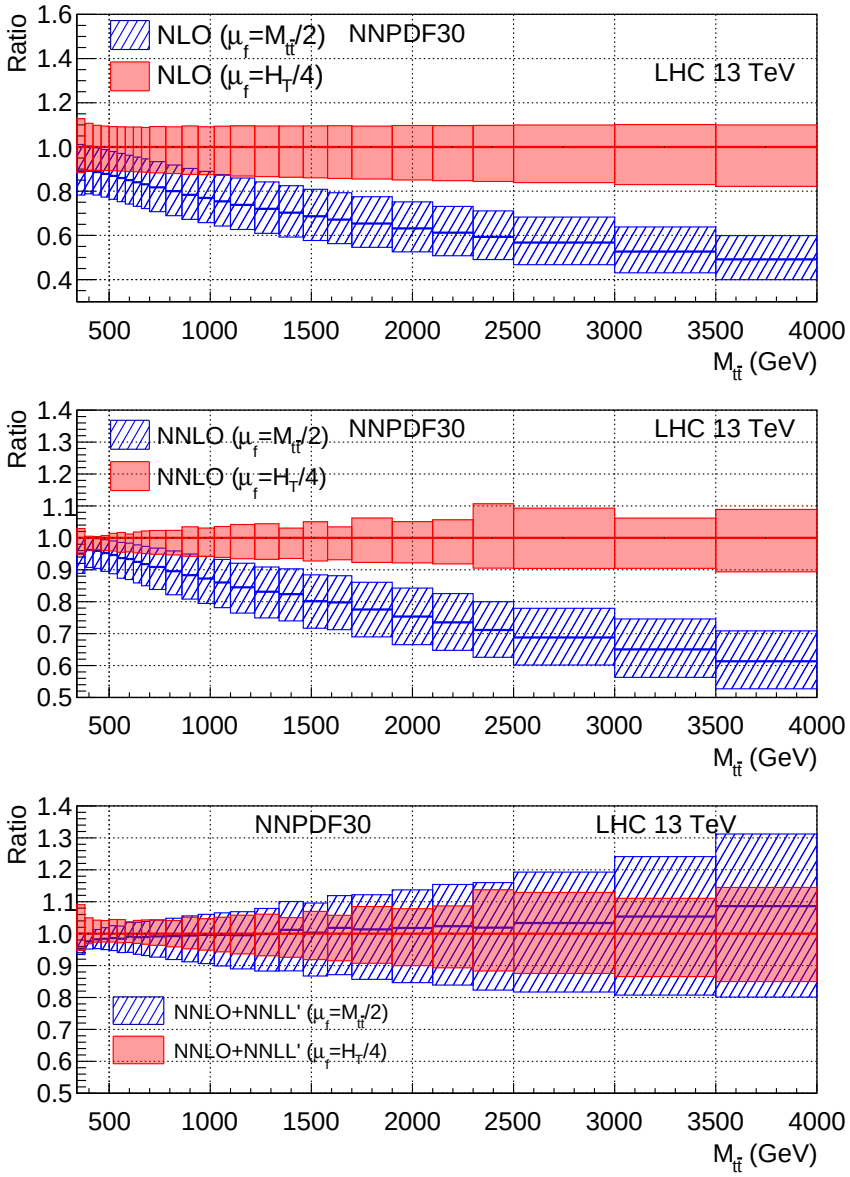

Figure 4.3: Predictions for the M distribution from fixed order (top/middle) and resummed (bottom) calculations for different scale choices $\mu_f = H_T/4$ (red) and $\mu_f = M/2$ (blue hatched). In each case the result is normalized to the prediction with $\mu_f = H_T/4$.

different scales however, are much more consistent with each other, the difference in central values not exceeding 10% across the displayed range. The fact that the resummed calculation produces results more consistent with each other suggests that most terms contributing to the difference in fixed order are accounted for through the resummation. In Figure 4.4 we plot the variation of the PIM distribution from two sample bins as a function of the factorisation scale. The top plot displays the variation in a bin at the peak of the differential cross section $M \in [380, 420]$ GeV while the bottom plot shows a region of high energy kinematics $M \in [2500, 3000]$ GeV. In each plot we give the variation of the bin with respect to two different choices of factorisation scale, $\mu_f \sim H_T$ (red shade) and $\mu_f \sim M$ (blue shade). In both plots we see the resummed results (dash lines) are less sensitive to the choice of μ_f than their fixed order counterparts. We can also see that in the lower energy bin the (N)NLO and resummed results are more consistent between scale choices i.e. that (N)NLO results from $\mu_f = M/2$ and $\mu_f = H_T/4$ give almost identical predictions, which can also be seen from the first few bins in Figure 4.3. We also see that this consistency is maintained across a wide variation of the scale choice. In the higher energy bin (lower plot), it can be seen that the choice of a lower factorisation scale in general leads to better perturbative convergence.

4.1.2 Factorisation Scale Studies

In order to further probe the differences between the scale choices $\mu_f \sim M$ and $\mu_f \sim H_T$, it is instructive to know how they compare numerically across the PIM distribution. It is straightforward to assess the size of $\mu_f \sim M$ in a given bin along the distribution, since it is in one-to-one correspondence with bin range. This is not the case for H_T based scales however, which can take on a range of values for a given value of M. Using the code developed to implement the resummed formulas (Eqs. (3.4.42) and (3.4.44)), we can study the relative magnitude of H_T to that of M. Since the resummed formulas are developed in the soft limit, the produced top quarks are back to back. In this limit we can relate H_T directly to M and $\sin\theta$, the

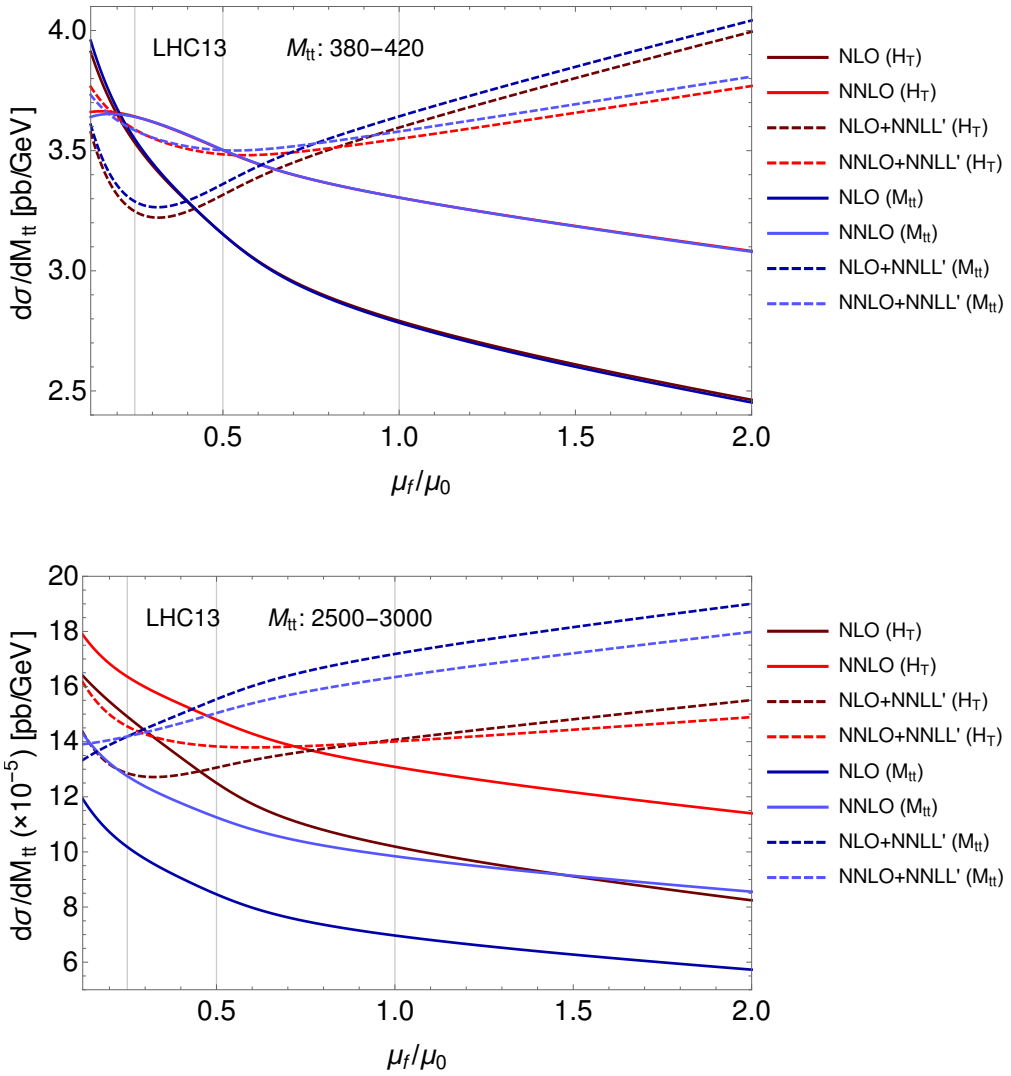

Figure 4.4: Impact of factorisation scale variation for PIM distributions in two separate kinematic regions; a high cross section region (top) and a high energy region (bottom). Grey lines mark typical choices for the default factorisation scale.

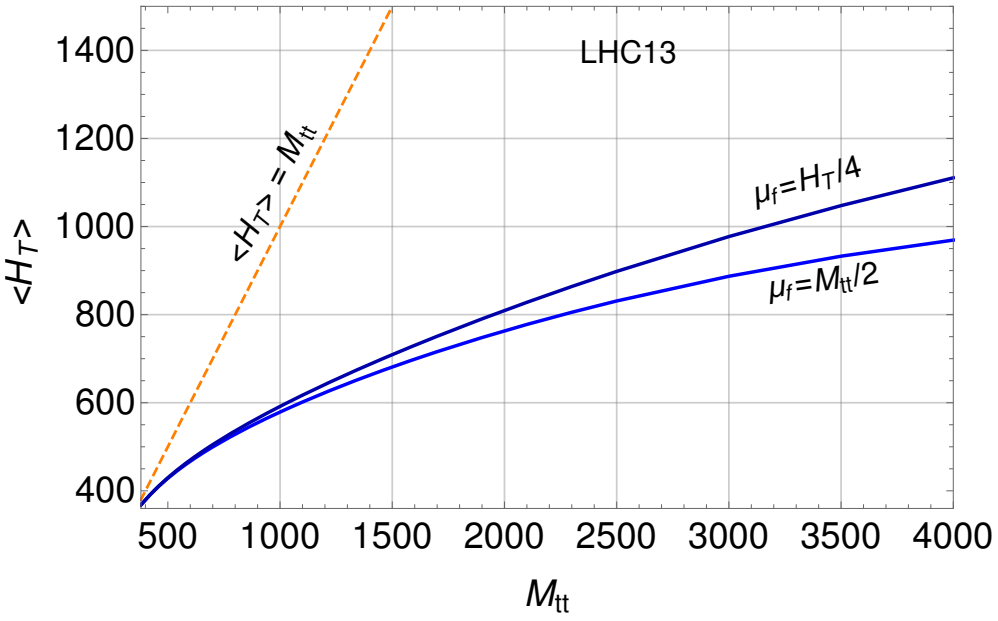

Figure 4.5: The average numerical value of H_T sampled for a given fixed value of M. The blue lines represent the resummed result, matched to soft resummation, but not to any fixed order, see Eq. 4.1.4 for details.

angle between the produced quarks and the initial incident partons, as

$$H_T = 2\sqrt{m_t^2 + \left(\frac{M^2}{4} - m_t^2\right)\sin^2\theta}\,. \tag{4.1.3}$$

In producing the PIM distributions the angle θ is integrated over and so H_T can vary between $H_{T,\min} = 2m_t$ and $H_{T,\max} = M$. In Figure 4.5 we plot the *average* H_T, $< H_T >$ that is sampled as a function of M. Explicitly, we compute $< H_T >$ from,

$$< H_T >= \frac{\displaystyle\int_{H_{T,\min}}^{H_{T,\max}} \frac{d\sigma^{\rm res}}{dM\; dH_T}\; H_T\; dH_T}{\displaystyle\int_{H_{T,\min}}^{H_{T,\max}} \frac{d\sigma^{\rm res}}{dM\; dH_T}\; dH_T}\,, \tag{4.1.4}$$

which gives the average H_T used for computing a point in the $d\sigma^{\rm res}/dM$ distribution for each value of M. This double differential distribution is obtained using a change of variables; formally the same procedure as that used to obtain p_T distributions as outlined at the end of Section 3.2. The notation $d\sigma^{res}$ indicates that this calculation only includes the resummed results and is not matched to any fixed order calculation. Specifically, it is the small-mass resummation in the threshold limit matched with pure threshold resummation (the top line of Eq. (3.5.6) only). Comparing typical

numerical values for μ_f, we see that at $M = 1$ TeV for example, $\mu_f \sim 500$ GeV for $\mu_f = M/2$ while $\mu_f \sim 150$ GeV for $\mu_f = H_T/4$, which is significantly lower. We see then that the scale choice $\mu_f = H_T/4$ leads to a smaller value of the factorisation scale than $\mu_f = M/2$ for a given bin in the PIM distribution. This disparity widens as one goes to higher values of M. It is known that picking a lower scale choice for $t\bar{t}$ predictions generally raises the cross section (see Figure 4.4), so it is not so surprising that the choice $H_T/4$ leads to lower K factors; the NLO result rises faster than the NNLO prediction, closing the gap between them.

4.1.3 Convergence of Perturbative Series

A key criterion in determining an appropriate scale choice in [42] was that of maximizing the convergence of the perturbative series. We therefore now turn to this question with regards to the resummed results. There is more than one way to look at the progression of resummed results. In what follows we look at a number of different comparisons. Figure 4.6 displays the traditional K-factor for fixed order calculations (top plot) as well as a K-factor for beyond NNLO corrections due to resummation (bottom plot). Examining first the fixed order K-factors we see that the choice of scale $\mu_f = M/2$ in general leads to K-factors which are rather large, leading to poor convergence of the perturbative series. On the other hand the scale choice $\mu_f = H_T/4$ leads to a much better convergence with K-factors closer to unity. In the lower plot, we show the K-factors for the corresponding resummed distributions. Here we define the K-factor as

$$K_{\mathrm{NNLO+NNLL'/NNLO}} = \frac{d\sigma^{\mathrm{NNLO+NNLL'}}}{d\sigma^{\mathrm{NNLO}}(\mu_f = \mu_f^{\mathrm{default}})} \,.$$

In the resummed case, we also see large K-factors for the prediction from $\mu_f = M/2$. This is perhaps not surprising given that we saw in Figure 4.3 that the resummation was able to bridge the gap between the fixed order results evaluated at the two different scale choices.

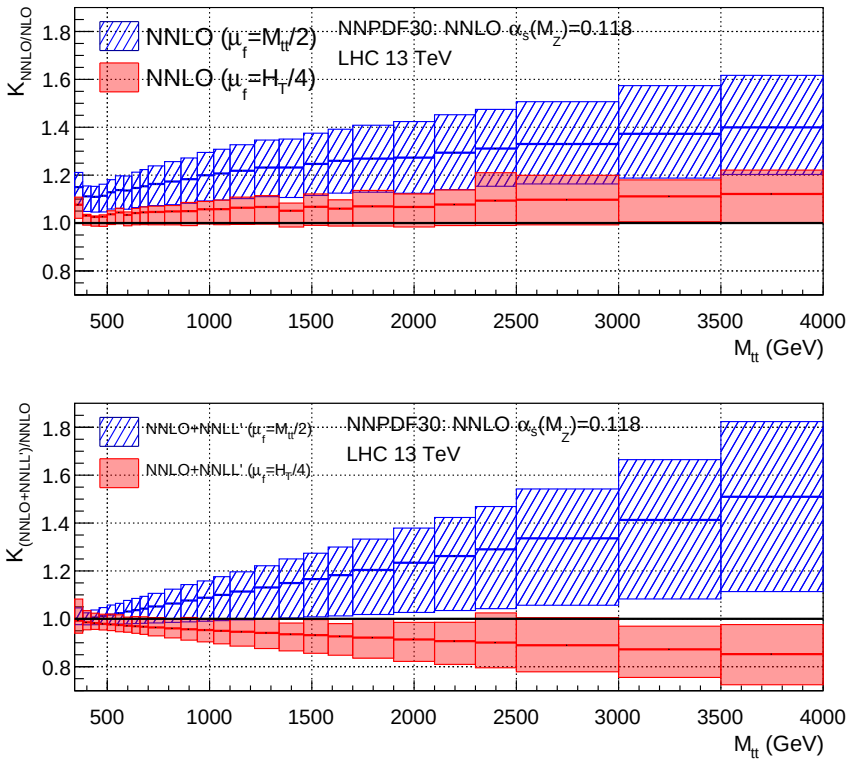

Figure 4.6: The K-factors obtained from fixed order NNLO/NLO, (top plot) and RG improved perturbation theory NNLO+NNLL′/NNLO, (bottom plot). In both cases the results are normalised to predictions of the same scale choice.

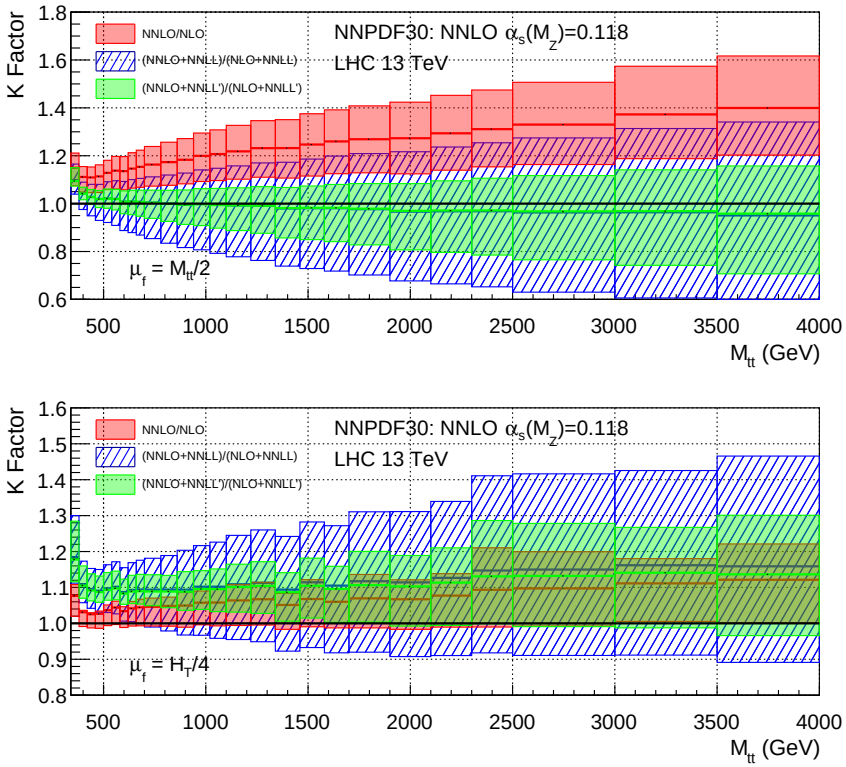

Figure 4.7: K-factors obtained from comparing NNLO and NLO at different levels of logarithmic accuracy, for $\mu_f = M/2$ (top) and $\mu_f = H_T/4$ (bottom).

We can consider other types of K-factor by computing different logarithmic accuracies of our resummed formulas. In Figure 4.7 we present three different K-factors for resummed results. Namely; NNLO/NLO (red), NNLO+NNLL/NLO+NNLL (blue hatched) and NNLO+NNLL′/NLO+NNLL′ (green). For each K-factor individually, exactly the same higher order (beyond NNLO) logarithms appear in both the NLO and NNLO matched results, and therefore the only difference between the numerator and denominator in each of the K-factors are the NNLO *constant terms*[1] and terms subleading in the soft limit at NNLO. The difference between each K-factor is the number of logarithms captured by the resummation at each order in perturbation theory. The top plot shows results from the scale choice $\mu_f = M/2$ where we see that progressively increasing the accuracy of the resummation between differing orders leads to K-factors which approach unity. Especially in the higher energy bins, we see that the central value of the K-factor NNLO+NNLL′/NLO+NNLL′ is almost identically one indicating that terms subleading in the soft limit at NNLO do not greatly contribute to the cross section in this region of phase space. Large corrections are still present in the first few bins however, emphasising the importance of matching to fixed order calculations near threshold. The lower plot shows the analogous predictions for the scale choice $\mu_f = H_T/4$. The K-factors are generally constant between the different logarithmic accuracies for this scale choice, straddling around 10% for most of the distribution. For this scale choice then we see the importance of matching to fixed order across the whole of the distribution, with the subleading and constant terms at NNLO still contributing significantly even in the tail.

Since we have seen in Figure 4.3 that the resummation closes the gap between the fixed order distributions at the two scale choices, it is interesting to also ask if such an effect is present at lower orders in perturbation theory. Figure 4.8 presents NLO results supplemented with NLL, NNLL and NNLL′ resummation, as well as the NNLO+NNLL′ result for comparison. Each result is normalised to the one for which

[1] Non-logarithmic contributions not captured by resummation.

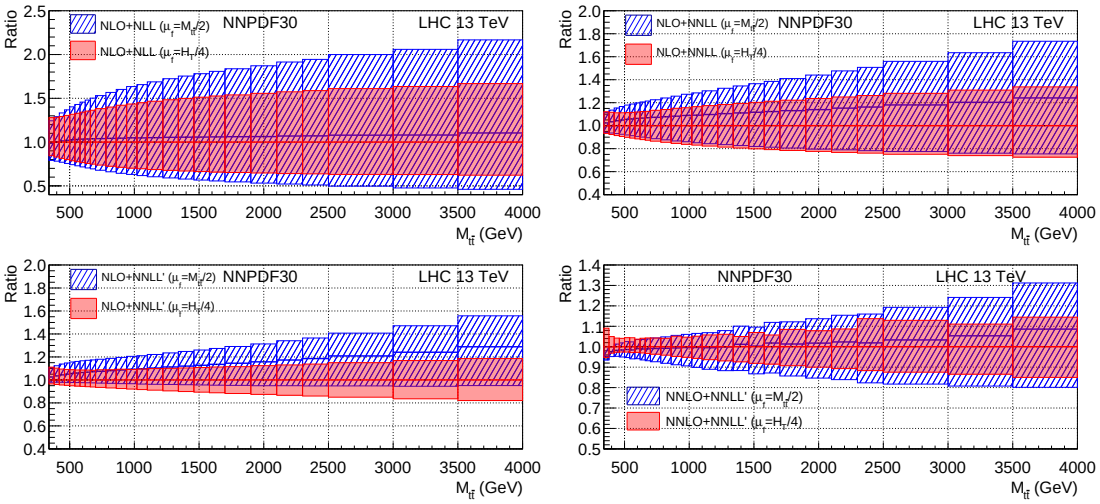

Figure 4.8: Predictions for the PIM distribution from NLO+NLL (top left), NLO+NNLL (top right), NLO+NNLL′ (bottom left) and NNLO+NNLL′ (bottom right) calculations for different scale choices $\mu_f = H_T/4$ (red) and $\mu_f = M/2$ (blue hatched). In each case the result is normalized to the prediction with $\mu_f = H_T/4$. Note the NLO+NLL result is computed using NLO PDFs.

$\mu_f = H_T/4$. Here we use NLO PDFs for the NLO+NLL resummed result. While the central values for the two scale choices at NLO+NLL (top left) lie close together compared with the fixed order NLO result, the associated uncertainties are incredibly large. At NLO+NNLL (top right), these uncertainties have somewhat diminished and though the central values are no longer as close to each other, both lie inside the uncertainty band of the other. At NLO+NNLL′ (bottom left) the uncertainties have again reduced, though the central values are not appreciably closer together. The final plot on the bottom right shows the last stage in this evolution, NNLO+NNLL′. Compared to NLO+NNLL′ we see again a drastic reduction in uncertainties as well as a more comfortable overlap between the central values of each prediction and the uncertainty band of the other.

The plots in Figure 4.8 allow us to check the convergence of predictions from differing scale choices as one includes more higher order logarithms, however we can also check the convergence of the series within a certain scale choice. That is, for each choice of scale, how do the results from NLO+NLL to NNLO+NNLL′ compare?

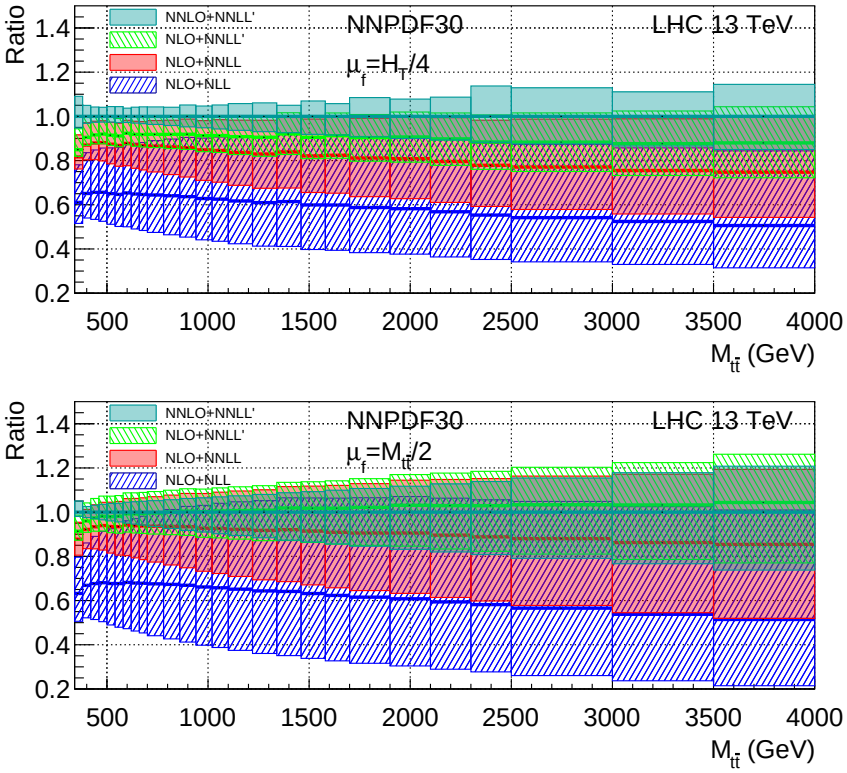

Figure 4.9: Predictions for the PIM distribution from NLO+NLL (blue hatched), NLO+NNLL (red), NLO+NNLL′ (green hatched) and NNLO+NNLL′ (blue transparent) calculations for different scale choices $\mu_f = H_T/4$ (top plot) and $\mu_f = M/2$ (bottom plot). In each case the result is normalized to the NNLO+NNLL′ prediction. Note that the NLO+NLL result is computed using NLO PDFs.

Figure 4.9 shows this progression for $\mu_f = H_T/4$ (top plot) and $\mu_f = M/2$ (bottom plot) normalised to the NNLO+NNLL′ prediction. This result contrasts to fixed order where the perturbative stability is quite different between $\mu_f = H_T/4$ and $\mu_f = M/2$. Instead, the resummed predictions have a more stable perturbative progression between the two scale choices.

4.1.4 Comparison of Joint and Threshold Resummation

Another question one might ask relates to what is gained by performing the combined small-mass and threshold resummation, compared with standard threshold resummation on its own. We address this question in Figure 4.10 where results from performing threshold resummation obtained using Eq. (3.5.1)(green) are shown

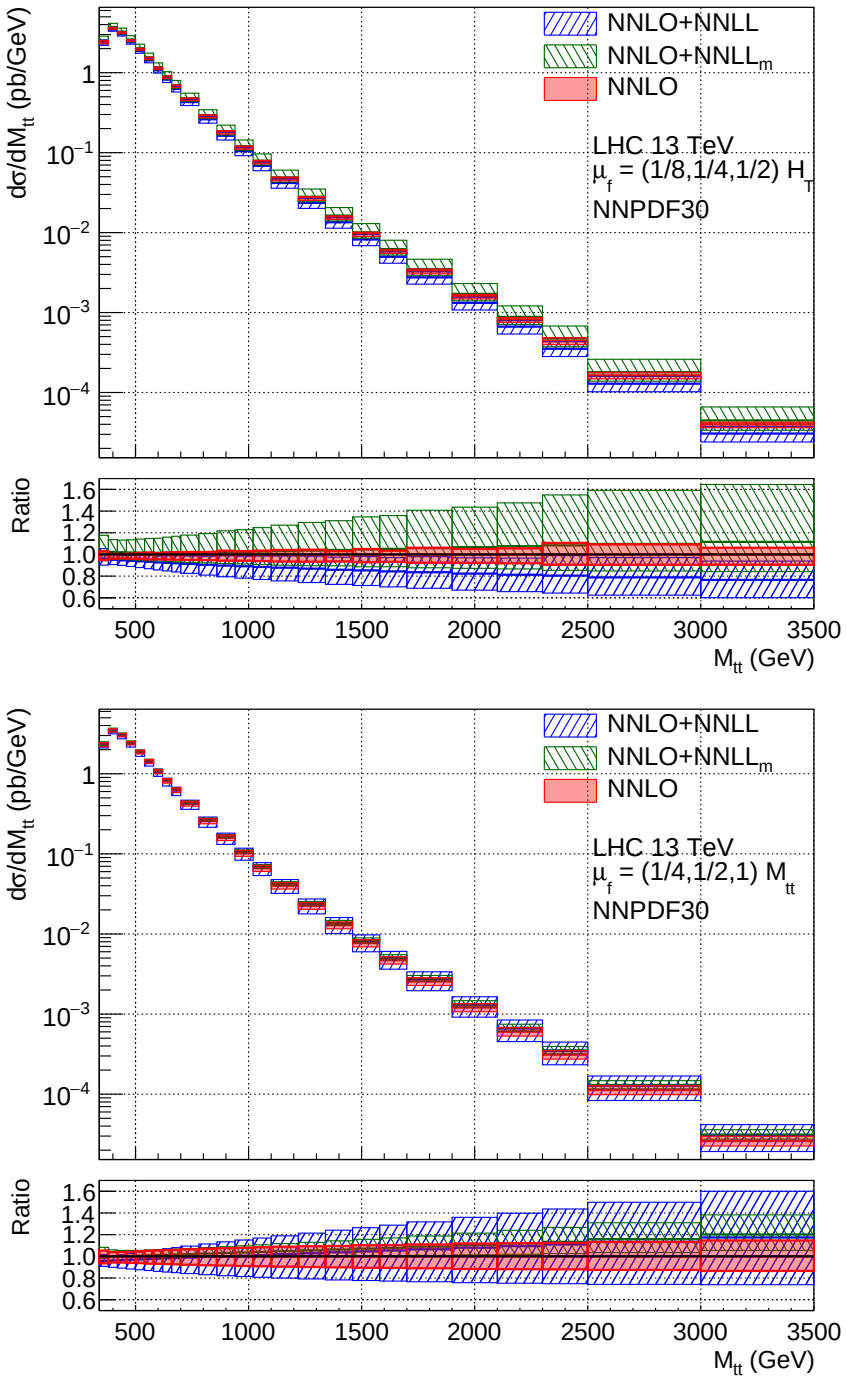

Figure 4.10: Pair invariant mass distributions for $\mu_f = H_T/4$ (top plot) and $\mu_f = M/2$ (bottom plot). Shown are predictions from fixed order NNLO (red), threshold resummed NNLO+NNLL (green hatched) and joint threshold and boosted-soft NNLO+NNLL (blue hatched) calculations.

alongside results from the joint resummation obtained from Eq. (3.5.6) (blue). Since threshold resummation was only computed to NNLO+NNLL, we also only compute the joint resummation to this order for a fair comparison and hence implement Eq. (3.5.6) to NNLL accuracy only. For comparison the ratios shown in the lower panels are normalised to the NNLO result shown in red. Examination of the upper plot, which gives results for the scale choice $\mu_f = H_T/4$ reveals that performing purely threshold resummation leads to a slight enhancement of the cross section for large M. Supplementing this with small-mass resummation in the threshold limit however leads to the opposite effect at large M, namely a softening in the tail of the spectrum relative to the fixed order result. This isn't so surprising since this is exactly the region where one might expect logarithms of the form $\ln^p(m_t/M)$ to play an increasingly important contribution to the cross section. Interestingly, in the lower plot, which shows predictions for the scale choice $\mu_f = M/2$, we see that the threshold resummation and joint resummation produce almost identical central values. Thus it would appear, at least in this instance, that the effect of the scale choice $\mu_f = M/2$ in pure threshold resummation seems to mimic the effect of resumming these small-mass logarithms in the threshold limit.

4.1.5 Rapidity Cuts

We noted from Figure 4.5 that the value of H_T in a given bin is generally considerably lower than M. We note that for a given value of M, H_T can be related to the angle the top quarks are produced at via Eq. (4.1.3). The fact that H_T is numerically quite small compared to M is suggestive that θ is also quite small, i.e. the angle of production is quite shallow.

In Figure 4.11, we show the average value of $\cos\theta$ sampled by the Monte-Carlo when computing the resummed results. This is computed analogously to the average H_T in Figure 4.5 and therefore only includes the resummed pieces of the calculation, in which the top quarks are produced back-to-back and we have no hard emissions.

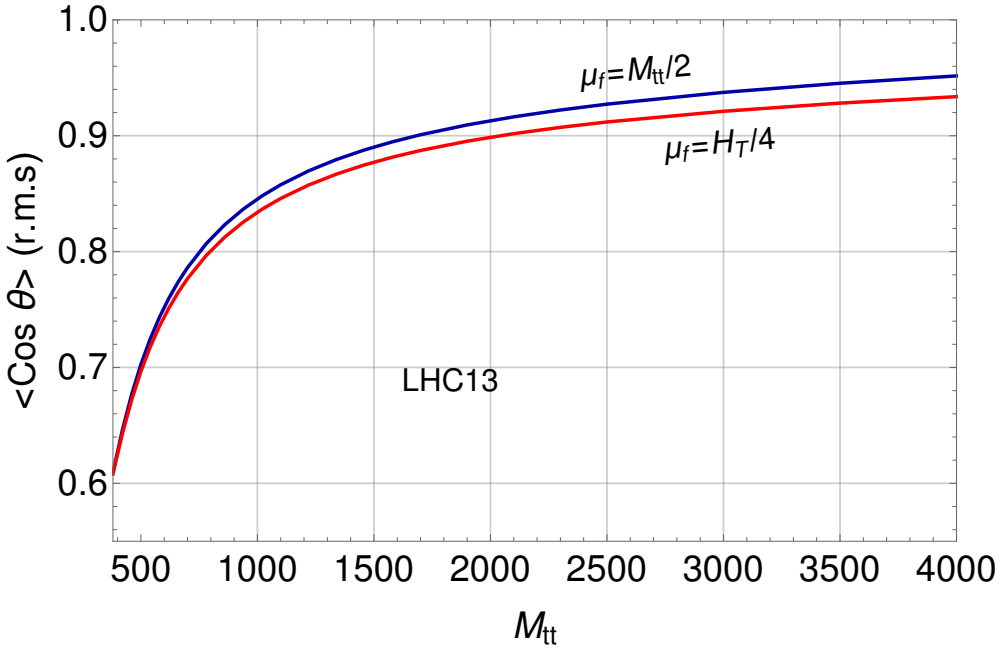

Figure 4.11: Average value of $\cos\theta$ as a function of M.

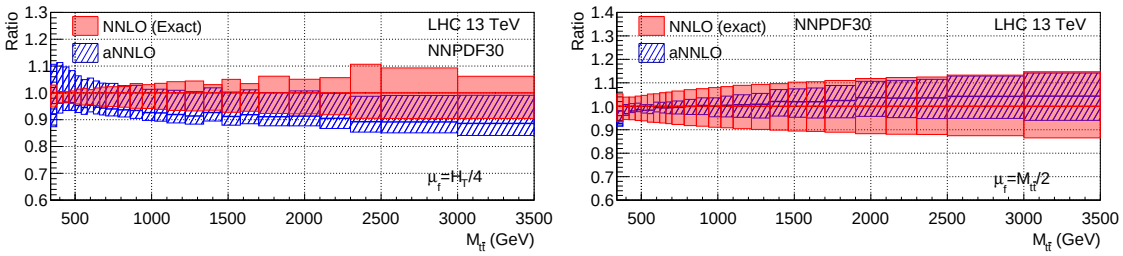

Figure 4.12: Comparison of approximate (aNNLO) and exact NNLO distributions.

By $M = 2$ TeV, the average value of $\cos\theta$ approaches 0.9, which corresponds to an angle of roughly 26° in the rest frame of the top pair.

An interesting thing to do therefore is place a cut on the rapidities of the top quarks, capturing only events which are central enough. Unfortunately, we cannot place cuts directly on the rapidities of the individual quarks. This is because the formalism used to perform the resummation in Chapter 4 loses information about the relative boost of the incoming partons. We can constrain the rapidity difference, $\Delta y = y_t - y_{\bar{t}}$ however, which is frame independent. As an example, we select a cut on the rapidity difference of $|\Delta y| < 4$, which corresponds to a cut of $|y| < 2$ for each quark in the soft limit. Since we do not have direct access to NNLO results with such cuts, we can perform the analysis using the approximate NNLO numbers produced by the

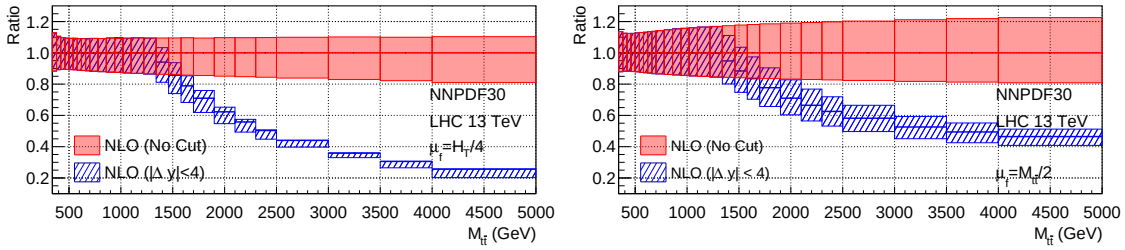

Figure 4.13: Comparison of NLO exact results with and without the rapidity difference cut at the two scale choices $\mu_f = H_T/4$ (left) and $\mu_f = M/2$ (right).

resummation formula. The approximate result is exact to NLO and includes all information from the RG equations for the matching functions in both the threshold and boosted soft limits to construct as much of the NNLO contribution as possible. It is prudent to check how well the approximate results actually replicate the exact ones. In Figure 4.12 we plot the aNNLO distributions compared with the exact NNLO result at the same scale choice, $\mu_f = H_T/4$ on the left and $\mu_f = M/2$ on the right. We see that the choice $\mu_f = M/2$ more accurately reflects the NNLO result than the choice $\mu_f = H_T/4$ does. The aNNLO result for the choice $\mu_f = M/2$ produces a much smaller uncertainty band and the central value stays within 5% of the exact result for most of the distribution. The choice $\mu_f = H_T/4$ on the other hand produces a central value which straddles the lower bound of the uncertainty from the fixed order result.

We can now look at the effect of the rapidity cuts on these distributions. For NLO results, we can use MCFM [76] to generate distributions with the relevant cuts. Figure 4.13 shows the effect of the rapidity difference cut $|\Delta y| \leq 4$ on the NLO results. Here predictions with the cut are compared to those without the cut at the same scale choice. The cut has no effect for $M \leq 1.3$ TeV since $|\Delta y| > 4$ is not accessible for such low energies. Beyond this energy however, the effect of the cut is quite severe, with the cross section less than half of its uncut value in the higher energy bins. We see that the cut has more of an effect on the distribution obtained with the scale choice $\mu_f = H_T/4$. Given that the uncut NLO distribution obtained using this choice of scale is larger than that obtained using $\mu_f = M/2$, one might

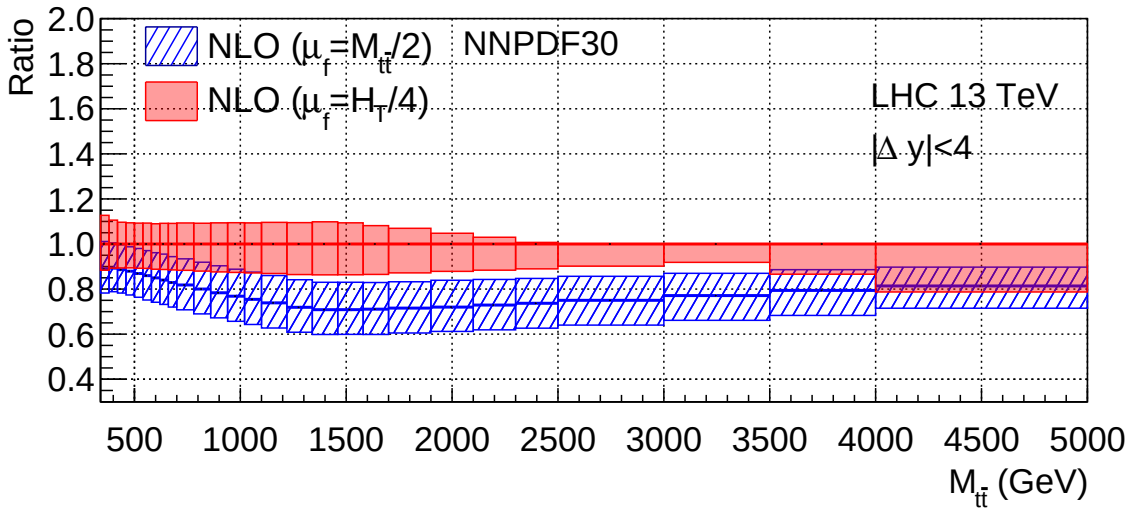

Figure 4.14: Comparison of the NLO distributions at two different scales with the rapidity cut.

suspect that the cut could bring the two results into better agreement.

In Figure 4.14 we plot the two distributions with cuts together. We see clearly that the effect of the cut is to bring the NLO results from the two different scale choices into better agreement. We see that the distribution using $\mu_f = M/2$ begins to fall compared to the $\mu_f = H_T/4$ result for $M \leq 1.3$ TeV. Beyond this, the cut takes effect and the difference between distributions with the two scale choices begins to diminish.

We will also assess the effect of the cut on the approximate NNLO distributions. We stress again that these are only approximate results and the actual effect must be left to a full NNLO calculation. However, it will be illustrative to investigate what happens in this approximate case nonetheless. Much like the NLO case, we see from Figure 4.15 that the effect of placing a cut of $|\Delta y| < 4$ is to drastically lower the cross section at high M. The cross section is reduced by half for $M \gtrsim 2.5$ TeV. Again the effect is strongest for $\mu_f = H_T/4$. Figure 4.16 displays the two aNNLO results with the $|\Delta y|$ cut applied. At least for these approximate distributions, the cut appears to bring the two distributions into better agreement. One might then expect that in a full NNLO calculation similar behaviour might be observed.

With these cut distributions we can also ask if the large K-factor present in fixed

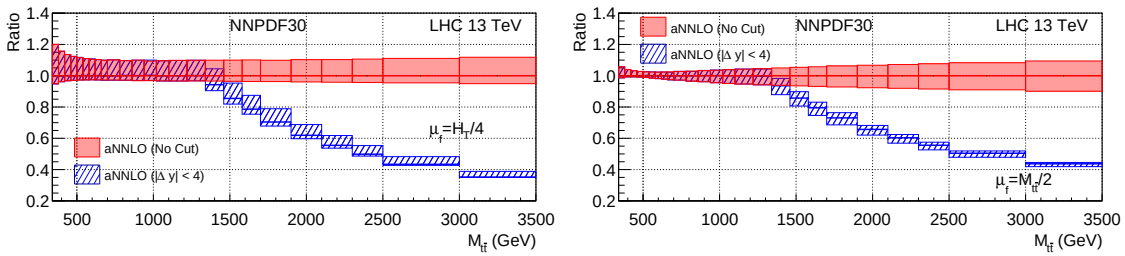

Figure 4.15: Effect of the $|\Delta y| < 4$ cut on aNNLO distributions for $\mu_f = H_T/4$ (left) and $\mu_f = M/2$ (right). Plots show the distributions without the cut (red) compared to the same distribution with the cut (blue hatched).

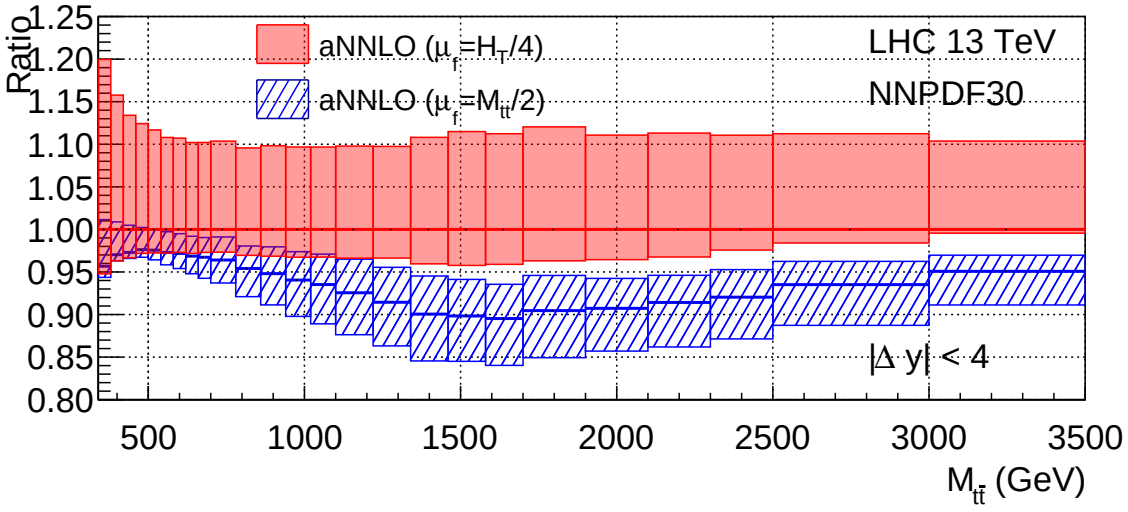

Figure 4.16: Comparison of aNNLO distributions with $|\Delta y| \leq 4$ for the two difference scale choices considered $\mu_f = H_T/4$ (red) and $\mu_f = M/2$ (blue hatched).

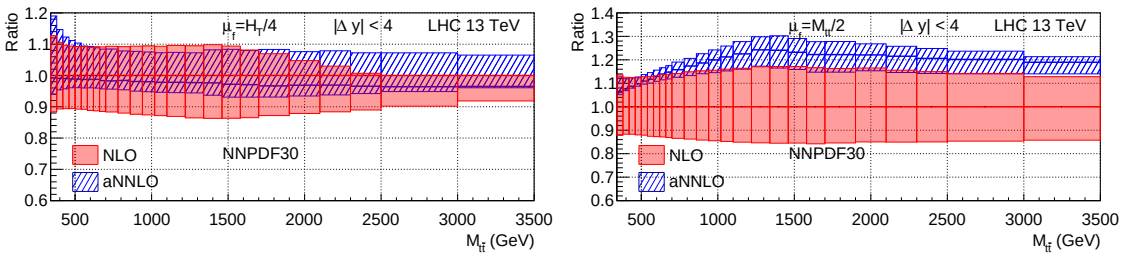

Figure 4.17: K-factors for the approximate NNLO distributions with the $|\Delta y| \leq 4$ cut for $\mu_f = H_T/4$ (left) and $\mu_f = M/2$ (right).

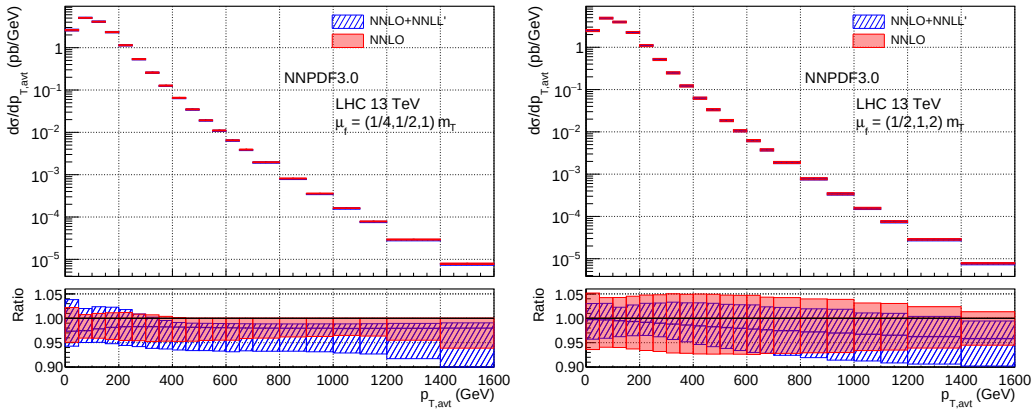

Figure 4.18: Transverse momentum distributions for the LHC with $\sqrt{s} = 13$ TeV at NNLO (red) and NNLO+NNLL′ (blue hatched) accuracy using $\mu_f = m_T/2$ (left) and $\mu_f = m_T$ (right).

order without the rapidity cuts remains? In Figure 4.17 we show the ratio of the approximate NNLO and exact NLO distributions with the cut $|\Delta y| \leq 4$. We see the scale choice $\mu_f = M/2$ still gives a large K-factor even after the cut. However, unlike the exact NNLO result without the cut, the K-factor does not grow monotonically with M and in fact shows a slight depression for $M \gtrsim 1.3$ TeV.

4.2 Transverse Momentum Distributions

As highlighted at the end of Section 3.2 it is also possible to produce distributions for the (anti-)top quark transverse momentum distribution. In this section we present results obtained using Eq. (3.2.4). In Figure 4.18 we present results using two commonly used factorisation scale choices, $\mu_f = m_T/2$ (left hand plot) as

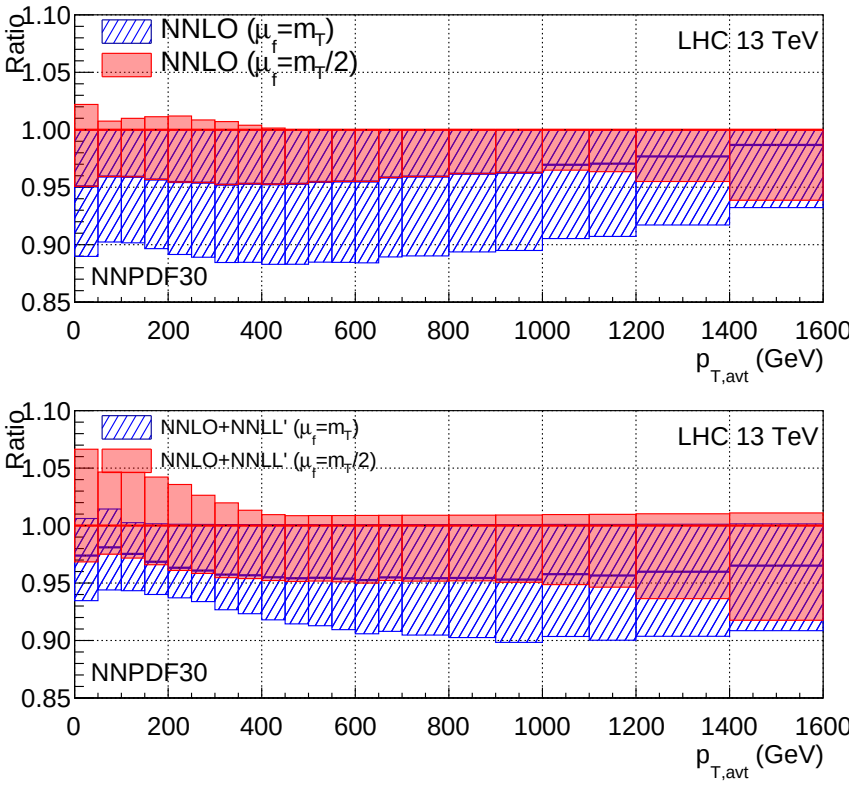

Figure 4.19: Predictions for the p_T distribution from fixed order (top) and resummed (bottom) calculations for different scale choices $\mu_f = m_T/2$ (red) and $\mu_f = m_T$ (blue hatched). In each case the result is normalized to the prediction with $\mu_f = m_T/2$.

recommended in [42] and the related choice $\mu_f = m_T$ (right hand plot). For both choices the central value obtained from the resummed results is slightly lower than the central value obtained by the NNLO calculation, it is well within the uncertainty band from the fixed order calculation. The scale choice $\mu_f = m_T/2$ however, produces no upper uncertainty band for the fixed order results in bins where $p_T \gtrsim 400$ GeV. The resummed result provides some uncertainty in this direction, but only marginally. Predictions obtained using the scale choice $\mu_f = m_T$ indicate that the effect of the resummation is to produce a softening of the high energy tails with increasing effect for larger p_T. In the top plot of Figure 4.19 we show the ratio of the fixed order calculations from the two different scale choices. For $p_T \lesssim 1$ TeV we see that the lower uncertainty on the result obtained from the scale choice $\mu_f = m_T/2$ coincides with the central value from the $\mu_f = m_T$ result. However, for $p_T \gtrsim 1$ TeV the

two no longer coincide indicating that there is a swap in the variation which gives rise to the lower bound. The fact that for most of the distribution, we only get a lower bound from the scale variation indicates that the choice $\mu_f = m_T/2$ sits on a peak of the distribution with respect to changes in the factorisation scale. As such, varying the factorisation scale by factors of two in either direction gives only lower uncertainties. We can see this in Figure 4.20 which shows the variation of the cross section in two sample bins as a function of the factorisation scale. The upper plot shows the variation in a region where the cross section is large ($p_T \in [50, 100]$ GeV), while the lower plot shows the variation in a high energy region of phase space ($p_T \in [1200, 1400]$ GeV). In the high energy bin, we can see the NNLO result evaluated at $\mu_f = m_T/2$ produces only lower uncertainties when varied as the cross section begins to dip for very low factorisation scales. This is in contrast to the NLO result which, though less stable under variations, appears to fall monotonically as one raises the factorisation scale in both the low and high energy bins examined.

4.3 Total Cross Section

While the main focus of this work has been to analyse the effects of resummation on differential distributions, particularly in the high energy tails, it is also prudent to check the effects on the total cross section. The predictions in this section are obtained by integrating over the differential distributions obtained in the previous sections. In addition to the dynamical scale choices considered so far, we also include $\mu_f = m_t$ for the (N)NLO predictions, another commonly used scale choice when calculating the total cross section. Such results are obtained through the use of the `top++` program [77]. Figure 4.21 shows the total cross section for top pair production evaluated at a range of different scale choices and perturbative accuracies. It can be seen that the NNLO+NNLL′ prediction produces a slightly larger cross section than the corresponding NNLO prediction with the scale choice $\mu_f = M/2$, but with the uncertainty bands still comfortably overlapping. This is consistent with our earlier

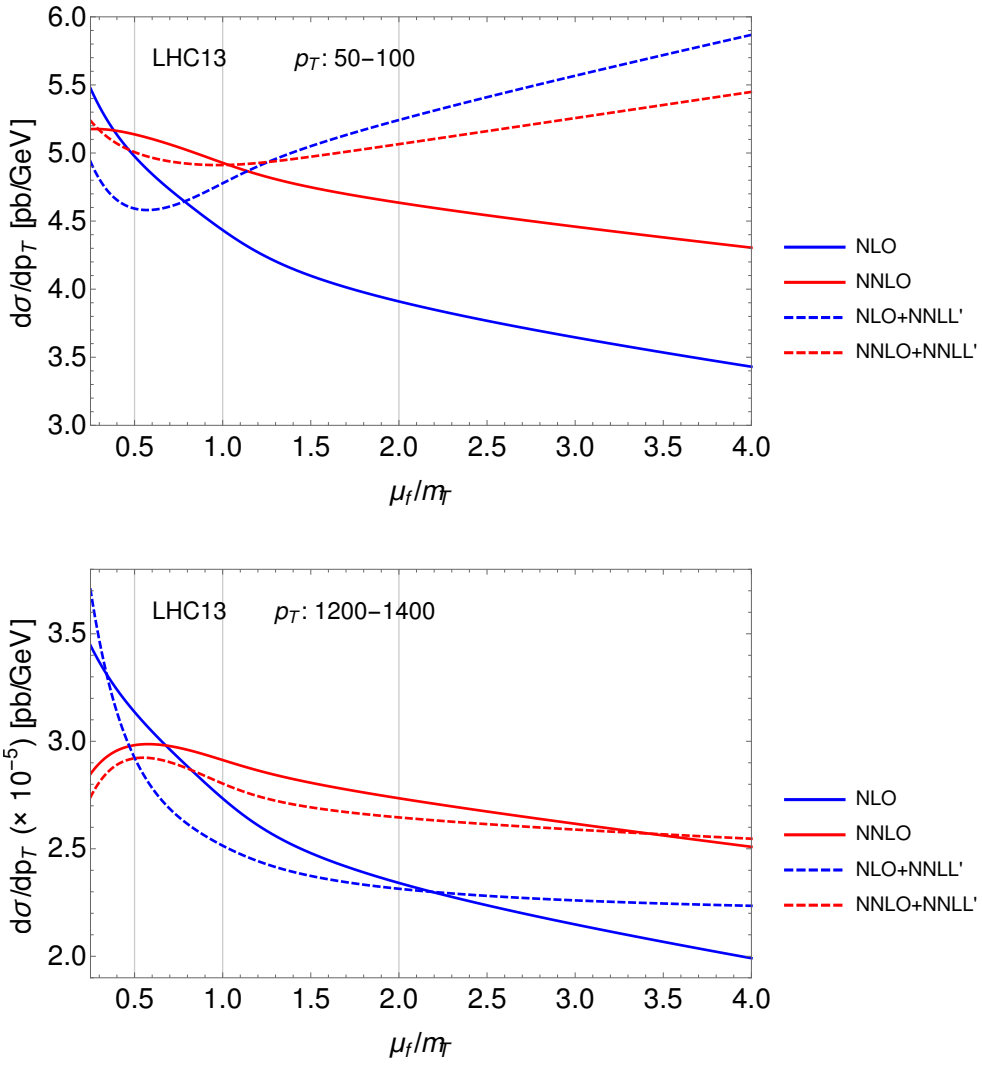

Figure 4.20: Impact of factorisation scale variation for p_T differential distributions in two separate kinematic regions; a high cross section region (top) and a high energy region (bottom). Grey lines mark typical choices for the default factorisation scale.

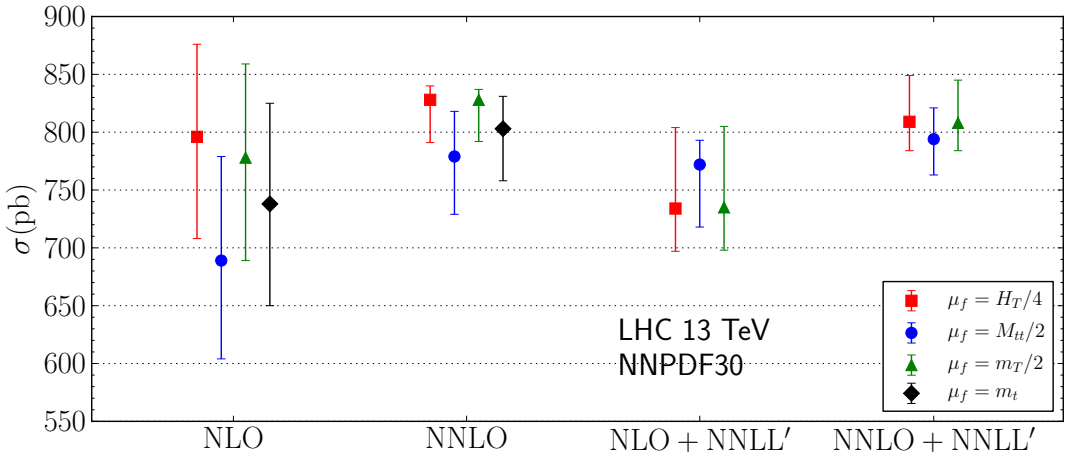

Figure 4.21: Predictions for the total cross section for top pair production at the LHC for different perturbative accuracies. Results are given for each of the different scale choices considered; $\mu_f = H_T/4$ (red square), $\mu_f = M_{t\bar{t}}/2$ (blue circle), $\mu_f = m_T/2$ (green triangle) as well as $\mu_f = m_t$ (black diamond). As usual NLO fixed order results are computed using NLO PDFs.

observations from the right hand plot of Figure 4.2, where we noted the effect of resummation was to enhance the cross section for large M. Similarly, performing the same comparison for the scale choice $\mu_f = H_T/4$ we see that the resummed result produces a slightly lower cross section than the NNLO prediction, again consistent with observations of the left hand plot in Figure 4.2. We can also see the fact that the resummed results are more stable under changes in the parametric choice of factorisation scale reflected in Figure 4.21. The effect of resummation on the total cross section however is mostly minimal. This is not unexpected since the effect of the resummation performed here is most prevalent in the tails of the distributions, most notably for the PIM predictions. Since the bulk of the cross section comes not from the tails but from phase space nearer threshold, we expect the resummation to have only a minimal effect. Finally, Figures 4.22 and 4.23 present the total cross section as a function of the factorisation scale. Figure 4.22 gives results from integrating the p_T distributions at different perturbative accuracies (but all with $\mu_f \sim m_T$) while Figure 4.23 provides the same information from the invariant mass distributions at the two different scales. In both plots we can see the greater stability

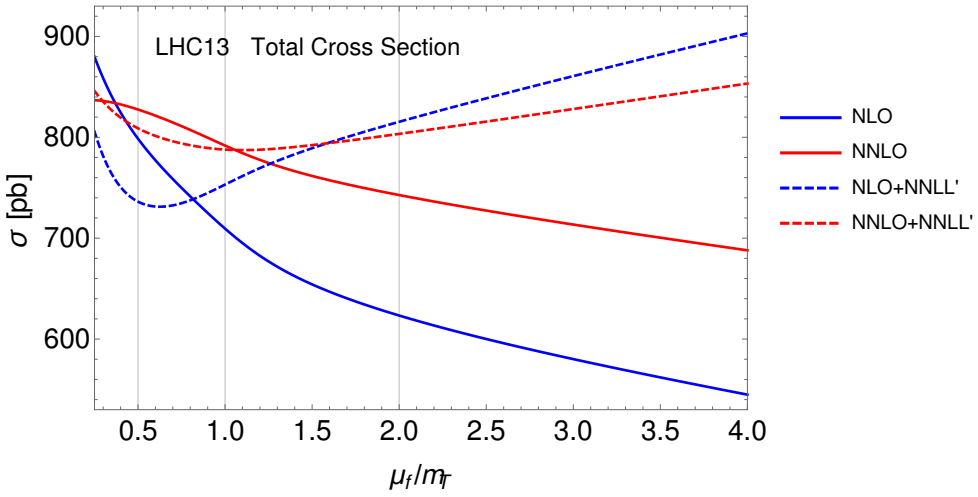

Figure 4.22: Comparison of the total cross section from integrating p_T distributions produced with different default values for μ_f and at varying perturbative accuracies.

of the resummed predictions (dashed lines) under scale variations with respect to their fixed order counterparts. In Figure 4.23 we see that the resummed results are also generally more consistent in the prediction of the total cross section for higher values of the factorisation scale. The difference between NLO and NNLO at such scales is more profound suggesting that the resummation is able to account for the higher order corrections which unaccounted for in fixed order lead to such a discrepancy. In both plots we also see that for lower values of the factorisation scale more of the results generally coincide.

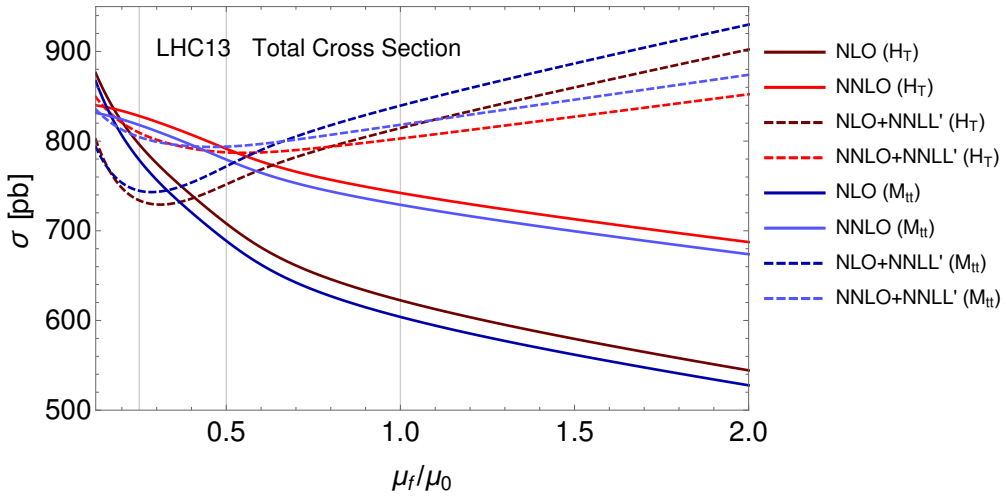

Figure 4.23: Comparison of the total cross section from integrating the PIM distributions produced with different default values for μ_f and at at varying perturbative accuracies.

Chapter 5

NLO QCD Higgs Decays in The SMEFT

5.1 Motivation and Goal

The Higgs boson, being the newest discovered particle, is one of the least well studied experimentally thus far. It plays a crucial role in the theory despite this, some details of which we explored in Section 1.2. An important test of the SM therefore is to measure the couplings of the Higgs boson to the other SM particles. As we saw in Chapter 1, the coupling of the Higgs to other SM particles is directly proportional to their mass. In Chapter 2 however, we saw from Eq. (2.2.13) that the presence of as yet undiscovered new physics existing at higher energies could alter this behaviour of the Higgs. In order to characterise the effects that possible new physics might have, without deference to a particular UV complete model, we can calculate the decay rate of the Higgs boson within the framework of the SMEFT. The result will be the usual result from the SM calculations plus additional contributions proportional to Wilson coefficients from higher dimensional operators. In the rest of this chapter we restrict ourselves exclusively to additional contributions from dimension-6 operators as discussed in Section 2.2. Long term, the goal would be to fit/constrain such Wilson coefficients using a number of different experimental

measurements and theoretical predictions. This requires calculations beyond the Higgs partial width calculated here. A large amount of work has already been done in this direction. Examples include the SMEFT in connection with top physics [78–83], muon decay [84], Z decay [85], other applications in Higgs physics [86–99] and more general or theoretical considerations [2, 35, 100–106].

In this Chapter, we consider the decays of the Higgs boson to b-quarks. In particular, we calculate a subset of the full NLO corrections to this process, namely those from QCD. This supplements those from four-fermion operators and EW results leading in (α/M_W) presented in [94]. The NLO corrections from QCD to this process are one power of α_s greater than the LO process in the SM. In order to ensure the same power counting in this calculation we rescale the operator $Q_{dG} \to g_s Q_{dG}$. This is because after EWSB this operator produces a coupling $\sim (\bar{b}\,\sigma^{\mu\nu} T^A b)\,\partial_\mu G^A_\nu$ and therefore alters the gbb vertex. The rescaling ensures this vertex also produces a factor of g_s as in the SM and preserves the power counting structure mentioned earlier. Note that in order to preserve the form of the term in the Lagrangian the Wilson coefficient C_{dG} is simultaneously rescaled $C_{dG} \to C_{dG}/g_s$. This is left implicit however but will be important when we consider the RG equations for this coefficient in Section 5.5. In order to facilitate the calculation we employ the use of `FeynRules` [107] to implement the dimension-6 operators. We then use `FeynArts` [108] and `FormCalc` [109]. In addition, we shall assume Minimal Flavour Violation as described in Section 2.2 such that the effective Yukawa and mass matrices are simultaneously diagonalisable and that there are no additional flavour violating effects beyond those in the SM. In practise we will work exclusively with 3rd generation fermions and so we will dispense with the flavour indices on operators which contain fermions and instead label the handedness. For example, for Q_{dG} we write $(\bar{b}_L \sigma^{\mu\nu} T^A b_R)\, H G^A_{\mu\nu} + \text{h.c.}$.

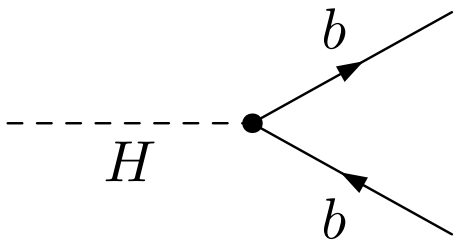

Figure 5.1: Diagram contributing to the process $h \to b\bar{b}$ at leading order.

5.2 Leading Order Calculation

In this section, we derive some preliminary results. We begin with the Leading Order (LO) decay of the Higgs boson to b quarks with the dimension-6 SMEFT. There is only one diagram contributing to the decay $h \to b\bar{b}$ at tree level, shown in Figure 5.1. Using the Feynman rules for the Higgs coupling to fermions in the dimension-6 SMEFT given in Eq. (2.2.13) and accounting for the redefinition of the Higgs field in Eq. (2.2.10), we can write the leading order amplitude as

$$i\mathcal{M}^{(0)} = -i\bar{U}(p_1)\left[\mathcal{M}_L^{(0)} P_L + \mathcal{M}_L^{(0)*} P_R\right] V(p_2)\,, \tag{5.2.1}$$

where

$$\begin{aligned}\mathcal{M}_L^{(0)} &= \frac{y_b}{\sqrt{2}}\left(1 + C_{H,\text{kin}}\right) - \frac{3}{2} v_T^2 C_{bH}^* \\ &= \frac{m_b}{v_T}\left(1 + C_{H,\text{kin}}\right) - \frac{v_T^2}{\sqrt{2}} C_{bH}^*\,.\end{aligned} \tag{5.2.2}$$

In the second line of Eq. (5.2.2) we have rewritten the SM Yukawa coupling in terms of the mass using Eq. (2.2.15). The superscript (0) on $\mathcal{M}_L$ indicates that this is the amplitude for the leading order process. There are still contributions from dimension-6 operators not explicit in this expression arising from v_T as can be seen through Eq. (2.2.19). We keep these implicit since it is v_T which is the physically measured VEV, not $\hat{v}_T$. To obtain the decay rate we square the amplitude, sum over spins and colours and integrate over the phase space of the final state particles. For the LO calculation this is simply a 2-body phase space, at NLO we will require a 3-body phase space, details on both are presented in Appendix A.2. We split

contributions to the decay rate into those from the SM ($\Gamma^{(4,0)}$) and those which arise from dimension-6 operators ($\Gamma^{(6,0)}$).

$$\Gamma^{(0)}(h \to b\bar{b}) = \Gamma^{(4,0)} + \Gamma^{(6,0)} \,. \tag{5.2.3}$$

We obtain the decay width

$$\Gamma^{(4,0)} = \frac{N_c m_h m_b^2 \beta^3}{8\pi v_T^2} \,, \tag{5.2.4}$$

and

$$\Gamma^{(6,0)} = \left(2C_{H,\text{kin}} - \frac{\sqrt{2} v_T^3}{m_b} \text{Re}(C_{bH}) \right) \Gamma^{(4,0)} \,, \tag{5.2.5}$$

where we have defined $\beta = \sqrt{1 - 4m_b^2/m_h^2}$. We see then at LO the contributions from the Wilson coefficients $C_{H\Box}$ and C_{HD} which appear because of the normalisation of the Higgs field, as well as the real part of C_{bH} which provides a modified Yukawa coupling. In principle, one could now go and fit these coefficients to data and determine bounds on the possible values. However, it is important for most processes to calculate NLO corrections. Firstly, calculating NLO corrections simply increases the accuracy of the prediction. In performing a perturbative expansion one should compute as many terms as possible in the series, the NLO result is the first step in this direction. Computing the NLO result also provides information on how quickly the series is converging. Another reason is that at NLO we begin to get a handle on the uncertainties related to the resulting predictions. These are obtained through varying the renormalisation scale, as was done in Chapter 4. While using the anomalous dimensions of the parameters appearing at tree level can tell us about the logarithmic contributions appearing at NLO, we cannot know the size of constant terms until they are explicitly calculated. Finally, another important reason for performing the NLO calculation, more specific to the SMEFT, is that we can get new dimension-6 operators contributing to the process at NLO which do not appear at tree level. It could be important to capture the effects of such operators.

5.3 Renormalisation

In performing the NLO calculation, we will encounter divergences of both UV and IR origin. We regulate these divergences using dimensional regularisation with $d = 4 - 2\epsilon$. In order to make sense of these we must renormalise the theory as discussed in Section 1.3. It is also necessary to decide which variables we wish to express our answer in terms of. Not all parameters in the SM are independent and so we can eliminate some in favour of others. We choose to parametrise our answer in terms of the masses, strong coupling, VEV and Wilson coefficients

$$m_h, M_W, M_Z, m_b, \alpha_s, v_T, C_i\,, \tag{5.3.1}$$

If we were considering other gauge interactions we would also use the electric charge $\bar{e}$ as one of our constants. In fact $\bar{e}$ will appear when we consider renormalisation of the VEV, but as we shall see does not contribute when considering the NLO QCD contributions. It is also necessary to specify a renormalisation scheme. We highlighted two such examples in Section 1.3; the on-shell scheme and the $\overline{\text{MS}}$ scheme. For the masses we choose to use the on-shell scheme, while for the Wilson coefficients we employ the $\overline{\text{MS}}$ scheme. The VEV will also be expressed in terms of physical parameters which are renormalised in the on-shell scheme. We will not actually need to renormalise α_s ourselves, however we will use the running coupling in Section 5.5 and as such is defined in the $\overline{\text{MS}}$ scheme. We now employ the tools of renormalised perturbation theory. By expanding the Lagrangian in terms of renormalised fields and counterterms we can express our UV-finite result from virtual corrections as

$$\mathcal{M}^{(1)}_{\text{Virt}} = \mathcal{M}^{(1),\text{bare}}_{\text{Virt}} + \mathcal{M}^{\text{C.T}}\,, \tag{5.3.2}$$

where we write

$$i\mathcal{M}^{\text{C.T}} = -i\overline{U}(p_1)\left(\delta\mathcal{M}_L P_L + \delta\mathcal{M}_L^* P_R\right) V(p_2)\,, \tag{5.3.3}$$

and $\mathcal{M}_{\text{Virt}}^{(1),\text{bare}}$ refers to the bare 1-loop amplitude obtained from virtual corrections. It is helpful to further separate the contributions in to those which do and those which do not depend on dimension-6 effects. As for when we presented the LO result we use the additional superscripts, (4) to denote SM contributions and (6) to denote contributions from dimension-6 operators. The counterterm for $\delta\mathcal{M}_L$ is thus expressed as

$$\delta\mathcal{M}_L = \frac{1}{16\pi^2}\left[\delta\mathcal{M}_L^{(4)} + \delta\mathcal{M}_L^{(6)}\right] . \tag{5.3.4}$$

In order to determine the form of $\delta\mathcal{M}_L$, we expand the LO amplitude in Eq. (5.2.2) in terms of renormalised parameters. This, as well as accounting for the field renormalisation from Eq. (1.3.2) will dictate the form of the counterterm to the amplitude. As mentioned earlier the amplitude in Eq. (5.2.2) does not explicitly show the full dependence on dimension-6 Wilson coefficients. Recall from Eq. (2.2.19) that v_T has dependence on C_{HWB} and C_{HD}. Writing this dependence explicitly, we arrive at

$$\mathcal{M}^{(0)} = \frac{m_b}{\hat{v}_T} + m_b\hat{v}_T\frac{\hat{c}_w}{\hat{s}_w}C_{HWB} + m_b\hat{v}_T C_{H\Box} + m_b\hat{v}_T\frac{\hat{c}_w^2-\hat{s}_w^2}{4\hat{s}_w^2}C_{HD} - \frac{v_T^2}{\sqrt{2}}C_{bH}^* . \tag{5.3.5}$$

This is the bare 1-loop amplitude which we must now expand in terms of renormalised quantities and counterterms. Considering first the SM contributions as well as including the contributions from field redefinitions we arrive at

$$\delta\mathcal{M}_L^{(4)} = \frac{m_b}{\hat{v}_T}\left(\frac{\delta m_b^{(4)}}{m_b} - \frac{\delta\hat{v}_T^{(4)}}{\hat{v}_T} + \frac{1}{2}\delta Z_h^{(4)} + \frac{1}{2}\delta Z_b^{(4)}\right) . \tag{5.3.6}$$

where we have defined $\delta Z_b^{(4)} = \delta Z_b^{L,(4)} + \delta Z_b^{R,(4)\,*}$. This is the form of the counterterm required to remove all the UV divergences proportional to Λ_{NP}^0. For greater clarity, we split the contributions to the counterterm from dimension-6 terms $\delta\mathcal{M}_L^{(6)}$ into three parts; those from SM counterterms which have dependence on the higher dimensional Wilson coefficients (e.g. $\delta m_b^{(6)}$), those from SM parameters multiplying Wilson Coefficients (e.g. $\delta m_b^{(4)} C_{HD}$), and those from the counterterms of the Wilson coefficients themselves (e.g. δC_{bH}). The sum of these contributions gives the form

of the counterterm required to cancel the UV divergences proportional to $\Lambda_{\rm NP}^{-2}$

$$\delta\mathcal{M}_L^{(6)} = \delta\mathcal{M}_{1,L}^{(6)} + \delta\mathcal{M}_{2,L}^{(6)} + \delta\mathcal{M}_{3,L}^{(6)}\,. \tag{5.3.7}$$

The first of these contributions, the dimension-6 contributions to SM counter terms takes the same form as Eq. (5.3.6) and is given by

$$\delta\mathcal{M}_{1,L}^{(6)} = \frac{m_b}{\hat{v}_T}\left(\frac{\delta m_b^{(6)}}{m_b} - \frac{\delta\hat{v}_T^{(6)}}{\hat{v}_T} + \frac{1}{2}\delta Z_h^{(6)} + \frac{1}{2}\delta Z_b^{(6)}\right)\,. \tag{5.3.8}$$

The second set of counterterms comes from expanding the coefficients of dimension-6 Wilson coefficients in Eq. (5.3.5) and gives

$$\begin{aligned}
\delta\mathcal{M}_{2,L}^{(6)} = \frac{m_b\hat{v}_T}{2}C_{HD}\Bigg[&\left(\frac{\delta m_b^{(4)}}{m_b} + \frac{\hat{v}_T^{(4)}}{\hat{v}_T} + \frac{1}{2}\delta Z_b^{(4)} + \frac{1}{2}\delta Z_h^{(4)}\right)\frac{\hat{c}_w^2 - \hat{s}_w^2}{2\hat{s}_w^2} \\
&+ \left(\frac{\delta\hat{c}_w^{(4)}}{\hat{c}_w} - \frac{\hat{s}_w^{(4)}}{\hat{s}_w}\right)\frac{\hat{c}_w^2}{\hat{s}_w^2}\Bigg] \\
&+ m_b\hat{v}_T C_{H\Box}\left[\frac{\delta m_b^{(4)}}{m_b} + \frac{\delta\hat{v}_T}{\hat{v}_T} + \frac{1}{2}\delta Z_b^{(4)} + \frac{1}{2}\delta Z_h^{(4)}\right] \\
&- \frac{\hat{v}_T^2}{\sqrt{2}}C_{bH}^*\left[2\frac{\delta\hat{v}_T^{(4)}}{\hat{v}_T} + \frac{1}{2}\delta Z_b^{(4)} + \frac{1}{2}\delta Z_h^{(4)}\right] \\
&+ \hat{v}_T\frac{\hat{c}_w}{\hat{s}_w}m_b C_{HWB}\left[\frac{\delta\hat{c}_w^{(4)}}{\hat{c}_w} - \frac{\delta\hat{s}_w^{(4)}}{\hat{s}_w} + \frac{\delta m_b^{(4)}}{m_b} + \frac{\delta\hat{v}_T^{(4)}}{\hat{v}_T} + \frac{1}{2}\delta Z_b^{(4)} + \frac{1}{2}\delta Z_h^{(4)}\right]\,.
\end{aligned} \tag{5.3.9}$$

The final contribution comes from the counterterms to the Wilson Coefficients themselves

$$\delta\mathcal{M}_{3,L}^{(6)} = \hat{v}_T m_b\left(\frac{\hat{c}_w^2 - \hat{s}_w^2}{4\hat{s}_w^2}\delta C_{HD} + \frac{\hat{c}_w}{\hat{s}_w}\delta C_{HWB} - \frac{\hat{v}_T}{\sqrt{2}m_B}\delta C_{bH}^* + \delta C_{H\Box}\right)\,. \tag{5.3.10}$$

The counterterms δm_b and δZ are determined by the renormalisation conditions given in Eqs. (1.3.9)-(1.3.13). In order to obtain the counterterms for $\hat{c}_w$, $\hat{s}_w$ and $\hat{v}_T$ we use Eqs. (1.2.10) and (1.2.9) to express them in terms of our chosen observables and then expand these in terms of renormalised quantities. The resulting expressions

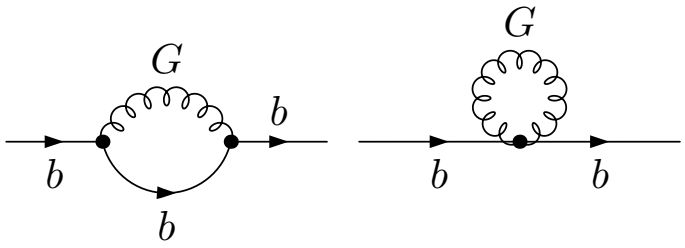

Figure 5.2: Diagrams contributing to the b-quark self energy from QCD at 1-loop. The diagram on the left is only generated through dimension-6 operators.

are given by

$$\begin{aligned}\frac{\delta\hat{c}_w}{\hat{c}_w} &= \frac{\delta M_W}{M_W} - \frac{\delta M_Z}{M_Z}\,, \qquad \frac{\delta\hat{s}_w}{\hat{s}_w} = -\frac{\hat{c}_w^2}{\hat{s}_w^2}\frac{\delta\hat{c}_w}{\hat{c}_w}\,,\\ \frac{\delta\hat{v}_T}{\hat{v}_T} &= \frac{\delta M_W}{M_W} + \frac{\delta\hat{s}_w}{\hat{s}_w} - \frac{\delta\bar{e}}{\bar{e}}\,.\end{aligned} \tag{5.3.11}$$

Constructing the full counterterm is now simply a matter of calculating the necessary 2-point functions used in Eqs. (1.3.9) and (1.3.12). We start with the b-quark 2-point function. In the SM, there is only one diagram which contributes to the self energy from QCD and is shown in the left of Figure 5.2. Computing the SM counterterm we find

$$\frac{\delta m_b^{(4)}}{m_b} = -\frac{\alpha_s C_F}{\pi}\left(\frac{3}{4}\frac{C_\epsilon^b}{\hat{\epsilon}} + 1\right)\,, \tag{5.3.12}$$

where for convenience we have introduced

$$C_\epsilon^b = 1 + \epsilon\ln\left[\frac{\mu^2}{m_b^2}\right]\,, \quad \frac{1}{\hat{\epsilon}} = \frac{1}{\epsilon} - \gamma_E + \ln(4\pi)\,. \tag{5.3.13}$$

However, there is also a contribution to this 2-point function from a dimension-6 operator. Namely the class 6 operator $g_s C_{bG}\left(\bar{b}_L\sigma^{\mu\nu}T^A b_R\right)HG^A_{\mu\nu} + \text{h.c.}$, where we have included the scaling of g_s as indicated at the start of this Chapter. This operator contributes not only to the diagram on the left of Figure 5.2, but also generates the new diagram on the right. The diagram on the right however contains a scaleless loop integral. Such integrals vanish in dimensional regularisation,

$$\sim \int \frac{d^dk}{(2\pi)^d}\frac{1}{k^2} \to 0\,. \tag{5.3.14}$$

The diagram on the left however does give a non-zero contribution. The dimension-6 contributions to the b quark mass counterterm is found to be

$$\frac{\delta m_b^{(6)}}{m_b} = -\frac{\alpha_s C_F}{\pi}\frac{m_b \hat{v}_T}{2\sqrt{2}}\left(3\frac{C_\epsilon^b}{\hat{\epsilon}}+1\right)(C_{bG}+C_{bG}^*)\,. \tag{5.3.15}$$

Using the same two point function, we can also calculate the counterterm for the b quark field renormalisation using Eqs. (1.3.10) and (1.3.11). The SM contributions give

$$\begin{aligned}\delta Z_b^{(4),L} &= \delta Z_b^{(4),R} = \delta Z_b^{(4),L*} = \delta Z_b^{(4),R*}\,,\\ \delta Z_b^{(4)} &= 2\delta Z_b^{(4),L} = -\frac{\alpha_s C_F}{\pi}\left(\frac{3}{2}\frac{C_\epsilon^b}{\hat{\epsilon}}+2\right)\,,\end{aligned} \tag{5.3.16}$$

while for the dimension-6 contributions we find

$$\begin{aligned}\delta Z_b^{(6),L} &= \frac{\alpha_s C_F}{\pi}\frac{m_b^2 v_T}{4\sqrt{2}}\left(3\frac{C_\epsilon^b}{\hat{\epsilon}}+1\right)(C_{bG}-3C_{bG}^*)\,,\\ \delta Z_b^{(6),R} &= -\frac{\alpha_s C_F}{\pi}\frac{m_b^2 v_T}{4\sqrt{2}}\left(3\frac{C_\epsilon^b}{\hat{\epsilon}}+1\right)(C_{bG}+C_{bG}^*)\,.\end{aligned} \tag{5.3.17}$$

For QCD corrections, there are no contributions to the other field/SM parameter counterterms to the order we are working to. For example, the class 4 operators Q_{HG} and $Q_{H\tilde{G}}$ generate diagrams which could contribute to the Higgs 2-point function. But these are either produce scaleless integrals or contribute starting at $\mathcal{O}(\Lambda_{\rm NP}^{-4})$.

The final terms we need are the counterterms to the Wilson coefficients themselves. These can be obtained through the use of the anomalous dimensions for the dimension-6 Wilson coefficients which were fully calculated in [2, 35, 102] for the baryon number conserving operators. The corresponding results for Wilson coefficients of operators which do not conserve baryon number were also calculated in [103], though we shall not make use of these here. The anomalous dimensions take the form

$$\frac{dC_i}{d\ln\mu} = \gamma_{ij}C_j\,. \tag{5.3.18}$$

We see that γ_{ij} is a matrix in the space of operators, so the anomalous dimension for a given operator C_i mixes it with other operators under RG running. The counterterms

in the $\overline{\text{MS}}$ scheme can obtained from the anomalous dimension as follows

$$\delta C_i = \frac{1}{2\hat{\epsilon}} \frac{dC_i}{d\ln\mu} \,. \tag{5.3.19}$$

The anomalous dimensions are written in the afore mentioned references as $\dot{C}_i = 16\pi^2 \mu \frac{dC_i}{d\mu}$. Thus the expansion of the bare Wilson coefficient in terms of counterterms is written

$$C_i^{(0)} = C_i(\mu) + \frac{1}{2\hat{\epsilon}} \frac{1}{16\pi^2} \dot{C}_i(\mu) \,. \tag{5.3.20}$$

The anomalous dimensions in [2, 35, 102] are calculated in the unbroken phase of the theory. Because we are using the $\overline{\text{MS}}$ scheme however, we can still use these results to construct counterterms in the broken phase which rely only on the pole structure by construction. In the current case, only δC_{bH} gives contributions proportional to g_s. It is found to be [35]

$$\delta C_{bH} = \frac{\alpha_s C_F}{\pi} \frac{3}{v_T^2} \frac{1}{\hat{\epsilon}} \left(2m_b^2 C_{bG} + v_T \left(\sqrt{2} m_b (C_{HG} + i C_{H\tilde{G}}) - \frac{v_T}{4} C_{bH} \right) \right) \,, \tag{5.3.21}$$

when written in terms of m_b instead of y_b.

At this point we have all we need to renormalise the bare NLO virtual corrections. We now turn to the computation of these bare 1-loop amplitudes.

5.4 NLO Corrections

5.4.1 Virtual Corrections

In the SM, there is only one diagram which provides a vertex correction to the LO process of the decay $h \to b\bar{b}$. At dimension-6 we get contributions proportional to C_{bH} and $C_{H,\text{kin}}$ from corrections to the SM-like diagrams in Figure 5.3. However, there are additional diagrams which can appear from the presence of dimension-6 operators and are displayed in Figure 5.4. These diagrams arise from operators which first appear at NLO in the calculation. Specifically, we get contributions from C_{dG}, C_{HG} and $C_{H\tilde{G}}$. The first of these produces the first three diagrams from the

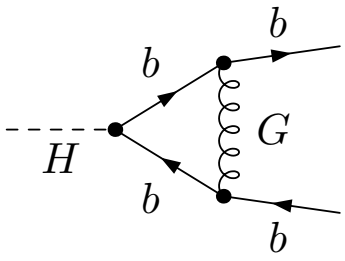

Figure 5.3: Diagram contributing to the QCD virtual correction of the decay $h \to b\bar{b}$.

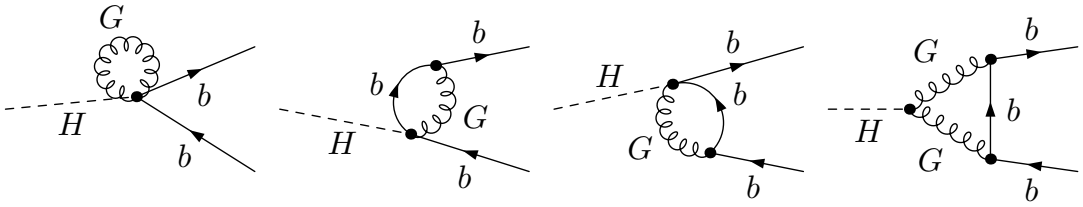

Figure 5.4: Additional diagrams contributing to the QCD virtual correction of the decay $h \to b\bar{b}$ from dimension-6 operators.

left in Figure 5.4, while C_{HG} and $C_{H\tilde{G}}$ each produce a new hGG vertex contributing to the final diagram. Summing the bare 1-loop amplitude and counterterm produces a UV finite result. The contribution from virtual corrections is then obtained by squaring the sum of the LO and UV finite virtual corrections,

$$|\mathcal{M}_{h\to b\bar{b}}|^2 = \left|\mathcal{M}^{(0)} + \mathcal{M}^{(1)}_{\text{Virt}}\right|^2 , \tag{5.4.1}$$

and keeping only terms up to $\mathcal{O}(\alpha_s)$. Finally we sum over final state spins and colours. The contribution from the **CP** violating operator which gives rise to $C_{H\tilde{G}}$ does not appear in the final result for the virtual corrections; its interference with the SM result gives no contribution. Such contributions would begin to survive if one considered contributions $\mathcal{O}(\Lambda_{\text{NP}}^{-4})$. And so in order to get a handle on the **CP** violating operators one would need to extend the calculation to next order in the effective theory. This result is still IR divergent however, and to obtain a finite cross section it is necessary to include the possibility of emitting gluons into the final state. Such diagrams also produce divergences when the emitted gluon becomes soft which cancel the IR singularities from the virtual corrections.

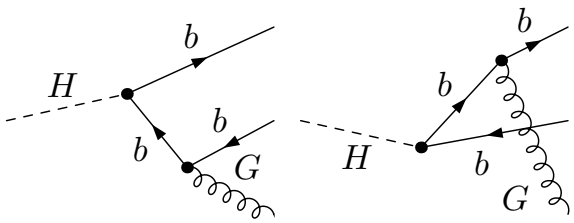

Figure 5.5: SM diagrams contributing to the process $h \to b\bar{b}G$.

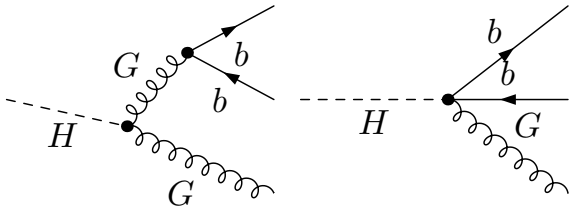

Figure 5.6: Additional diagrams contributing to $h \to b\bar{b}G$ from dimension-6 operators.

5.4.2 Real Emission

We now consider the emission of additional gluon radiation into the final state. In the SM there are only two such diagrams which contribute to this process. These are shown in Figure 5.5. The SM result is given by summing these diagrams, taking the square and integrating over the 3-body phase space. The squared matrix element is found to depend on a number of kinematic structures and we find agreement with the analogus calculation of $h \to f\bar{f}\gamma$ in [110]. The presence of the dimension-6 operators produce additional diagrams which can arise and these are shown in Figure 5.6. These produce new kinematic dependence in the phase space integrals compared to the SM ones. Again we find dependence on the class 4 operators C_{HG} and $C_{H\tilde{G}}$ and the class 6 operator C_{bG}. Summing the diagrams, squaring the result, truncating to $\mathcal{O}\left(\Lambda_{\text{NP}}^{-2}\right)$ and summing over final state spins, polarisations and colours gives our result for the real emissions. In performing the sum over polarisation states of the gluon, the dependence on the operator $C_{H\tilde{G}}$ is removed.

5.4.3 Combined Result

Obtaining the full NLO QCD correction to the decay rate is now a matter of integrating the virtual corrections over 2-body phase space, the real corrections over

3-body phase space and dividing by the appropriate flux factors. In this instance our initial state is simply the Higgs, so our flux factor is given as $1/(2m_H)$. We thus write

$$\Gamma_{h\to b\bar{b}(G)} = \frac{1}{2m_H}\int \mathrm{dPS}_2 \sum |\mathcal{M}_{h\to b\bar{b}}|^2 + \frac{1}{2m_H}\int \mathrm{dPS}_3 \sum |\mathcal{M}_{h\to b\bar{b}G}|^2 \qquad (5.4.2)$$

where dPS_n denotes the integration measure for the Lorentz invariant n-body phase space measure. Details are given in Appendix A.2. The Wilson coefficient C_{bH} can be complex in general. However, as in the LO result in Eq. (5.2.5) the results we obtain in the rest of this Chapter depend only on the real part of this coefficient. To avoid clutter we do not write Re explicitly everywhere and the understanding is that only the real part of the Wilson coefficient contributes.

$$\Gamma^{(4,1)} = \Gamma^{(4,0)}\frac{\alpha_s C_F}{\pi}\frac{A(\beta)}{\beta^3}\,. \qquad (5.4.3)$$

We have introduced the kinematic factor $A(\beta)$

$$\begin{aligned} A(\beta) = {} & \frac{3\beta}{8}\left(-1+7\beta^2\right) + \beta^3\left(3\ln[y] - 4\ln[\beta]\right) \\ & + \ln[x]\left\{\frac{1}{16}(-3-34\beta^2+13\beta^4)\right. \\ & \left. + \beta^2(1+\beta^2)\left(-\frac{3}{2}\ln[y] + 2\ln[\beta]\right)\right\} \\ & + \beta^2(1+\beta^2)\left(\frac{3}{2}\ln^2[x] + 2\mathrm{Li}_2[x] + \mathrm{Li}_2\left[x^2\right]\right)\,, \end{aligned} \qquad (5.4.4)$$

and further defined

$$x = \frac{1-\beta}{1+\beta}\,, \qquad y = \frac{1-\beta^2}{4} = \frac{m_b^2}{m_h^2}\,.$$

The NLO SM result is not new, but it is an important check that we reproduce the result. Our result agrees with those in [111, 112]. The NLO result proportional to

dimension-6 contributions is found to be

$$\begin{aligned}
\Gamma^{(6,1)} =& C_{bG}\frac{\alpha_s C_F}{\pi}\frac{N_c m_h^3 m_b}{8\sqrt{2}\pi v_T}\Bigg\{\frac{\beta}{8}\left(15+28\beta^2-35\beta^4\right)\\
&-\frac{3}{16}\left(-5+3\beta^2-15\beta^4+17\beta^6\right)\ln[x]\\
&-3\beta^3\left(1-\beta^2\right)\ln[y]\Bigg\}\\
&+C_{HG}\frac{\alpha_s C_F}{\pi}\frac{N_c m_h^2 m_b\sqrt{y}}{2\pi}\Bigg\{\frac{\beta}{8}\left(15-2\pi^2\beta+23\beta^2\right)\\
&-\frac{3}{4}\beta^2\ln^2[x]-\frac{3}{2}\beta^3\ln[y]\\
&+\ln[x]\left(\frac{1}{16}(15+2\beta^2+7\beta^4)+\beta^2\ln[y]\right)\\
&+3\beta^2\left(\mathrm{Li}_2[x]-\frac{1}{2}\mathrm{Li}_2\left[x^2\right]\right)\Bigg\}\\
&+2\,\Gamma^{(4,1)}C_{H,\mathrm{kin}}-C_{bH}\frac{\alpha_s C_F}{\pi}\frac{N_c m_h m_b v_T}{4\sqrt{2}\pi}\left(A(\beta)+\beta^3-\frac{3}{4}\beta^3\ln[y]\right)\\
&+\Gamma^{(4,0)}\frac{v_T^3}{\sqrt{2}m_b}\frac{\dot{C}_{bH}}{(4\pi)^2}\ln\left[\frac{\mu^2}{m_H^2}\right],
\end{aligned}\tag{5.4.5}$$

where the $\mathcal{O}(\alpha_s)$ corrections on the final line are provided using $\dot{C}_{bH} = 2\hat{\epsilon}(16\pi^2)\delta C_{bH}$ together with Eq. (5.3.21). There are a number of features of this result which can be discussed. The first is the appearance of new Wilson coefficients in the NLO result which do not appear at tree level. Although these are subleading in α_s they may have important numerical consequences, especially if the tree level Wilson coefficients are zero or heavily suppressed compared to the ones appearing at NLO. We also see that, unlike the SM NLO corrections, which are proportional to the LO result, this is no longer the case for the dimension-6 pieces, with the sole exception of $C_{H,\mathrm{kin}}$. Ideally one would evaluate this decay rate using $\mu = m_h$ in order to remove the logarithm on the final line. However, the result still contains a number of large logarithms of the ratio of the Higgs and b-quark masses. We can attempt to remove these logarithms by renormalising m_b in the $\overline{\mathrm{MS}}$ scheme rather than in the on-shell scheme.

5.5 Resummation of Large Logs and The Massless Limit

The presence of logarithms of the ratio of m_b and m_H in Eq. (5.4.5) is in general not a small ratio and one might be worried about the size of the logarithms and their potential to ruin the perturbative series. At any rate the presence of such logarithms will hamper the convergence of the perturbative series. However, we can attempt to remedy this situation by converting from the on-shell b quark mass to the $\overline{\text{MS}}$ mass. Since the mass will now depend on the renormalisation scale, we may be able to use the RG running of the b mass to resum these large logarithmic contributions.

In the on-shell scheme, the finite part of the counterterm is set such that the renomalised mass is equal to the pole mass at all orders in perturbation theory. In the $\overline{\text{MS}}$-scheme the finite part is set to zero save the universal γ_E and $\ln(4\pi)$ terms. Thus to convert the on-shell scheme to the $\overline{\text{MS}}$-scheme we simply drop the finite part. We denote results in the $\overline{\text{MS}}$-scheme by a bar, e.g. $\overline{m}_b(\mu)$. Writing the bare mass in the two different ways allows us to relate the two

$$\begin{aligned} m_b &= \overline{m}_b + \delta\overline{m}_b - \delta m_b \\ &= \overline{m}_b \left(1 - \delta(\mu)\right) . \end{aligned} \tag{5.5.1}$$

Using the notation and results of Eqs. (5.3.12) and (5.3.15) and that $\delta\overline{m}_b$ is simply the divergent part of δm_b we find

$$\delta^{(4)}(\mu) = -\frac{\alpha_s C_F}{\pi}\left(1 + \frac{3}{4}\ln\left[\frac{\mu^2}{\overline{m}_b^2}\right]\right) , \tag{5.5.2}$$

$$\delta^{(6)}(\mu) = -\frac{\alpha_s C_F}{\pi}\frac{v_T \overline{m}_b}{\sqrt{2}} C_{bG}\left(1 + 3\ln\left[\frac{\mu^2}{\overline{m}_b^2}\right]\right) . \tag{5.5.3}$$

The schemes differ starting at $\mathcal{O}(\alpha_s)$ and so we can write the tree level results in the $\overline{\text{MS}}$-scheme as

$$\overline{\Gamma}^{(4,0)} = \frac{N_c m_h \overline{m}_b^2 \beta^3}{8\pi v_T^2} ,$$

$$\overline{\Gamma}^{(6,0)} = \left(2C_{H,\text{kin}} - \frac{\sqrt{2}v_T^3}{\overline{m}_b}C_{bH}\right)\overline{\Gamma}^{(4,0)}\,. \tag{5.5.4}$$

Here we have not made the substitution in the β terms. These are related to the kinematics and phase space of the final state particles and not the Yukawa couplings. The substitution in Eq. (5.5.1) generates terms at $\mathcal{O}(\alpha_s)$ compared to the LO result that will appear in the $\overline{\text{MS}}$ NLO result. Specifically

$$\begin{aligned}
\Gamma^{(4,0)} &\to \overline{\Gamma}^{(4,0)} - 2\delta^{(4)}(\mu)\overline{\Gamma}^{(4,0)} - 2\delta^{(6)}(\mu)\overline{\Gamma}^{(4,0)}\,,\\
\Gamma^{(6,0)} &\to \overline{\Gamma}^{(6,0)} - 2\delta^{(4)}(\mu)\overline{\Gamma}^{(6,0)} - \frac{\sqrt{2}v_T^3}{\overline{m}_b}C_{bH}\delta^{(4)}(\mu)\overline{\Gamma}^{(4,0)}\,.
\end{aligned} \tag{5.5.5}$$

These will contribute to the NLO results in the $\overline{\text{MS}}$-scheme. These are

$$\overline{\Gamma}^{(4,1)} = \Gamma^{(4,1)} - 2\delta^{(4)}(\mu)\overline{\Gamma}^{4,0}\,, \tag{5.5.6}$$

$$\overline{\Gamma}^{(6,1)} = \Gamma^{(6,1)} - 2\delta^{(6)}(\mu)\overline{\Gamma}^{4,0} - 2\delta^{(4)}\left(2C_{H\text{kin}} - \frac{v_T^3}{\sqrt{2}\overline{m}_b}C_{bH}\right)\overline{\Gamma}^{(4,0)}\,, \tag{5.5.7}$$

where on the right hand side it is understood that one should use the $\overline{\text{MS}}$ mass in each of the terms, except βs as mentioned earlier. In the $\overline{\text{MS}}$-scheme the b-quark mass now depends on the renormalisation scale μ. In order to resum large logarithmic contributions we will need to derive and solve the RG equations related the b mass at differing scales. In the SMEFT this now gains dimension-6 contributions. Note that we use the following convention for the β-function

$$\frac{\beta(\alpha_s)}{\pi} = \frac{1}{\pi}\frac{d\alpha_s(\mu)}{d\ln\mu} = -2\beta_0\left(\frac{\alpha_s}{\pi}\right)^2 + \mathcal{O}(\alpha_s^3) \tag{5.5.8}$$

where $\beta_0 = (11N_c - 2n_f)/12$ and n_f denotes the number of active flavours; here $n_f = 5$. The RG equation for $\overline{m}_b(\mu)$ can be found by taking the derivative of Eq. (5.5.1) with respect to μ. To Leading Log (LL) accuracy (i.e. keeping only contributions to $\mathcal{O}(\alpha_s)$), this results in

$$0 = \frac{d\overline{m}_b(\mu)}{d\ln\mu}(1-\delta(\mu)) - \overline{m}_b(\mu)\frac{d\delta(\mu)}{d\ln\mu}\,. \tag{5.5.9}$$

Using Eqs. (5.5.2)-(5.5.3) and that $\mu\partial_\mu\alpha_s \sim \mathcal{O}(\alpha_s^2)$ and $\mu\partial_\mu C_{bG} \sim \mathcal{O}\alpha$ we find

$$\frac{d\delta(\mu)}{d\ln\mu} = -\frac{2\alpha_s}{\pi} - \frac{2\alpha_s}{\pi}\sqrt{2}v_T\left(C_{bG}\frac{d\overline{m}_b(\mu)}{d\ln\mu}\right)\left(\frac{1}{3}+\ln\frac{\mu^2}{\overline{m}_b^2}\right). \tag{5.5.10}$$

So the RG equation for $\overline{m}_b$ is found to be

$$\frac{d\overline{m}_b(\mu)}{d\ln\mu} = -\frac{\alpha_s C_F}{\pi}\frac{3}{2}\overline{m}_b(\mu)\left(1+2\sqrt{2}v_T\overline{m}_b(\mu)\,C_{bG}(\mu)\right). \tag{5.5.11}$$

Although we can divide out one factor of $\overline{m}_b$ from the right hand side of Eq. (5.5.11), since the coefficient of C_{bG} is quadratic in $\overline{m}_b$ we will still have dependence on on the $\overline{\text{MS}}$ mass (and hence μ) on the right hand side. In addition, the Wilson coefficient itself also depends on μ. In order to solve the RG equation we can find the LL result for these terms to express them in terms of some fixed scale μ_0 and an evolution factor. This appears recursive since the RG equation for $\overline{m}_b$ is the very thing we are trying to solve for in the first place. However, because we are only working to terms up to Λ_{NP}^{-2} and because the remaining factor of $\overline{m}_b$ on the right hand side multiplies a dimension-6 Wilson coefficient, we only require the solution to the RG equation as given by the SM. This is given by

$$\frac{d\overline{m}_b^{(4)}(\mu)}{d\ln\mu} = -\frac{\alpha_s C_F}{\pi}\frac{3}{2}\overline{m}_b^{(4)}(\mu), \tag{5.5.12}$$

with solution

$$\overline{m}_b^{(4)}(\mu) = \overline{m}_b(\mu_0)\left(\frac{\alpha_s(\mu)}{\alpha_s(\mu_0)}\right)^{\frac{\gamma_m^0}{\beta_0}}, \tag{5.5.13}$$

where $\gamma_m^0 = 3C_F/4$. To obtain the LL result for the Wilson coefficient C_{bG} we require the anomalous dimension as given in [2,35,102]. In principle this involves the contributions from many different operators. However, the numerically dominant terms proportional to g_s^2 are those from self mixing, and so we consider only those contributions. Note that the anomalous dimension given in [35] is for the unscaled Wilson coefficient. Recall, we rescaled this Wilson coefficient by an additional factor of g_s such that $\overline{C}_{dG} = g_s C_{dG}$ where $\overline{C}_{dG}$ refers to the unscaled Wilson coefficient.

This leads to

$$\frac{d\overline{C}_{dG}}{d\ln\mu} = \frac{dg_s}{d\ln\mu}C_{bG} + g_s\frac{dC_{bG}}{d\ln\mu}\,. \tag{5.5.14}$$

The left hand side in Eq. (5.5.14) can be obtained from [35] which gives

$$16\pi^2\frac{d\overline{C}_{dG}}{d\ln\mu} = Ag_s^2\overline{C}_{dG}\,, \tag{5.5.15}$$

where $A = 10C_F - 4N_c - 4\beta_0$. The first term on the right hand side in Eq. (5.5.14) can be obtained using the QCD β-function

$$\frac{d\alpha_s}{d\ln\mu} = \frac{g_s}{2\pi}\frac{dg_s}{d\ln\mu}\,. \tag{5.5.16}$$

Thus Eq. (5.5.14) becomes

$$\frac{2\pi}{g_s}\beta(\alpha_s)C_{bG} + g_s\frac{dC_{bG}}{d\ln\mu} = \frac{A}{16\pi^2}g_s^3C_{bG}\,. \tag{5.5.17}$$

Expanding this to first order in α_s we can solve for C_{bG}. We find

$$\frac{1}{C_{bG}}\frac{dC_{bG}}{d\alpha_s} = \frac{-5C_F + 2N_c}{4\beta_0\alpha_s}\,,$$

$$C_{bG}(\mu) = C_{bG}(\mu_0)\left(\frac{\alpha_s(\mu)}{\alpha_s(\mu_0)}\right)^{\frac{\gamma_c^0}{\beta_0}}\,, \tag{5.5.18}$$

where $\gamma_c^0 = \frac{-5C_F+2N_c}{4}$. We can now substitute the solutions for $\overline{m}_b^{(4)}(\mu)$ in Eq. (5.5.13) and $C_{bG}(\mu)$ in Eq. (5.5.18) into Eq. (5.5.11) to facilitate a solution. We find

$$\ln\frac{\overline{m}_b(\mu)}{\overline{m}_b(\mu_0)} = \frac{\gamma_m^0}{\beta_0}\ln\left(\frac{\alpha_s(\mu)}{\alpha_s(\mu_0)}\right) + \frac{3C_F}{4(\gamma_c^0+\gamma_m^0)}2\sqrt{2}\hat{v}_T\left[\overline{m}_b^{(4)}(\mu)C_{bG}(\mu) - \overline{m}_b^{(4)}(\mu_0)C_{bG}(\mu_0)\right]\,, \tag{5.5.19}$$

$$\begin{aligned}\overline{m}_b(\mu) = \overline{m}_b(\mu_0)\left(\frac{\alpha_s(\mu)}{\alpha_s(\mu_0)}\right)^{\frac{\gamma_m^0}{\beta_0}}\Bigg(1 + \frac{2\sqrt{2}v_T}{\gamma_m^0+\gamma_c^0} \\ \left[\overline{m}_b^{(4)}(\mu)C_{bG}(\mu) - \overline{m}_b^{(4)}(\mu_0)C_{bG}(\mu_0)\right]\Bigg)\,,\end{aligned} \tag{5.5.20}$$

where on the last line we have truncated the result to $\mathcal{O}(\Lambda_{\text{NP}^{-2}})$. Since we are considering the ratio of the b-quark and Higgs mass as a large scale separation, it is also interesting to consider the decay rate in the limit $m_b/m_H \to 0$, or equivalently $\beta \to 1$. In order to retain possibly interesting dependence on Wilson coefficients

which are subleading in this limit, we keep the first terms which do not vanish in this limit. In order to take the limit we use the result

$$A(\beta \to 1) = \frac{9}{4} + \frac{3}{2} \ln \left[\frac{m_b^2}{m_h^2} \right] . \tag{5.5.21}$$

The resulting expressions for the decay rates are found to be

$$\begin{aligned}
\overline{\Gamma}^{(4,0)}_{\beta\to 1} =& \frac{N_c m_h \overline{m}_b^2}{8\pi v_T^2} , \\
\overline{\Gamma}^{(4,1)}_{\beta\to 1} =& \frac{\alpha_s C_F}{\pi} \frac{1}{4} \left(17 + 6 \ln \left[\frac{\mu^2}{m_h^2} \right] \right) \overline{\Gamma}^{(4,0)}_{\beta\to 1} , \\
\overline{\Gamma}^{(6,0)}_{\beta\to 1} =& \left(2C_{H,\text{kin}} - \frac{\sqrt{2} v_T^3}{\overline{m}_b} C_{bH} \right) \overline{\Gamma}^{(4,0)}_{\beta\to 1} , \\
\overline{\Gamma}^{(6,1)}_{\beta\to 1} =& \left(2C_{H,\text{kin}} - \frac{\sqrt{2} v_T^3}{\overline{m}_b} C_{bH} \right) \overline{\Gamma}^{(4,1)}_{\beta\to 1} \\
& + \frac{\alpha_s C_F}{\pi} \frac{N_c m_h^3 \overline{m}_b}{8\sqrt{2}\pi v_T} C_{bG} + \frac{\alpha_s C_F}{\pi} \frac{N_c m_h \overline{m}_b^2}{8\pi} C_{HG} \\
& \times \left(19 - \pi^2 + \ln^2 \left[\frac{\overline{m}_b^2}{m_h^2} \right] + 6 \ln \left[\frac{\mu^2}{m_h^2} \right] \right) .
\end{aligned} \tag{5.5.22}$$

This limit for $\overline{\Gamma}^{(4)}$ was also considered in [111, 112] and we find agreement with their result. In this limit a number of features arise. The first is that we notice the NLO dimension-6 contributions from C_{bH} and $C_{H,\text{kin}}$ are proportional to the SM ones, they factorise. These are the Wilson coefficients already present at tree level. The other Wilson coefficients C_{bG} and C_{HG} which appear for first time at NLO, are not proportional to the SM in the same way. Also, we have kept the dependence on the Wilson coefficient C_{HG} despite it being formally subleading in the $m_b/m_h \to 0$ limit compared with C_{bG}. The reason we have done this is the presence of the large logarithm $\ln^2(m_b^2/m_h^2)$ which survives the conversion to the $\overline{\text{MS}}$-scheme. This logarithm can have a numerically significant impact on the relative contribution between C_{bG} and C_{HG} as we will see shortly.

Converting the b-quark renormalised mass to the $\overline{\text{MS}}$-scheme and subsequently taking the massless limit successfully removed many of the large logs, except the squared log multiplying C_{HG}, and simplified the resulting expression, it is important to check

to what extent this result approximates the full one. To this end we compare the $\overline{\text{MS}}$-scheme decay rates with and without the $m_b/m_h \to 0$ limit applied. We denote the full result as

$$\overline{\Gamma} = \overline{\Gamma}^{(4,0)} + \overline{\Gamma}^{(4,1)} + \overline{\Gamma}^{(6,0)} + \overline{\Gamma}^{(6,1)}\,, \tag{5.5.23}$$

and similarly for $\overline{\Gamma}_{\beta\to 1}$. In order to evaluate the expressions we use $\alpha_s\left(m_Z\right) = 0.1184$, $m_Z = 91.1876$ GeV, $\overline{m}_b(\overline{m}_b) = 4.18$ GeV and $m_h = 125.0$ GeV. We numerically evaluate the VEV by making the replacement $v_T \to (\sqrt{2}G_F)^{-\frac{1}{2}}$ and using $G_F = 1.16637 \cdot 10^{-5}$ GeV^{-2}. Additionally, we separate out the scale of new physics from the Wilson coefficients, writing $C_i = \widetilde{C}_i/\Lambda_{\text{NP}}^2$. In doing so, we keep explicit factors of v_T^2 for each $\Lambda_{\text{NP}^{-2}}$ in order to express the contributions from the Wilson coefficients relative to the electroweak scale. We also extract the factor of v_T^2 from the expression for $C_{H,\text{kin}}$ so that

$$\widetilde{C}_{H,\text{kin}} = \left(\frac{\Lambda_{\text{NP}}}{v_T}\right)^2 C_{H,\text{kin}} = \left(\widetilde{C}_{H\Box} - \frac{1}{4}\widetilde{C}_{DH}\right).$$

We evaluate the decay rates with $\mu = m_h$ to remove logarithms of $\ln\left(\mu^2/m_h^2\right)$ from the NLO results in Eq. (5.5.22). Results for $\overline{m}_b(m_h)$ (which requires $C_{bG}(m_h)$) are obtained using the solutions to the RG for these parameters in Eqs. (5.5.13), (5.5.18) and (5.5.20). Keeping only results to $\mathcal{O}(\Lambda_{\text{NP}}^{-2})$ we find

$$\begin{aligned}
\frac{\overline{\Gamma}}{\text{MeV}} &= \kappa^{\text{QCD}}\Bigg\{2.22\left[1 + 2\left(\frac{v_T}{\Lambda_{\text{NP}}}\right)^2 \widetilde{C}_{H,\text{kin}}\right] \\
&\qquad - 258\left(\frac{v_T}{\Lambda_{\text{NP}}}\right)^2 \widetilde{C}_{bH}\Bigg\} \\
&\quad + \left(\frac{v_T}{\Lambda_{\text{NP}}}\right)^2 \left(1.55\widetilde{C}_{bG} + 6.88\widetilde{C}_{HG}\right), \\
\frac{\overline{\Gamma}_{\beta\to 1}}{\text{MeV}} &= \kappa^{\text{QCD}}_{\beta\to 1}\Bigg\{2.23\left[1 + 2\left(\frac{v_T}{\Lambda_{\text{NP}}}\right)^2 \widetilde{C}_{H,\text{kin}}\right] \\
&\qquad - 257\left(\frac{v_T}{\Lambda_{\text{NP}}}\right)^2 \widetilde{C}_{bH}\Bigg\} \\
&\quad + \left(\frac{v_T}{\Lambda_{\text{NP}}}\right)^2 \left(1.57\widetilde{C}_{bG} + 6.91\widetilde{C}_{HG}\right),
\end{aligned} \tag{5.5.24}$$

where the remaining Wilson coefficients are evaluated at a scale $\mu = m_h$. To compare the impact of the NLO corrections with those from tree-level we have introduced

$\kappa^{\rm QCD} \approx \kappa^{\rm QCD}_{\beta\to 1} \approx 1.20$ as is conventionally done in the SM. First, we see the results in the massless case are an excellent approximation (almost identical) to the results with full mass dependence. Giving all Wilson coefficients equal importance we see that the coefficient for C_{bH} is numerically the most important dimension-6 contribution. We also see however the importance of having kept the C_{HG} term which was formally subleading in the massless limit, it's coefficient being much more significant than that of C_{bG}. Of course, one should not make such uninformed assumptions about the relative size of such coefficients to justify the importance or not of any given Wilson coefficient. Differing UV complete models will result in different suppressions or enhancements of the Wilson coefficients. For example a common result highlighted in [98] is that for Minimal Flavour Violating (MFV) scenarios, one expects the Wilson coefficient $\widetilde{C}_{bH}$ instead to scale as $\widetilde{C}^{\rm MFV}_{bH} \sim y_b \widetilde{C}_{bH}$. This would bring the coefficient into the same range of sensitivity as that for C_{bG} and C_{HG}.

The main use of the results in Eq. (5.5.22) lies in fitting the Wilson coefficients based on experimental measurements. In the absence of a direct discovery of new physics this would constrain the possible effects new physics beyond the SM could possibly have. Simply measuring the Higgs partial width at some future collider would not suffice on its own. Instead the results obtained here would need to be combined with other measurements performed in the SMEFT and a global fit performed. The allowed ranges of such Wilson coefficients could then be used to make informed assumptions about how physics beyond the SM might manifest itself. Another important aspect of the results obtained here is that performing the NLO calculation exposes the role of potentially important dimension-6 operators which are absent at tree-level. Specifically C_{bG} and C_{HG} which can appear in equal weight to the tree level operator C_{bH} in certain scenarios. That these operators would also be missed by performing a naïve RG analysis of the NLO corrections only underlines the importance in computing to NLO in the SMEFT.

Chapter 6

Conclusions

This thesis has focused on two different Effective Field Theories (EFTs) and their applications to top quark pair production and the decay of the Higgs boson to bottom quarks. We started in Chapter 1 with a short review of the Standard Model focussing on QCD and the Higgs sector. Chapter 2 is where we introduced the two EFTs; Soft Collinear Effective Field Theory (SCET) and Standard Model Effective Field Theory (SMEFT). The first of these is an example of a top down EFT which can be derived from QCD, useful for separating our the physics associated with different scales in collider scenarios. The EFT essentially works by integrating out hard momentum exchanges. In doing so the theory is described in terms of fields with with momenta which scale collinear to the directions of the particles they describe, as well as soft momenta. In this way one is able to separate scales associated with different energetic particles and resum potentially dangerous logarithms. The SMEFT on the other hand is a bottom up EFT used to parametrise the effects of heavier physics beyond the SM in a model independent way. It does this by introducing higher dimensional operators which one could imagine arising as the low energy limit of some new high scale physics.

We studied an application of SCET to the problem of top quark pair production at hadron colliders in Chapter 3. A factorisation theorem derived within the SCET framework was analysed which separates the scales associated with the hard scatter-

ing from those dynamically generated through the emission of soft gluon radiation. The emission of these soft gluons leads to the presence of threshold logarithms in the perturbative expansion of the partonic cross section, possibly endangering the convergence of the series. The factorisation theorem separating these scales is derived in the threshold limit $z \to 1$. Using this it was then possible to derive the form of a resummed partonic cross section in Mellin space following the example set out in the original paper which did so directly in momentum space. This gave us the ability to resum such logarithmic contributions to all orders in α_s.

A further factorisation theorem, building on the one used to perform threshold resummation was also considered. Here in contributions subleading in m_t/M were also neglected and in this joint $z \to 1$, $m_t/M \to 0$ limit, the partonic cross section further factorised. The factorisation theorem results in four distinct scales; the hard scattering scales, the top mass, and two soft scales. Again solving for the form of the resummed partonic cross section in Mellin space allowed us to resum logarithms of m_t/M in the threshold limit.

These results, although containing resummed towers of logarithms were still only to leading power in their respective limits. In order to make full use of the results we outlined a matching procedure to combine the two resummed results without double counting logarithmic contributions which appear in both, as well as matching on to (N)NLO fixed order. In this manner we were able to produce results at NNLO+NNLL$'$ accuracy.

In Chapter 4 we produced a number of predictions using these resummed formulas. The resummed formulas allowed predictions for the pair invariant mass (PIM) of the top quark pair, as well as the p_T of the (anti)top. We examined the differences between the NNLO+NNLL$'$ resummed results and those from fixed order NNLO. In particular, the different choices one might make for the factorisation scale were compared. It was noted that while the fixed order (N)NLO predictions for the resulting PIM distributions depend strongly on the choice of scale (particularly in the high energy tails), the resummed distributions do not. Thus we saw one of effects

of the resummation was to bridge the gap between the differing results at NNLO. Given that this was the case, we also examined the rate at which this happens as one increases the accuracy of the logarithmic resummation by considering matched NLL, NNLL, and NNLL$'$ predictions. The lowest accuracy result produces very large uncertainties, but as one increases the order of resummation the uncertainties quickly drop. The central values of the results tend to coincide in each case however suggesting the resummation is able to bridge the gap between the two scale choices rather quickly. We also examined a number of K factors and found results for the resummed results produce a more stable perturbative series than those from fixed order. A comparison between pure threshold resummation and that from the joint resummation performed in this work. It was shown that for the scale choice $\mu_f = H_T/4$, the joint resummation changes the behaviour of the resulting distribution compared with pure threshold resummation completely. While pure threshold resummation lead to an enhancement in the tail of the distribution, incorporating the small mass resummation ended up producing a suppression in the tail compared to fixed order. The threshold and joint resummed results produce almost identical distributions for the scale choice $\mu_f = M/2$ however. Finally for PIM distributions we also looked at the effect of placing a cut on the magnitude of the rapidity difference between the top and the antitop. Placing a cut $|\Delta y| \leq 4$, we notice a sharp reduction in the cross section at large values of M. This then had the effect of brining the NLO distributions at the two different scale choices into better agreement. We performed the same analysis with approximate NNLO results which suggests the same effect would be observed there as well. The resulting uncertainties associated with the resummed results however are still larger than one might have hoped for and are not significantly more competitive than the NNLO uncertainty bands. In the factorisation theorems used to construct the EFT at the start, the Mandelstam variables $\hat{s}$ and t_1 are assumed to be of roughly the same value $\hat{s}/t_1 \sim 1$. However, for top quarks produced at shallow angles we can have $\hat{s} \gg t_1$. We studied the average angle of production in the top pair frame and together with the results from

the rapidity cut distributions suggests that a large part of the cross section at high energies is dominated by forward produced top quarks. The assumption that $\hat{s} \sim t_1$ may not be a good one in this region and so it may be interesting in the future to resum logarithms of $\ln \hat{s}/t_1$ which can appear in the perturbative cross section.

We also considered the resulting p_T distributions using the factorisation scale choice $\mu_f = m_T/2$, with m_T the transverse mass of the top quark. Here the effect of the resummation was more muted, producing only a slight softening of the distribution compared with the NNLO result. The central values of both calculation lie comfortably within the uncertainty band of the other.

In Chapter 5 we considered the application of the SMEFT to the decays of the Higgs boson to bottom quarks. Specifically, we augmented the SM with all dimension-6 operators and calculated the decay rate $h \to b\bar{b}$ to NLO in QCD using the resulting Lagrangian. The renormalisation procedure was outlined and the form of the resulting counterterms presented. SM parameters and masses were renormalised using the on-shell scheme while the Wilson coefficients of the dimension-6 operators were renormalised in the $\overline{\text{MS}}$ scheme. The counterterms for the Wilson coefficients were constructed using anomalous dimensions which had been recently calculated. The dimension-6 operators already have an effect on the decay rate at LO and are proportional to the SM result. At NLO we saw the emergence of new diagrams compared to the SM calculation and as such Wilson coefficients which only appear at $\mathcal{O}(\alpha_s)$ and as such would be missed by simply working with the EFT to leading order. The main result of this chapter are the dimension-6 Wilson coefficient contributions to the NLO QCD decay rate. The result contained a number of large logarithms of the ratios of the Higgs and bottom quark mass. In order to attempt to remedy the situation and remove these large logs we converted the renormalised bottom quark mass from the on shell scheme to the $\overline{MS}$ scheme. In addition, we also considered the limit $m_b/m_h \to 0$ (except when m_b results from a Yukawa coupling). However, in taking the limit we kept the first non-vanishing term for each Wilson coefficient. In particular we noticed the coefficient of C_{HG} was formally subleading

compared to that of C_{bG} but that the former multiplied a large logarithm which survived the conversion of m_b to the $\overline{\text{MS}}$ scheme. Comparing numerically the results in the $\overline{\text{MS}}$ scheme in the massive and massless limits as just described, we noted that the massless limit is in excellent agreement with the result retaining full mass dependence. In particular we noticed the importance of keeping the coefficient of C_{HG} which has a non-negligible numerical coefficient.

One cannot really judge the expected size of such Wilson coefficients from theory without some input from a UV complete model. Such models might result in particular scalings for the Wilson coefficients and some may be completely absent in particular models. The utility of such calculations then, lies in comparing the predictions to experimental results and fitting the resulting Wilson coefficients. This requires many other calculations also to be performed in the SMEFT such that it would be possible to constrain Wilson coefficients uniquely.

Appendix A

Appendix

A.1 g-Functions

In this appendix we present the form of the g-functions appearing in Eqs. (3.4.53), (3.4.54) and (3.4.55). In order to ease notation we introduce

$$L_h = \ln \frac{M^2}{\mu_h^2}\,, \quad L_s = \ln \frac{M^2}{\bar{N}^2 \mu_s^2}\,, \quad L_{dh} = \ln \frac{m_t^2}{\mu_{dh}^2}\,, \quad L_{ds} = \ln \frac{m_t^2}{\bar{N}^2 \mu_{ds}^2}\,,$$

where

$$\lambda_i = \frac{\alpha_s(\mu_h)}{2\pi} \beta_0 \ln \frac{\mu_h}{\mu_i}\,.$$

Expressions for the beta functions coefficients and anomalous dimensions can be found in [36] and [37].

A.1.1 Soft limit

First, we present the g_i^m functions appearing in the evolution factor Eq. (3.4.53) for the threshold resummed result.

$$g_1^m(\lambda_s, \lambda_f) = \frac{\Gamma_0}{2\beta_0^2} \Big[\lambda_s + (1-\lambda_s)\ln(1-\lambda_s) + \lambda_s \ln(1-\lambda_f) \Big]\,,$$

$$
\begin{aligned}
g_2^m(\lambda_s,\lambda_f) &= \frac{\Gamma_0\beta_1}{2\beta_0^3}\left[\ln(1-\lambda_s)+\frac{1}{2}\ln^2(1-\lambda_s)\right]-\frac{\Gamma_1}{2\beta_0^2}\ln(1-\lambda_s)+\frac{\gamma_0^\phi}{\beta_0}\ln\frac{1-\lambda_s}{1-\lambda_f}\\
&+\frac{\Gamma_0}{2\beta_0}L_s\ln\frac{1-\lambda_s}{1-\lambda_f}+\frac{\Gamma_0}{2\beta_0}L_h\ln(1-\lambda_f)\\
&+\frac{1}{1-\lambda_f}\left\{\frac{\Gamma_0\beta_1}{2\beta_0^3}\lambda_s\left[1+\ln(1-\lambda_f)\right]-\frac{\Gamma_1}{2\beta_0^2}\lambda_s\right\},\\
g_3^m(\lambda_s,\lambda_f) &= \frac{1}{1-\lambda_s}\left\{\frac{\Gamma_0\beta_1^2}{4\beta_0^4}\left[\lambda_s+2\lambda_s\ln(1-\lambda_s)+\ln^2(1-\lambda_s)\right]\right.\\
&\quad+\frac{\Gamma_0\beta_2}{2\beta_0^3}\left[\frac{\lambda_s}{2}+(1-\lambda_s)\ln(1-\lambda_s)\right]\\
&\quad-\frac{\Gamma_1\beta_1}{2\beta_0^3}\left[\frac{3}{2}\lambda_s+\ln(1-\lambda_s)\right]+\frac{\Gamma_2}{4\beta_0^2}\lambda_s+\frac{\beta_1\gamma_0^\phi}{\beta_0^2}\Big[1+\ln(1-\lambda_s)\Big]\\
&\quad-\frac{\gamma_1^\phi}{\beta_0}+\frac{\Gamma_0\beta_1}{2\beta_0^2}\Big[\Big[1+\ln(1-\lambda_s)\Big]L_s-(1-\lambda_s)L_h\Big]\\
&\quad\left.+\frac{\Gamma_1}{2\beta_0}\Big[(1-\lambda_s)L_h-L_s\Big]\right\}\\
&+\frac{1}{1-\lambda_f}\left\{-\frac{\Gamma_0\beta_1^2}{2\beta_0^4}\lambda_s+\frac{\Gamma_0\beta_2}{2\beta_0^3}\lambda_s-\frac{\gamma_0^\phi\beta_1}{\beta_0^2}\Big[1+\ln(1-\lambda_f)\Big]+\frac{\gamma_1^\phi}{\beta_0}\right.\\
&\quad\left.+\frac{\Gamma_1}{2\beta_0}\Big[L_s-L_h\Big]+\frac{\Gamma_0\beta_1}{2\beta_0^2}\Big[L_h-L_s\Big]\Big[1+\ln(1-\lambda_f)\Big]\right\}\\
&+\frac{\lambda_s}{(1-\lambda_f)^2}\left\{\frac{\Gamma_0\beta_1^2}{4\beta_0^4}\left[1-\ln^2(1-\lambda_f)\right]-\frac{\Gamma_0\beta_2}{4\beta_0^3}\right.\\
&\quad\left.+\frac{\Gamma_1\beta_1}{2\beta_0^3}\left[\frac{1}{2}+\ln(1-\lambda_f)\right]-\frac{\Gamma_2}{4\beta_0^2}\right\}.
\end{aligned}
$$

A.1.2 Boosted soft limit

Here we present the g_i and g_i^D functions which appear in the evolution factors Eqs. (3.4.54) and (3.4.55) for the boosted resummation formula. First we present the g_i functions.

$$
\begin{aligned}
g_1(\lambda_s,\lambda_f) &= \frac{A_0}{2\beta_0^2}\left[\ln(1-\lambda_s)+\lambda_s\left[1-\ln\left(\frac{1-\lambda_{dh}}{1-\lambda_f}\right)\right]\right],\\
g_2(\lambda_s,\lambda_f) &= \frac{\beta_1 A_0}{4\beta_0^3}\left[2\ln(1-\lambda_s)+\ln^2(1-\lambda_s)+\frac{2\lambda_s}{1-\lambda_f}(1+\ln(1-\lambda_f))\right]\\
&+\frac{A_1}{2\beta_0^2}\left[\frac{\lambda_s}{\lambda_f-1}-\ln(1-\lambda_s)\right]
\end{aligned}
$$

$$
\begin{aligned}
&+\frac{1}{\beta_0}\Bigg\{A_0\ln(1-\lambda_s)\ln\left(\frac{M}{\mu_h}\right)+\ln\left(\frac{1-\lambda_s}{1-\lambda_f}\right)\left[A_0\ln\left(\frac{\mu_h}{\mu_s\bar{N}}\right)+\gamma_0^{\phi}+\gamma_0^{\phi_q}\right]\Bigg\}\\
g_3(\lambda_s,\lambda_f)=&\frac{1}{(1-\lambda_s)(1-\lambda_f)}\Bigg\{\\
&+\frac{A_0\beta_1^2}{\beta_0^4}\frac{1}{1-\lambda_f}\Bigg[\lambda_s(-2\lambda_s\lambda_f+\lambda_s+\lambda_f^2)+(\lambda_s-1)\lambda_s\ln^2(1-\lambda_f)\\
&\qquad+(1-\lambda_f)^2\ln(1-\lambda_f)(2\lambda_s+\ln(1-\lambda_s))\Bigg]\\
&+\frac{1}{\beta_0^3}\Bigg[\frac{1}{2}(\lambda_f-1)\ln(1-\lambda_s)\Big(A_0\beta_2(\lambda_s-1)+A_1\beta_1\Big)\\
&\qquad+\frac{\lambda_s}{4(\lambda_f-1)}\Big(A_0\beta_2(-2\lambda_s\lambda_f+\lambda_s-(\lambda_f-4)\lambda_f-2)\\
&\qquad+A_1\beta_1(\lambda_s+3(\lambda_f-2)\lambda_f+2)+2A_1\beta_1(\lambda_s-1)\ln(1-\lambda_f)\Big)\Bigg]\\
&+\frac{\beta_1}{\beta_0^2}\Bigg[-A_0(\lambda_f-1)(\lambda_s+\ln(1-\lambda_s))\ln\left(\frac{M}{\mu_h}\right)\\
&\qquad+A_0((1-\lambda_f)\ln(1-\lambda_s)-(1-\lambda_s)\ln(1-\lambda_f)\\
&\qquad+\lambda_s-\lambda_f)\ln\left(\frac{\mu_h}{\mu_s\bar{N}}\right)+(\gamma_0^{\phi}+\gamma_0^{\phi_q})((\lambda_s-1)\ln(1-\lambda_f)\\
&\qquad-(\lambda_f-1)\lambda_((1-\lambda_s))\Bigg]\\
&+\frac{A_2\lambda_s}{4\beta_0^2}\left(\lambda_s+(\lambda_f-2)\lambda_f\right)\\
&+\frac{\beta_1}{\beta_0^2}(\gamma_0^{\phi}+\gamma_0^{\phi_q})(\lambda_s-\lambda_f)\\
&+\frac{A_1\lambda_s}{\beta_0}(\lambda_f-1)\ln\left(\frac{M}{\mu_h}\right)-(\lambda_s-\lambda_f)\left(A_1\ln\left(\frac{\mu_h}{\mu_s\bar{N}}\right)+\gamma_1^{\phi}+\gamma_1^{\phi_q}\right)\Bigg\}
\end{aligned}
$$

We decompose each of the g_i^D, which are functions of three arguments into two two-argument functions $g_{i,dh}^D$ and $g_{i,ds}^D$ as follows

$$g_i^D(\lambda_{dh},\lambda_{ds},\lambda_f)=g_{i,dh}^D(\lambda_{dh},\lambda_f)+g_{i,ds}^D(\lambda_{ds},\lambda_f)\,.$$

Using this decomposition, we present below the functions as used in this work.

$$
\begin{aligned}
g_{1,dh}^D(\lambda_{dh},\lambda_f)&=\frac{\Gamma_0}{2\beta_0^2}\left[\ln(1-\lambda_{dh})+\lambda_{dh}\left[1-\ln\left(\frac{1-\lambda_{dh}}{1-\lambda_f}\right)\right]\right],\\
g_{1,ds}^D(\lambda_{ds},\lambda_f)&=-\frac{\Gamma_0}{2\beta_0^2}\left[\ln(1-\lambda_{ds})+\lambda_{ds}\left[1-\ln\left(\frac{1-\lambda_{ds}}{1-\lambda_f}\right)\right]\right],
\end{aligned}
$$

$$
\begin{aligned}
g^D_{2,dh}(\lambda_{dh},\lambda_f) &= \frac{\beta_1\Gamma_0}{2\beta_0^3}\left[\left[1+\frac{1}{2}\ln(1-\lambda_{dh})\right]\ln(1-\lambda_{dh})\right] - \frac{\Gamma_1}{2\beta_0^2}\ln(1-\lambda_{dh}) \\
&\quad - \frac{\gamma_0^S}{\beta_0}\ln(1-\lambda_{dh}) \\
&\quad + \frac{\Gamma_0}{2\beta_0}L_{dh}\ln(1-\lambda_{dh}) - \frac{\gamma_0^{\phi_q}}{\beta_0}\ln\left(\frac{1-\lambda_{dh}}{1-\lambda_f}\right) \\
&\quad + \frac{1}{1-\lambda_f}\left\{\frac{\beta_1\Gamma_0}{2\beta_0^3}\lambda_{dh}\Big[1+\ln(1-\lambda_f)\Big] - \frac{\Gamma_1}{2\beta_0^2}\lambda_{dh}\right\}, \\
g^D_{2,ds}(\lambda_{ds},\lambda_f) &= -\frac{\beta_1\Gamma_0}{2\beta_0^3}\left[\left[1+\frac{1}{2}\ln(1-\lambda_{ds})\right]\ln(1-\lambda_{ds})\right] + \frac{\Gamma_1}{2\beta_0^2}\ln(1-\lambda_{ds}) \\
&\quad + \frac{\gamma_0^S}{\beta_0}\ln(1-\lambda_{ds}) \\
&\quad - \frac{\Gamma_0}{2\beta_0}L_{dh}\ln(1-\lambda_{ds}) - \frac{\Gamma_0}{2\beta_0}\Big[L_{ds}-L_{dh}\Big]\ln\left(\frac{1-\lambda_{ds}}{1-\lambda_f}\right) \\
&\quad + \frac{1}{1-\lambda_f}\left\{-\frac{\beta_1\Gamma_0}{2\beta_0^3}\lambda_{ds}\Big[1+\ln(1-\lambda_f)\Big] + \frac{\Gamma_1}{2\beta_0^2}\lambda_{ds}\right\}, \\
g^D_{3,dh}(\lambda_{dh},\lambda_f) &= -\frac{\beta_1^2\,\Gamma_0}{2\beta_0^4}\ln(1-\lambda_{dh}) + \frac{\beta_2\Gamma_0}{2\beta_0^3}\ln(1-\lambda_{dh}) \\
&\quad + \frac{1}{1-\lambda_{dh}}\left\{\frac{\beta_1^2\Gamma_0}{4\beta_0^4}\Big[1+\ln(1-\lambda_{dh})\Big]^2 + \frac{\beta_2\Gamma_0}{4\beta_0^3} - \frac{\beta_1\Gamma_1}{2\beta_0^3}\left[\frac{3}{2}+\ln(1-\lambda_{dh})\right]\right. \\
&\qquad + \frac{\Gamma_2}{4\beta_0^2} - \frac{\beta_1}{\beta_0^2}\Big(\gamma_0^{\phi_q}+\gamma_0^S\Big)\Big[1+\ln(1-\lambda_{dh})\Big] + \frac{1}{\beta_0}\Big(\gamma_1^{\phi_q}+\gamma_1^S\Big) \\
&\qquad \left. + \frac{\beta_1\Gamma_0}{2\beta_0^2}\Big[1+\ln(1-\lambda_{dh})\Big]L_{dh} - \frac{\Gamma_1}{2\beta_0}L_{dh}\right\} \\
&\quad + \frac{1}{1-\lambda_f}\left\{-\frac{\beta_1^2\Gamma_0}{2\beta_0^4}\lambda_{dh} + \frac{\beta_2\Gamma_0}{2\beta_0^3}\lambda_{dh} + \frac{\beta_1}{2\beta_0^2}\gamma_0^{\phi_q}\Big[1+\ln(1-\lambda_f)\Big] - \frac{\gamma_1^{\phi_q}}{2\beta_0}\right. \\
&\qquad \left. + \frac{\beta_1\Gamma_0}{4\beta_0^2}\Big[L_{ds}-L_{dh}\Big]\Big[1+\ln(1-\lambda_f)\Big] - \frac{\Gamma_1}{4\beta_0}\Big[L_{ds}-L_{dh}\Big]\right\} \\
&\quad + \frac{1}{(1-\lambda_f)^2}\left\{\frac{\beta_1^2\Gamma_0}{4\beta_0^4}\lambda_{dh}\Big[1-\ln^2(1-\lambda_f)\Big] - \frac{\beta_2\Gamma_0}{4\beta_0^3}\lambda_{dh}\right. \\
&\qquad \left. + \frac{\beta_1\Gamma_1}{2\beta_0^3}\lambda_{dh}\left[\frac{1}{2}+\ln(1-\lambda_f)\right] - \frac{\Gamma_2}{\beta_0^2}\lambda_{dh}\right\}, \\
g^D_{3,ds}(\lambda_{ds},\lambda_f) &= \frac{\beta_1^2\,\Gamma_0}{2\beta_0^4}\ln(1-\lambda_{ds}) - \frac{\beta_2\Gamma_0}{2\beta_0^3}\ln(1-\lambda_{ds}) \\
&\quad + \frac{1}{1-\lambda_{ds}}\left\{-\frac{\beta_1^2\Gamma_0}{4\beta_0^4}\Big[1+\ln(1-\lambda_{ds})\Big]^2 - \frac{\beta_2\Gamma_0}{4\beta_0^3}\right. \\
&\qquad \left. + \frac{\beta_1\Gamma_1}{2\beta_0^3}\left[\frac{3}{2}+\ln(1-\lambda_{ds})\right] - \frac{\Gamma_2}{4\beta_0^2}\right.
\end{aligned}
$$

$$
\begin{aligned}
&+\frac{\beta_1}{\beta_0^2}\gamma_0^S\Big[1+\ln(1-\lambda_{ds})\Big]-\frac{\gamma_1^S}{\beta_0}\\
&-\frac{\beta_1\Gamma_0}{2\beta_0^2}\Big[1+\ln(1-\lambda_{ds})\Big]L_{ds}+\frac{\Gamma_1}{2\beta_0}L_{ds}\Bigg\}\\
&+\frac{1}{1-\lambda_f}\Bigg\{\frac{\beta_1^2\Gamma_0}{2\beta_0^4}\lambda_{ds}-\frac{\beta_2\Gamma_0}{2\beta_0^3}\lambda_{ds}+\frac{\beta_1}{2\beta_0^2}\gamma_0^{\phi_q}\Big[1+\ln(1-\lambda_f)\Big]-\frac{\gamma_1^{\phi_q}}{2\beta_0}\\
&+\frac{\beta_1\Gamma_0}{4\beta_0^2}\Big[L_{ds}-L_{dh}\Big]\Big[1+\ln(1-\lambda_f)\Big]-\frac{\Gamma_1}{4\beta_0}\Big[L_{ds}-L_{dh}\Big]\Bigg\}\\
&+\frac{1}{(1-\lambda_f)^2}\Bigg\{-\frac{\beta_1^2\Gamma_0}{4\beta_0^4}\lambda_{ds}\Big[1-\ln^2(1-\lambda_f)\Big]+\frac{\beta_2\Gamma_0}{4\beta_0^3}\lambda_{ds}\\
&-\frac{\beta_1\Gamma_1}{2\beta_0^3}\lambda_{ds}\left[\frac{1}{2}+\ln(1-\lambda_f)\right]-\frac{\Gamma_2}{\beta_0^2}\lambda_{ds}\Bigg\}.
\end{aligned}
$$

A.2 Phase Space Integrals

Here we present the necessary phase space integrals used in computing the decay of the Higgs to b-quarks at LO and NLO. Specifically, these are 2- and 3-body phase space integrals. We also only deal with the cases required for the calculation, namely a massive particle (the Higgs) decaying to two identical massive particles (b-quarks) with the possible emission of an additional gluon into the final state. Throughout we work in d-dimensional spacetime. Setting $d = 4 - 2\epsilon$ will allow dimensional regularisation of the IR poles generated through the emission of soft gluons. We define an n-body phase space as

$$
\int \mathrm{dPS}_n\left(p_0; p_1, \ldots, p_n\right) = \int \prod_{i=1}^{n} \frac{d^{d-1}\vec{p}_i}{(2\pi)^{d-1}2p_i^0}\,(2\pi)^d\delta^{(d)}\left(p_0 - \sum_{i=1}^{n} p_i\right) \tag{A.2.1}
$$

A.2.1 2-Body Phase Space

We start with the 2-body case,

$$
\Gamma_{h\to\bar{b}b} = \frac{1}{2m_h}\int \mathrm{dPS}_2\,\overline{\sum}|\mathcal{M}|^2\,. \tag{A.2.2}
$$

In general, the matrix element will depend on various Lorentz invariant kinematic structures. We shall not worry about these for now, but account for their presence

in the integral by keeping the matrix element squared present throughout. We also start labelling the final state momenta p_i from $i = 3$ onwards. Ignoring the initial flux factor, the phase space integral becomes

$$I_2 = \int \frac{d^{d-1}\vec{p}_3}{(2\pi)^{d-1}2p_3^0} \frac{d^{d-1}\vec{p}_4}{(2\pi)^{d-1}2p_4^0} (2\pi)^d \delta^{(d)} (p_h - p_3 - p_4) |\mathcal{M}|^2 . \tag{A.2.3}$$

Because the matrix element squared is Lorentz invariant, we can compute this integral in any frame. We choose the rest frame of the Higgs. In this frame we parametrise the momenta as

$$p_h = (m_h, \vec{0})$$
$$p_3 = (p_3^0, \vec{p}_3)$$
$$p_4 = (p_4^0, \vec{p}_4)$$

The $\vec{p}_4$ integral is straightforward to compute using the delta function which we can write as $\delta^{(d)} (p_h - p_3 - p_4) = \delta(m_h - p_3^0 - p_4^0)\delta^{(d-1)}(\vec{p}_3 + \vec{p}_4)$. Performing the integral, we get $\vec{p}_4 = -\vec{p}_3$. This also sets

$$p_4^0 = \sqrt{m_b^2 + |\vec{p}_4|^2} = \sqrt{m_b^2 + |\vec{p}_3|^2} = p_3^0 .$$

Our phase space integral thus reduces to

$$I_2 = \int \frac{d^{d-1}\vec{p}_3}{(2\pi)^{d-2}4(p_3^0)^2} \delta(m_h - 2p_3^0) |\mathcal{M}|^2_{\vec{p}_4 \to -\vec{p}_3} . \tag{A.2.4}$$

It is most convenient to write the final integral in spherical coordinates. We write

$$d^{d-1}\vec{p}_3 = |\vec{p}_3|^{d-2} d|\vec{p}_3| d\Omega_{d-1} , \tag{A.2.5}$$

where $d\Omega_d$ represents a unit surface element of a d-dimensional sphere and is given by

$$d\Omega_d = \sin^{d-2}(\phi_{d-1}) \dots \sin(\phi_2) d\phi_1 \dots d\phi_{d-2} , \tag{A.2.6}$$

and we integrate $\phi_1 \in [0, 2\pi]$ and $\phi_{n>1} \in [0, \pi]$. In order to evaluate this integral, we must rewrite the delta function in the form $\delta (|\vec{p}_3| - f)$, where f is some function of

the other variables involved but not of $|\vec{p}_3|$. We use the identity

$$\delta\left(f(x)\right) = \sum_{x_0 \in \text{roots}} \frac{\delta(x - x_0)}{|f'(x)|_{x=x_0}} \tag{A.2.7}$$

where x_0 are the roots of $f(x)$ and $f'(x) = \partial_x f(x)$. Expressing p_3^0 in terms of the momentum $\vec{p}_3$ we arrive at,

$$\delta\left(m_h - 2\sqrt{|\vec{p}_3|^2 + m_b^2}\right) = \frac{1}{2\beta}\delta\left(|\vec{p}_3| - \frac{m_h}{2}\beta\right), \tag{A.2.8}$$

where $\beta = \sqrt{1 - \frac{4m_b^2}{m_h^2}}$. The integral over $|\vec{p}_3|$ can now be performed in a straightforward way using the delta function. We are left with

$$I_2 = \frac{1}{2m_h^2\beta(2\pi)^{d-2}}\left[\frac{m_h}{2}\beta\right]^{d-2}\int d\Omega_{d-1}\,|\mathcal{M}|^2\,, \tag{A.2.9}$$

where in the matrix element we have that $\vec{p}_4 = -\vec{p}_3$ and $|\vec{p}_3| = \beta\, m_h/2$. In general, one would now have to consider the possible angular dependence in $|\mathcal{M}|^2$ to proceed. However, for the 2-body decay in the rest frame of the decaying particle there will not be any such dependence and we can evaluate the angular piece using the result

$$\int d\Omega_d = \frac{2\pi^{d/2}}{\Gamma\left(\frac{d}{2}\right)}\,. \tag{A.2.10}$$

Thus our final result for the 2-body phase space integral becomes

$$I_2 = \frac{\beta}{8\pi}|\mathcal{M}|^2\,. \tag{A.2.11}$$

A.2.2 3-Body Phase Space

We now consider the 3-body phase space integral necessary when considering radiative corrections to Higgs decay. Specifically, this is the decay to two particles of equal mass and one massless particle. We write the 3-body phase space analogous to the 2-body one

$$I_3 = \int \frac{d^{d-1}\vec{p}_3}{(2\pi)^{d-1}2p_3^0}\frac{d^{d-1}\vec{p}_4}{(2\pi)^{d-1}p_4^0}\frac{d^{d-1}\vec{p}_g}{(2\pi)^{d-1}2p_g^0}\,(2\pi)^d\delta^{(d)}\left(p_h - p_3 - p_4 - p_g\right)|\mathcal{M}|^2\,. \tag{A.2.12}$$

A common method for solving such integrals is to split the 3-body phase space into two 2-body phase space integrals

$$I_3 = \frac{dQ^2}{2\pi}\mathrm{dPS}_2(p_h; Q, p_g)\mathrm{dPS}_2(Q; p_3, p_4)\,. \tag{A.2.13}$$

We can easily do each of the two 2-body phase space integrals in its rest frame. We refer to $\mathrm{dPS}_2(Q; p_3, p_4)$ as phase space 1 (PS1) and $\mathrm{dPS}_2(p_h; Q, p_g)$ as phase space 2 (PS2). Considering PS1 first, we choose the frame in which $Q = (Q^0, \vec{0})$. Carrying out the trivial $(d-1)$-dimensional integral, which simply sets the b-quarks back-to-back, the momenta can be parametrised as

$$\begin{aligned}
p_H &= (E_H, 0, \ldots, 0, |\vec{p}_H|)\,, \\
p_3 &= (E_3, 0, \ldots, |\vec{p}_3|\sin\theta, |\vec{p}_3|\cos\theta)\,, \\
p_4 &= (E_3, 0, \ldots, -|\vec{p}_3|\sin\theta, -|\vec{p}_3|\cos\theta)\,, \\
p_g &= (E_g, 0, \ldots, 0, E_g)\,,
\end{aligned}$$

where we have additionally used the fact that the gluon is on-shell. We can also see from total momentum conservation that in this frame $E_g = |\vec{p}_H|$. We perform the rest of this integral in complete analogy to the 2-body case except in the fact that we keep dependence on one angle. We write

$$\int d\Omega_{d-1} = \frac{2\pi^{\frac{d-2}{2}}}{\Gamma\left(\frac{d-2}{2}\right)}\int_0^\pi d\phi\ \sin^{d-3}(\phi)\,, \tag{A.2.14}$$

and obtain the resulting PS1 integral

$$I_{\mathrm{PS1}} = \int_0^\phi d\phi \frac{4^{2-d}\pi^{1-\frac{d}{2}}(Q^2)^{\frac{d}{2}-2}\beta_Q^{d-3}}{\Gamma\left(\frac{d}{2}-1\right)}\sin^{d-3}(\phi)|\mathcal{M}|^2\,. \tag{A.2.15}$$

We now insert this into the PS2 integral and compute in the same fashion. Since the result for the PS1 integral is written in terms of invariants[1] we can evaluate PS2 in a different frame. We choose the rest frame of the Higgs. The integral over $d^{d-1}\vec{p}_g$ is again evaluated with the spatial part of the delta function and sets the

[1] The angle is technically not invariant, but we integrate over the entire range.

gluon back-to-back with the $b\bar{b}$ system.

$$\vec{p}_g = -\vec{Q}\,, \qquad \implies E_g = |\vec{p}_g| = |\vec{Q}|\,. \tag{A.2.16}$$

Using the remaining delta function as before we arrive at the 3-body phase space integral

$$I_3 = \int_{4m_b^2}^{m_H^2} dQ^2 \int_0^\pi d\phi \sin^{d-3}(\phi) \frac{2^{4-3d} m_H^{2-d} \pi^{1-d} (Q^2)^{\frac{d}{2}-2} \beta_Q^{d-3} (m_H^2 - Q^2)^{d-3}}{\Gamma(d-2)} |\mathcal{M}|^2\,, \tag{A.2.17}$$

where we have left the integral over the angle and the energy of the $b\bar{b}$ system unevaluated. This is because the squared matrix element will in general depend on such quantities and so the final answer depends on the exact structures being integrated over.

A.3 SMEFT Operators in the Warsaw Basis

For reference, we list the baryon number conserving operators which comprise the *Warsaw Basis* [32] of dimension-6 operators.

$1 : X^3$

Q_G	$f^{ABC} G_\mu^{A\nu} G_\nu^{B\rho} G_\rho^{C\mu}$
$Q_{\widetilde{G}}$	$f^{ABC} \widetilde{G}_\mu^{A\nu} G_\nu^{B\rho} G_\rho^{C\mu}$
Q_W	$\epsilon^{IJK} W_\mu^{I\nu} W_\nu^{J\rho} W_\rho^{K\mu}$
$Q_{\widetilde{W}}$	$\epsilon^{IJK} \widetilde{W}_\mu^{I\nu} W_\nu^{J\rho} W_\rho^{K\mu}$

$2 : H^6$

Q_H	$(H^\dagger H)^3$

$3 : H^4 D^2$

$Q_{H\Box}$	$(H^\dagger H)\Box(H^\dagger H)$
Q_{HD}	$\left(H^\dagger D_\mu H\right)^* \left(H^\dagger D_\mu H\right)$

$4 : X^2 H^2$

Q_{HG}	$H^\dagger H\, G_{\mu\nu}^A G^{A\mu\nu}$
$Q_{H\widetilde{G}}$	$H^\dagger H\, \widetilde{G}_{\mu\nu}^A G^{A\mu\nu}$
Q_{HW}	$H^\dagger H\, W_{\mu\nu}^I W^{I\mu\nu}$
$Q_{H\widetilde{W}}$	$H^\dagger H\, \widetilde{W}_{\mu\nu}^I W^{I\mu\nu}$
Q_{HB}	$H^\dagger H\, B_{\mu\nu} B^{\mu\nu}$
$Q_{H\widetilde{B}}$	$H^\dagger H\, \widetilde{B}_{\mu\nu} B^{\mu\nu}$
Q_{HWB}	$H^\dagger \tau^I H\, W_{\mu\nu}^I B^{\mu\nu}$
$Q_{H\widetilde{W}B}$	$H^\dagger \tau^I H\, \widetilde{W}_{\mu\nu}^I B^{\mu\nu}$

$5 : \psi^2 H^3 + \text{h.c.}$

Q_{eH}	$(H^\dagger H)(\bar{l}_p e_r H)$
Q_{uH}	$(H^\dagger H)(\bar{q}_p u_r \widetilde{H})$
Q_{dH}	$(H^\dagger H)(\bar{q}_p d_r H)$

$6 : \psi^2 X H + \text{h.c.}$

Q_{eW}	$(\bar{l}_p \sigma^{\mu\nu} e_r)\tau^I H W_{\mu\nu}^I$
Q_{eB}	$(\bar{l}_p \sigma^{\mu\nu} e_r) H B_{\mu\nu}$
Q_{uG}	$(\bar{q}_p \sigma^{\mu\nu} T^A u_r)\widetilde{H}\, G_{\mu\nu}^A$
Q_{uW}	$(\bar{q}_p \sigma^{\mu\nu} u_r)\tau^I \widetilde{H}\, W_{\mu\nu}^I$
Q_{uB}	$(\bar{q}_p \sigma^{\mu\nu} u_r)\widetilde{H}\, B_{\mu\nu}$
Q_{dG}	$(\bar{q}_p \sigma^{\mu\nu} T^A d_r) H\, G_{\mu\nu}^A$
Q_{dW}	$(\bar{q}_p \sigma^{\mu\nu} d_r)\tau^I H\, W_{\mu\nu}^I$
Q_{dB}	$(\bar{q}_p \sigma^{\mu\nu} d_r) H\, B_{\mu\nu}$

$7 : \psi^2 H^2 D$

$Q_{Hl}^{(1)}$	$(H^\dagger i\overleftrightarrow{D}_\mu H)(\bar{l}_p \gamma^\mu l_r)$
$Q_{Hl}^{(3)}$	$(H^\dagger i\overleftrightarrow{D}_\mu^I H)(\bar{l}_p \tau^I \gamma^\mu l_r)$
Q_{He}	$(H^\dagger i\overleftrightarrow{D}_\mu H)(\bar{e}_p \gamma^\mu e_r)$
$Q_{Hq}^{(1)}$	$(H^\dagger i\overleftrightarrow{D}_\mu H)(\bar{q}_p \gamma^\mu q_r)$
$Q_{Hq}^{(3)}$	$(H^\dagger i\overleftrightarrow{D}_\mu^I H)(\bar{q}_p \tau^I \gamma^\mu q_r)$
Q_{Hu}	$(H^\dagger i\overleftrightarrow{D}_\mu H)(\bar{u}_p \gamma^\mu u_r)$
Q_{Hd}	$(H^\dagger i\overleftrightarrow{D}_\mu H)(\bar{d}_p \gamma^\mu d_r)$
$Q_{Hud} + \text{h.c.}$	$i(\widetilde{H}^\dagger D_\mu H)(\bar{u}_p \gamma^\mu d_r)$

$8:(\bar{L}L)(\bar{L}L)$	
Q_{ll}	$(\bar{l}_p\gamma_\mu l_r)(\bar{l}_s\gamma^\mu l_t)$
$Q_{qq}^{(1)}$	$(\bar{q}_p\gamma_\mu q_r)(\bar{q}_s\gamma^\mu q_t)$
$Q_{qq}^{(3)}$	$(\bar{q}_p\gamma_\mu \tau^I q_r)(\bar{q}_s\gamma^\mu \tau^I q_t)$
$Q_{lq}^{(1)}$	$(\bar{l}_p\gamma_\mu l_r)(\bar{q}_s\gamma^\mu q_t)$
$Q_{lq}^{(3)}$	$(\bar{l}_p\gamma_\mu \tau^I l_r)(\bar{q}_s\gamma^\mu \tau^I q_t)$

$8:(\bar{R}R)(\bar{R}R)$	
Q_{ee}	$(\bar{e}_p\gamma_\mu e_r)(\bar{e}_s\gamma^\mu e_t)$
Q_{uu}	$(\bar{u}_p\gamma_\mu u_r)(\bar{u}_s\gamma^\mu u_t)$
Q_{dd}	$(\bar{d}_p\gamma_\mu d_r)(\bar{d}_s\gamma^\mu d_t)$
Q_{eu}	$(\bar{e}_p\gamma_\mu e_r)(\bar{u}_s\gamma^\mu u_t)$
Q_{ed}	$(\bar{e}_p\gamma_\mu e_r)(\bar{d}_s\gamma^\mu d_t)$
$Q_{ud}^{(1)}$	$(\bar{u}_p\gamma_\mu u_r)(\bar{d}_s\gamma^\mu d_t)$
$Q_{ud}^{(8)}$	$(\bar{u}_p\gamma_\mu T^A u_r)(\bar{d}_s\gamma^\mu T^A d_t)$

$8:(\bar{L}L)(\bar{R}R)$	
Q_{le}	$(\bar{l}_p\gamma_\mu l_r)(\bar{e}_s\gamma^\mu e_t)$
Q_{lu}	$(\bar{l}_p\gamma_\mu l_r)(\bar{u}_s\gamma^\mu u_t)$
Q_{ld}	$(\bar{l}_p\gamma_\mu l_r)(\bar{d}_s\gamma^\mu d_t)$
Q_{qe}	$(\bar{q}_p\gamma_\mu q_r)(\bar{e}_s\gamma^\mu e_t)$
$Q_{qu}^{(1)}$	$(\bar{q}_p\gamma_\mu q_r)(\bar{u}_s\gamma^\mu u_t)$
$Q_{qu}^{(8)}$	$(\bar{q}_p\gamma_\mu T^A q_r)(\bar{u}_s\gamma^\mu T^A u_t)$
$Q_{qd}^{(1)}$	$(\bar{q}_p\gamma_\mu q_r)(\bar{d}_s\gamma^\mu d_t)$
$Q_{qd}^{(8)}$	$(\bar{q}_p\gamma_\mu T^A q_r)(\bar{d}_s\gamma^\mu T^A d_t)$

$8:(\bar{L}R)(\bar{R}L)+\text{h.c.}$	
Q_{ledq}	$(\bar{l}_p^j e_r)(\bar{d}_s q_{tj})$

$8:(\bar{L}R)(\bar{L}R)+\text{h.c.}$	
$Q_{quqd}^{(1)}$	$(\bar{q}_p^j u_r)\epsilon_{jk}(\bar{q}_s^k d_t)$
$Q_{quqd}^{(8)}$	$(\bar{q}_p^j T^A u_r)\epsilon_{jk}(\bar{q}_s^k T^A d_t)$
$Q_{lequ}^{(1)}$	$(\bar{l}_p^j e_r)\epsilon_{jk}(\bar{q}_s^k u_t)$
$Q_{lequ}^{(3)}$	$(\bar{l}_p^j \sigma_{\mu\nu} e_r)\epsilon_{jk}(\bar{q}_s^k \sigma^{\mu\nu} u_t)$

Table A.1: The 59 independent dimension-6 operators built from Standard Model fields which conserve baryon number, as given in Ref. [32]. The operators are divided into eight classes: X^3, H^6, etc. Operators with +h.c. in the table heading also have hermitian conjugates, as does the $\psi^2 H^2 D$ operator Q_{Hud}. The subscripts p, r, s, t are flavor indices, The notation is described in [2].

Bibliography

[1] Chen-Ning Yang and Robert L. Mills. Conservation of Isotopic Spin and Isotopic Gauge Invariance. *Phys. Rev.*, 96:191–195, 1954.

[2] Elizabeth E. Jenkins, Aneesh V. Manohar, and Michael Trott. Renormalization Group Evolution of the Standard Model Dimension Six Operators I: Formalism and lambda Dependence. *JHEP*, 10:087, 2013.

[3] Peter W. Higgs. Broken Symmetries and the Masses of Gauge Bosons. *Phys. Rev. Lett.*, 13:508–509, 1964.

[4] F. Englert and R. Brout. Broken Symmetry and the Mass of Gauge Vector Mesons. *Phys. Rev. Lett.*, 13:321–323, 1964.

[5] G. S. Guralnik, C. R. Hagen, and T. W. B. Kibble. Global Conservation Laws and Massless Particles. *Phys. Rev. Lett.*, 13:585–587, 1964.

[6] J. Goldstone. Field Theories with Superconductor Solutions. *Nuovo Cim.*, 19:154–164, 1961.

[7] Jeffrey Goldstone, Abdus Salam, and Steven Weinberg. Broken Symmetries. *Phys. Rev.*, 127:965–970, 1962.

[8] Nicola Cabibbo. Unitary Symmetry and Leptonic Decays. *Phys. Rev. Lett.*, 10:531–533, 1963. [,648(1963)].

[9] Makoto Kobayashi and Toshihide Maskawa. CP Violation in the Renormalizable Theory of Weak Interaction. *Prog. Theor. Phys.*, 49:652–657, 1973.

[10] Ansgar Denner. Techniques for calculation of electroweak radiative corrections at the one loop level and results for W physics at LEP-200. *Fortsch. Phys.*, 41:307–420, 1993.

[11] T. Kinoshita. Mass singularities of Feynman amplitudes. *J. Math. Phys.*, 3:650–677, 1962.

[12] T. D. Lee and M. Nauenberg. Degenerate Systems and Mass Singularities. *Phys. Rev.*, 133:B1549–B1562, 1964. [,25(1964)].

[13] L. D. Faddeev and V. N. Popov. Feynman Diagrams for the Yang-Mills Field. *Phys. Lett.*, 25B:29–30, 1967.

[14] David J. Gross and Frank Wilczek. Ultraviolet Behavior of Nonabelian Gauge Theories. *Phys. Rev. Lett.*, 30:1343–1346, 1973.

[15] H. David Politzer. Reliable Perturbative Results for Strong Interactions? *Phys. Rev. Lett.*, 30:1346–1349, 1973.

[16] M. Beneke and Vladimir A. Smirnov. Asymptotic expansion of Feynman integrals near threshold. *Nucl. Phys.*, B522:321–344, 1998.

[17] Vladimir A. Smirnov. Applied asymptotic expansions in momenta and masses. *Springer Tracts Mod. Phys.*, 177:1–262, 2002.

[18] Thomas Becher, Alessandro Broggio, and Andrea Ferroglia. Introduction to Soft-Collinear Effective Theory. *Lect. Notes Phys.*, 896:pp.1–206, 2015.

[19] Richard J. Hill and Matthias Neubert. Spectator interactions in soft collinear effective theory. *Nucl. Phys.*, B657:229–256, 2003.

[20] M. Beneke and T. Feldmann. Multipole expanded soft collinear effective theory with nonAbelian gauge symmetry. *Phys. Lett.*, B553:267–276, 2003.

[21] M. Beneke, A. P. Chapovsky, M. Diehl, and T. Feldmann. Soft collinear effective theory and heavy to light currents beyond leading power. *Nucl. Phys.*, B643:431–476, 2002.

[22] Christian W. Bauer, Dan Pirjol, and Iain W. Stewart. Soft collinear factorization in effective field theory. *Phys. Rev.*, D65:054022, 2002.

[23] Christian W. Bauer and Iain W. Stewart. Invariant operators in collinear effective theory. *Phys. Lett.*, B516:134–142, 2001.

[24] Christian W. Bauer, Sean Fleming, Dan Pirjol, and Iain W. Stewart. An Effective field theory for collinear and soft gluons: Heavy to light decays. *Phys. Rev.*, D63:114020, 2001.

[25] Christian W. Bauer, Sean Fleming, and Michael E. Luke. Summing Sudakov logarithms in B —> X(s gamma) in effective field theory. *Phys. Rev.*, D63:014006, 2000.

[26] Alexander M. Polyakov. Gauge Fields as Rings of Glue. *Nucl. Phys.*, B164:171–188, 1980.

[27] Richard A. Brandt, Filippo Neri, and Masa-aki Sato. Renormalization of Loop Functions for All Loops. *Phys. Rev.*, D24:879, 1981.

[28] Thomas Appelquist and J. Carazzone. Infrared Singularities and Massive Fields. *Phys. Rev.*, D11:2856, 1975.

[29] Steven Weinberg. A Model of Leptons. *Phys. Rev. Lett.*, 19:1264–1266, 1967.

[30] Chung Ngoc Leung, S. T. Love, and S. Rao. Low-Energy Manifestations of a New Interaction Scale: Operator Analysis. *Z. Phys.*, C31:433, 1986.

[31] W. Buchmuller and D. Wyler. Effective Lagrangian Analysis of New Interactions and Flavor Conservation. *Nucl. Phys.*, B268:621–653, 1986.

[32] B. Grzadkowski, M. Iskrzynski, M. Misiak, and J. Rosiek. Dimension-Six Terms in the Standard Model Lagrangian. *JHEP*, 10:085, 2010.

[33] Christopher Arzt. Reduced effective Lagrangians. *Phys. Lett.*, B342:189–195, 1995.

[34] Howard Georgi. On-shell effective field theory. *Nucl. Phys.*, B361:339–350, 1991.

[35] Rodrigo Alonso, Elizabeth E. Jenkins, Aneesh V. Manohar, and Michael Trott. Renormalization Group Evolution of the Standard Model Dimension Six Operators III: Gauge Coupling Dependence and Phenomenology. *JHEP*, 04:159, 2014.

[36] Valentin Ahrens, Andrea Ferroglia, Matthias Neubert, Ben D. Pecjak, and Li Lin Yang. Renormalization-Group Improved Predictions for Top-Quark Pair Production at Hadron Colliders. *JHEP*, 09:097, 2010.

[37] Andrea Ferroglia, Ben D. Pecjak, and Li Lin Yang. Soft-gluon resummation for boosted top-quark production at hadron colliders. *Phys. Rev.*, D86:034010, 2012.

[38] P. Nason, S. Dawson, and R. Keith Ellis. The Total Cross-Section for the Production of Heavy Quarks in Hadronic Collisions. *Nucl. Phys.*, B303:607–633, 1988.

[39] W. Beenakker, H. Kuijf, W. L. van Neerven, and J. Smith. QCD Corrections to Heavy Quark Production in p anti-p Collisions. *Phys. Rev.*, D40:54–82, 1989.

[40] Michał Czakon, Paul Fiedler, and Alexander Mitov. Total Top-Quark Pair-Production Cross Section at Hadron Colliders Through $\mathcal{O}(\alpha_S^4)$. *Phys. Rev. Lett.*, 110:252004, 2013.

[41] Michal Czakon, David Heymes, and Alexander Mitov. High-precision differential predictions for top-quark pairs at the LHC. *Phys. Rev. Lett.*, 116(8):082003, 2016.

[42] Michal Czakon, David Heymes, and Alexander Mitov. Dynamical scales for multi-TeV top-pair production at the LHC. *JHEP*, 04:071, 2017.

[43] John C. Collins, Davison E. Soper, and George F. Sterman. Factorization of Hard Processes in QCD. *Adv. Ser. Direct. High Energy Phys.*, 5:1–91, 1989.

[44] Thomas Becher, Matthias Neubert, and Gang Xu. Dynamical Threshold Enhancement and Resummation in Drell-Yan Production. *JHEP*, 07:030, 2008.

[45] Valentin Ahrens, Andrea Ferroglia, Matthias Neubert, Ben D. Pecjak, and Li Lin Yang. Threshold expansion at order alpha(s)**4 for the t t-bar invariant mass distribution at hadron colliders. *Phys. Lett.*, B687:331–337, 2010.

[46] B. Mele and P. Nason. The Fragmentation function for heavy quarks in QCD. *Nucl. Phys.*, B361:626–644, 1991.

[47] Kirill Melnikov and Alexander Mitov. Perturbative heavy quark fragmentation function through O(alpha**2(s)). *Phys. Rev.*, D70:034027, 2004.

[48] Matthias Neubert. Factorization analysis for the fragmentation functions of hadrons containing a heavy quark. 2007.

[49] W. Furmanski and R. Petronzio. A Method of Analyzing the Scaling Violation of Inclusive Spectra in Hard Processes. *Nucl. Phys.*, B195:237–261, 1982.

[50] Marco Bonvini and Simone Marzani. Resummed Higgs cross section at N^3LL. *JHEP*, 09:007, 2014.

[51] Marco Bonvini. *Resummation of soft and hard gluon radiation in perturbative QCD*. PhD thesis, Genoa U., 2012.

[52] Richard D. Ball, Marco Bonvini, Stefano Forte, Simone Marzani, and Giovanni Ridolfi. Higgs production in gluon fusion beyond NNLO. *Nucl. Phys.*, B874:746–772, 2013.

[53] V. N. Gribov and L. N. Lipatov. Deep inelastic e p scattering in perturbation theory. *Sov. J. Nucl. Phys.*, 15:438–450, 1972. [Yad. Fiz.15,781(1972)].

[54] Guido Altarelli and G. Parisi. Asymptotic Freedom in Parton Language. *Nucl. Phys.*, B126:298–318, 1977.

[55] Yuri L. Dokshitzer. Calculation of the Structure Functions for Deep Inelastic Scattering and e+ e- Annihilation by Perturbation Theory in Quantum Chromodynamics. *Sov. Phys. JETP*, 46:641–653, 1977. [Zh. Eksp. Teor. Fiz.73,1216(1977)].

[56] Einan Gardi. On the quark distribution in an on-shell heavy quark and its all-order relations with the perturbative fragmentation function. *JHEP*, 02:053, 2005.

[57] S. Moch, J. A. M. Vermaseren, and A. Vogt. Higher-order corrections in threshold resummation. *Nucl. Phys.*, B726:317–335, 2005.

[58] Andrzej J. Buras. Asymptotic Freedom in Deep Inelastic Processes in the Leading Order and Beyond. *Rev. Mod. Phys.*, 52:199, 1980.

[59] Andrzej J. Buras, Matthias Jamin, M. E. Lautenbacher, and Peter H. Weisz. Effective Hamiltonians for $\Delta S = 1$ and $\Delta B = 1$ nonleptonic decays beyond the leading logarithmic approximation. *Nucl. Phys.*, B370:69–104, 1992. [Addendum: Nucl. Phys.B375,501(1992)].

[60] Gerhard Buchalla, Andrzej J. Buras, and Markus E. Lautenbacher. Weak decays beyond leading logarithms. *Rev. Mod. Phys.*, 68:1125–1144, 1996.

[61] S. Moch, J. A. M. Vermaseren, and A. Vogt. The Three loop splitting functions in QCD: The Nonsinglet case. *Nucl. Phys.*, B688:101–134, 2004.

[62] Thomas Becher and Matthias Neubert. Infrared singularities of QCD amplitudes with massive partons. *Phys. Rev.*, D79:125004, 2009. [Erratum: Phys. Rev.D80,109901(2009)].

[63] Thomas Becher and Matthias Neubert. On the Structure of Infrared Singularities of Gauge-Theory Amplitudes. *JHEP*, 06:081, 2009. [Erratum: JHEP11,024(2013)].

[64] Andrea Ferroglia, Matthias Neubert, Ben D. Pecjak, and Li Lin Yang. Two-loop divergences of scattering amplitudes with massive partons. *Phys. Rev. Lett.*, 103:201601, 2009.

[65] Andrea Ferroglia, Matthias Neubert, Ben D. Pecjak, and Li Lin Yang. Two-loop divergences of massive scattering amplitudes in non-abelian gauge theories. *JHEP*, 11:062, 2009.

[66] Nikolaos Kidonakis. Two-loop soft anomalous dimensions and NNLL resummation for heavy quark production. *Phys. Rev. Lett.*, 102:232003, 2009.

[67] G. P. Korchemsky and A. V. Radyushkin. Renormalization of the Wilson Loops Beyond the Leading Order. *Nucl. Phys.*, B283:342–364, 1987.

[68] G. P. Korchemsky and A. V. Radyushkin. Infrared factorization, Wilson lines and the heavy quark limit. *Phys. Lett.*, B279:359–366, 1992.

[69] Alessandro Broggio, Andrea Ferroglia, Ben D. Pecjak, and Zhibai Zhang. NNLO hard functions in massless QCD. *JHEP*, 12:005, 2014.

[70] Andrea Ferroglia, Ben D. Pecjak, Li Lin Yang, Ben D. Pecjak, and Li Lin Yang. The NNLO soft function for the pair invariant mass distribution of boosted top quarks. *JHEP*, 10:180, 2012.

[71] Stefano Catani, Michelangelo L. Mangano, Paolo Nason, and Luca Trentadue. The Resummation of soft gluons in hadronic collisions. *Nucl. Phys.*, B478:273–310, 1996.

[72] Richard D. Ball et al. Parton distributions for the LHC Run II. *JHEP*, 04:040, 2015.

[73] Andy Buckley, James Ferrando, Stephen Lloyd, Karl Nordström, Ben Page, Martin Rüfenacht, Marek Schönherr, and Graeme Watt. LHAPDF6: parton density access in the LHC precision era. *Eur. Phys. J.*, C75:132, 2015.

[74] T. Hahn. CUBA: A Library for multidimensional numerical integration. *Comput. Phys. Commun.*, 168:78–95, 2005.

[75] T. Hahn. Concurrent Cuba. *J. Phys. Conf. Ser.*, 608(1):012066, 2015.

[76] John M. Campbell and R. K. Ellis. MCFM for the Tevatron and the LHC. *Nucl. Phys. Proc. Suppl.*, 205-206:10–15, 2010.

[77] Michal Czakon and Alexander Mitov. Top++: A Program for the Calculation of the Top-Pair Cross-Section at Hadron Colliders. *Comput. Phys. Commun.*, 185:2930, 2014.

[78] Cen Zhang and Fabio Maltoni. Top-quark decay into Higgs boson and a light quark at next-to-leading order in QCD. *Phys. Rev.*, D88:054005, 2013.

[79] Cen Zhang. Effective field theory approach to top-quark decay at next-to-leading order in QCD. *Phys. Rev.*, D90(1):014008, 2014.

[80] Celine Degrande, Fabio Maltoni, Jian Wang, and Cen Zhang. Automatic computations at next-to-leading order in QCD for top-quark flavor-changing neutral processes. *Phys. Rev.*, D91:034024, 2015.

[81] Diogo Buarque Franzosi and Cen Zhang. Probing the top-quark chromomagnetic dipole moment at next-to-leading order in QCD. *Phys. Rev.*, D91(11):114010, 2015.

[82] Cen Zhang. Single Top Production at Next-to-Leading Order in the Standard Model Effective Field Theory. *Phys. Rev. Lett.*, 116(16):162002, 2016.

[83] Olga Bessidskaia Bylund, Fabio Maltoni, Ioannis Tsinikos, Eleni Vryonidou, and Cen Zhang. Probing top quark neutral couplings in the Standard Model Effective Field Theory at NLO in QCD. *JHEP*, 05:052, 2016.

[84] Giovanni Marco Pruna and Adrian Signer. The $\mu \to e\gamma$ decay in a systematic effective field theory approach with dimension 6 operators. *JHEP*, 10:014, 2014.

[85] Christine Hartmann, William Shepherd, and Michael Trott. The Z decay width in the SMEFT: y_t and λ corrections at one loop. *JHEP*, 03:060, 2017.

[86] Giampiero Passarino. NLO Inspired Effective Lagrangians for Higgs Physics. *Nucl. Phys.*, B868:416–458, 2013.

[87] Chien-Yi Chen, S. Dawson, and Cen Zhang. Electroweak Effective Operators and Higgs Physics. *Phys. Rev.*, D89(1):015016, 2014.

[88] Christophe Grojean, Elizabeth E. Jenkins, Aneesh V. Manohar, and Michael Trott. Renormalization Group Scaling of Higgs Operators and $\Gamma(h- > \gamma\gamma)$. *JHEP*, 04:016, 2013.

[89] Christoph Englert and Michael Spannowsky. Effective Theories and Measurements at Colliders. *Phys. Lett.*, B740:8–15, 2015.

[90] Margherita Ghezzi, Raquel Gomez-Ambrosio, Giampiero Passarino, and Sandro Uccirati. NLO Higgs effective field theory and κ-framework. *JHEP*, 07:175, 2015.

[91] Ramona Grober, Margarete Muhlleitner, Michael Spira, and Juraj Streicher. NLO QCD Corrections to Higgs Pair Production including Dimension-6 Operators. *JHEP*, 09:092, 2015.

[92] Christine Hartmann and Michael Trott. On one-loop corrections in the standard model effective field theory; the $\Gamma(h \to \gamma\,\gamma)$ case. *JHEP*, 07:151, 2015.

[93] Christine Hartmann and Michael Trott. Higgs Decay to Two Photons at One Loop in the Standard Model Effective Field Theory. *Phys. Rev. Lett.*, 115(19):191801, 2015.

[94] Rhorry Gauld, Benjamin D. Pecjak, and Darren J. Scott. One-loop corrections to $h \to b\bar{b}$ and $h \to \tau\bar{\tau}$ decays in the Standard Model Dimension-6 EFT: four-fermion operators and the large-m_t limit. *JHEP*, 05:080, 2016.

[95] Martin Gorbahn and Ulrich Haisch. Indirect probes of the trilinear Higgs coupling: $gg \to h$ and $h \to \gamma\gamma$. *JHEP*, 10:094, 2016.

[96] Fabio Maltoni, Eleni Vryonidou, and Cen Zhang. Higgs production in association with a top-antitop pair in the Standard Model Effective Field Theory at NLO in QCD. *JHEP*, 10:123, 2016.

[97] J. Elias-Miró, J. R. Espinosa, E. Masso, and A. Pomarol. Renormalization of dimension-six operators relevant for the Higgs decays $h \to \gamma\gamma, \gamma Z$. *JHEP*, 08:033, 2013.

[98] J. Elias-Miro, J. R. Espinosa, E. Masso, and A. Pomarol. Higgs windows to new physics through d=6 operators: constraints and one-loop anomalous dimensions. *JHEP*, 11:066, 2013.

[99] Nicolas Deutschmann, Claude Duhr, Fabio Maltoni, and Eleni Vryonidou. Gluon-fusion Higgs production in the Standard Model Effective Field Theory. 2017.

[100] Brian Henning, Xiaochuan Lu, and Hitoshi Murayama. How to use the Standard Model effective field theory. *JHEP*, 01:023, 2016.

[101] André David and Giampiero Passarino. Through precision straits to next standard model heights. *Rev. Phys.*, 1:13–28, 2016.

[102] Elizabeth E. Jenkins, Aneesh V. Manohar, and Michael Trott. Renormalization Group Evolution of the Standard Model Dimension Six Operators II: Yukawa Dependence. *JHEP*, 01:035, 2014.

[103] Rodrigo Alonso, Hsi-Ming Chang, Elizabeth E. Jenkins, Aneesh V. Manohar, and Brian Shotwell. Renormalization group evolution of dimension-six baryon number violating operators. *Phys. Lett.*, B734:302–307, 2014.

[104] Alejandro Celis, Javier Fuentes-Martin, Avelino Vicente, and Javier Virto. DsixTools: The Standard Model Effective Field Theory Toolkit. *Eur. Phys. J.*, C77(6):405, 2017.

[105] Yi Liao and Xiao-Dong Ma. Perturbative Power Counting, Lowest-Index Operators and Their Renormalization in Standard Model Effective Field Theory. 2017.

[106] A. Dedes, W. Materkowska, M. Paraskevas, J. Rosiek, and K. Suxho. Feynman rules for the Standard Model Effective Field Theory in R_ξ -gauges. *JHEP*, 06:143, 2017.

[107] Adam Alloul, Neil D. Christensen, Céline Degrande, Claude Duhr, and Benjamin Fuks. FeynRules 2.0 - A complete toolbox for tree-level phenomenology. *Comput. Phys. Commun.*, 185:2250–2300, 2014.

[108] Thomas Hahn. Generating Feynman diagrams and amplitudes with FeynArts 3. *Comput. Phys. Commun.*, 140:418–431, 2001.

[109] T. Hahn and M. Perez-Victoria. Automatized one loop calculations in four-dimensions and D-dimensions. *Comput. Phys. Commun.*, 118:153–165, 1999.

[110] Bernd A. Kniehl. Radiative corrections for $H \to$ f anti-f (γ) in the standard model. *Nucl. Phys.*, B376:3–28, 1992.

[111] E. Braaten and J. P. Leveille. Higgs Boson Decay and the Running Mass. *Phys. Rev.*, D22:715, 1980.

[112] Manuel Drees and Ken-ichi Hikasa. NOTE ON QCD CORRECTIONS TO HADRONIC HIGGS DECAY. *Phys. Lett.*, B240:455, 1990. [Erratum: Phys. Lett.B262,497(1991)].